Alpha decay of deformed nuclei

Thesis submitted in accordance with the requirements of the University of Liverpool for the degree of Doctor in Philosophy

by

Tina Louise Stewart

August 1996

Declaration

I hereby declare that all work described in this thesis is the result of my own research activities unless reference is given to others. None of this material has been previously submitted to this or any other university. All work was carried out in the Department of Applied Mathematics and Theoretical Physics during the period October 1993 to August 1996 under the supervision of Dr. M. W. Kermode.

Contributions from this work are contained in the following references:

- T.L. Stewart, M.W. Kermode, D.J. Beachey, N. Rowley, I.S. Grant and A.T. Kruppa, Phys. Rev. Lett. **77** (1996) 36.
- T.L. Stewart, M.W. Kermode, D.J. Beachey, N. Rowley, I.S. Grant and A.T. Kruppa, submitted for publication to Nuclear Physics A.

Acknowledgements

Thanks first to my supervisor Mark Kermode and all staff and students in Theoretical Physics, especially to Dave for many late evening consultations and Pedro for the entertainment. Also to Neil Rowley for many stimulating discussions, scientific and otherwise. I must also thank my family and friends who have encouraged me, and finally Andy for endless support and inspiration.

Abstract

We consider the effects of nuclear deformation on alpha decay, in particular the effect on transmission of the alpha particle through the potential barrier. For a deformed nucleus, there is coupling between the alpha particle and daughter during barrier transmission which results in mixing of the orbital angular momenta L of emitted alpha particles in this region. We derive an approximate semi-classical transmission matrix to represent this mixing of angular momentum states, and verify its accuracy by comparison of results with those obtained from the numerical solution of coupled channels equations. We also compare our results with those assuming a spherical barrier and show that the treatment of deformation is indeed very important.

The semi-classical technique is applied to the alpha decay of both even–even and odd mass actinide nuclei. For the range of even–even nuclei considered, we make use of experimental branching ratios and factor out the effects of barrier penetration to obtain information on the alpha particle wave functions near the nuclear surface. With certain assumptions about asymptotic phases, we find that the amplitudes of these wave functions are practically constant for all the nuclei considered, suggesting some common nuclear structure in this mass region.

We assume that each odd mass nucleus is formed from the neighbouring even–even nucleus plus an odd nucleon which is strongly coupled to the even–even core in the intrinsic frame. Using this model and the constant amplitudes found for the even–even nuclei, we calculate branching ratios and the anisotropy of alpha particle emission for favoured decays. Our results are compared with experimental data where available and we find that the agreement is reasonable for this simple model.

Contents

Chapter 1

Introduction

Alpha decay occurs when a parent nucleus emits an alpha particle to leave a daughter nucleus. The process may be divided into two distinct parts: the formation of an alpha particle in the nuclear interior, followed by its penetration through the alpha-daughter potential barrier. There are two main approaches to the formation problem. One of these assumes a preformed alpha particle to be moving in the field of the daughter nucleus. Alternatively, one can calculate formation amplitudes by taking the overlap of the individual neutron and proton wave functions with an alpha particle at the nuclear surface. If the nucleus is not spherical in shape, deformed Nilsson-model states should be used in these microscopic calculations.

Whatever the formation mechanism, the decay proceeds by quantum mechanical tunnelling through the potential barrier. In 1928, Gamow [1] and Condon and Gurney [2] calculated the probability of transmission of the alpha particle through the potential barrier resulting from a spherical nucleus. They found that it is mainly dependent upon the energy of the alpha particle and the proton number of the decaying nucleus. This explained the logarithmic relationship between alpha decay half lives and energies for

chains of even–even isotopes, observed by Geiger and Nuttall (see Ref. [3]). Since they only considered the second part of the alpha decay process, the success of their calculations shows that the Geiger-Nuttall relationship does not depend significantly on nuclear structure effects.

In 1953, Hill and Wheeler [4] considered transmission through a deformed barrier and concluded that nuclear deformation should have a pronounced effect on the barrier penetration. They showed that for a prolate nucleus the transmission of an alpha particle is more likely from the poles of the daughter where the potential barrier is lower and thinner than at the equator. This is illustrated in Figure 1.1 where we show the Coulomb barrier for an alpha particle with energy E_L. Since the radius at the pole (r_p) is greater than that at the equator (r_e), the Coulomb barrier is lower and thinner and thus the alpha particle is more likely to be transmitted from the polar region.

Many papers were written during the 1950's and 1960's which considered alpha decay through a deformed barrier. The exact solution of this problem requires the numerical integration of coupled channels equations, but the problem may be solved approximately by a semi-classical approach. In 1957, Fröman [5] used a WKB (Wentzel - Kramers - Brillouin) technique to describe the transmission of an alpha particle through a deformed barrier. A significant part of this thesis is concerned with the derivation of a transmission matrix similar to that of Fröman and the determination of its accuracy compared with exact solutions.

Much of the work on alpha decay in recent years has been carried out by a small number of collaborations. Buck *et al.* [6] – [9] assumed a preformed alpha particle moving in the field of the daughter nucleus, but did not consider nuclear deformation. Berggren's model is similar, and although he considered deformation to be an important factor in the first part of the alpha decay process, he assumed a spherical barrier in the second part [10] – [12]. Finally, Delion *et al.* [13] – [15] derived alpha particle formation amplitudes

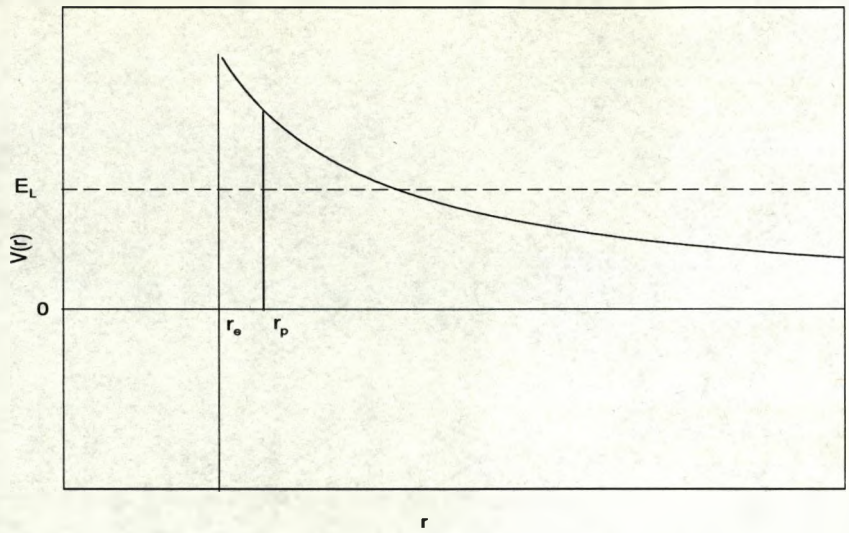

Figure 1.1: The Coulomb barrier for an alpha particle of energy E_L. r_p and r_e represent the radius of the prolate daughter nucleus at the pole and equator respectively. Since $r_p > r_e$ the alpha particle is more likely to be transmitted from the polar region where the barrier is lower and thinner.

using a microscopic approach. They considered the deformed single-particle (Nilsson) states in the vicinity of the Fermi surface and calculated the overlap of the correlated neutron and proton BCS wave functions with an alpha particle at the nuclear surface. The matrix introduced by Fröman was employed to describe transmission through the deformed barrier. It is clear, therefore, that not only is there a difference of approach to the alpha particle formation mechanism, but also to the barrier penetration problem. In this thesis we discuss both these aspects of the alpha decay problem and the validity of the various approaches to them. Most of our work is, however, concerned with the treatment of transmission through the barrier.

In the next chapter we derive a semi-classical transmission matrix and compare the results of alpha decay calculations with those obtained using Fröman's matrix. We also

make a comparison with results assuming a spherical barrier and show that the nuclear deformation does indeed make a significant difference to barrier transmission. Chapter 2 contains all the formal details of our deformation dependent transmission matrix which is used in subsequent work.

In Chapter 3 we consider the alpha decay of even–even nuclei (even Z, even N), in particular how to determine formation amplitudes for a range of deformed actinide nuclei. We investigate several possible models to explain the formation and emission of the alpha particle and compare theoretical results with experimental branching ratios. All of the models considered fail to reproduce the experimental trends, which leads us to reverse the problem and use experimental data to calculate some possible wave functions near the nuclear surface. This is done by factoring out the effects of barrier transmission using our semi-classical transmission matrix, similar to the calculation of reduced widths from absolute alpha decay widths as described in Ref. [16]. In this way, we gain information on the alpha particle formation amplitudes present in deformed actinide nuclei without assuming any model of internal dynamics.

With a particular choice of asymptotic phases, the amplitudes of wave functions near the nuclear surface are practically constant for the range of nuclei considered. This result suggests some common nuclear structure in the actinide region, independent of nuclear deformation or alpha particle energies. We shall show that the most likely physical model to explain such constant amplitudes is that of the alpha particle being formed from pair-correlated proton and neutron Nilsson-model states, i.e. a microscopic description similar to that of Delion *et al.*.

Finally, we consider the more complicated problem of the alpha decay of odd mass nuclei. Interest in this subject has been renewed recently because of new experiments to measure the angular distribution of emitted alpha particles using on-line low temperature nuclear orientation. In our calculations, we assume that the internal wave function of

the odd mass nucleus is closely related to that of the neighbouring even–even one. This allows us to make use of our results from Chapter 3 and calculate alpha decay anisotropies and branching ratios for a range of odd mass nuclei. Our results are compared with experimental data where available and we find that our simple model gives reasonable results. In particular, our model is capable of reproducing the trends of experimentally measured anisotropies in the actinide region. A similar model introduced by Fröman is not able to predict these trends correctly.

Experimental data

The work contained in this thesis employs a large amount of nuclear data for a wide range of nuclei. We take alpha decay lifetimes from the compilation by Buck *et al.* [9], which contains experimental data for all the nuclei we consider. All information on level schemes i.e. spin assignments, excitation energies and branching ratios, is taken from the relevant Nuclear Data Sheets. (These data have been updated since the calculations reported in Refs. [17] and [18].)

Nuclear deformation parameters are extracted from the compilation by Möller *et al.* [19], who obtain their values using a detailed nuclear model and a least-squares fit to experimental ground state masses and fission barrier heights. Although this is not strictly experimental data, it is a convenient source of deformation parameters collected together in one place. Alternatively, deformation parameters would be deduced from experimental data such as quadrupole moments or transition rates. This would be time consuming for the systematic studies included in this work, and since most of our work involves the calculation of normalized quantities such accuracy is not necessary. For the cases where experimentally determined deformation parameters are available, we have compared results to those obtained from Ref. [19] and found that our conclusions

remain unchanged. Since no errors are quoted in the compilation of Möller *et al.* we have investigated in each chapter the sensitivity of our results to these deformation parameters. We employ the deformation parameters of the daughter nucleus in all our work since it is this nucleus with which the alpha particle interacts during barrier transmission.

Chapter 2

Penetration of a deformed barrier

2.1 Schrödinger equation for the alpha decay problem

In the alpha decay process, the parent nucleus decays into two objects – the alpha particle and daughter nucleus. It is convenient to separate the Schrödinger equation into parts which describe the internal motion of each object and the relative motion of the two. We therefore write the Hamiltonian of the system in the form

$$H = H_\alpha + H_d + H_{rel} \tag{2.1.1}$$

where H_α and H_d are the internal Hamiltonians of the alpha and daughter respectively. The corresponding internal wave functions satisfy

$$\begin{aligned} H_\alpha \, \psi_\alpha &= E_\alpha \, \psi_\alpha \\ H_d \, \psi_d &= E_d \, \psi_d \end{aligned} \tag{2.1.2}$$

where E_α and E_d are the internal energies of each part. These wave functions will in general be functions of the object's angular momentum, position in space and isospin,

but we shall not consider isospin in our work since it does not change. The internal energy of the alpha particle remains constant since it does not get excited in the decay process. The internal energy of the daughter, however, may vary as the nucleus rotates. (The vibrational energy of the nucleus is not important in our work since vibrational states have relatively large excitation energies of around 1 MeV for actinide nuclei.)

The term H_{rel} contains the kinetic energy of the relative motion of the alpha and daughter and the potential V between the two parts:

$$H_{rel} = -\frac{\hbar^2}{2\mu}\nabla^2 + V(\mathbf{r}) \tag{2.1.3}$$

where $\mu = m_\alpha m_d/(m_\alpha + m_d)$ is the reduced mass of the system and $\mathbf{r}$ describes the relative co-ordinates of the alpha particle and daughter centres of mass. (This potential is an approximation since it averages over the interaction between the individual nucleons in the alpha particle and daughter nucleus.)

The total wave function Ψ satisfies the Schrödinger equation

$$H\Psi = E\Psi \tag{2.1.4}$$

where E is the total energy of the system, which remains constant. This Schrödinger equation is time-independent because we assume that the parent nucleus is in a quasi-stationary state, as we discuss in more detail in Section 3.4. The total wave function may be expanded as a sum over all possible daughter states,

$$\Psi = \sum_{d'} \psi_\alpha \; \psi_{d'} \; \psi_{\alpha d'}(\mathbf{r}) \tag{2.1.5}$$

where $\psi_{\alpha d'}(\mathbf{r})$ is the relative wave function.

We shall now describe each of these wave functions in more detail. Since the alpha particle has zero intrinsic spin, we shall only consider the space dependent part of its wave function. However, the daughter nucleus may have non-zero angular momentum

J_d, and so its wave function is written as a product of the space dependent wave function $\phi_{d'}$ and the spin dependent state vector,

$$\psi_{d'} = \phi_{d'} \, |J'_d M'_d\rangle. \tag{2.1.6}$$

(Where a label has a subscript we write the prime differently for clarity, i.e. we write J'_d rather than $J_{d'}$.) The spin dependent part is defined in the laboratory frame, but for even–even nuclei the transformation between frames does not change the amplitude of the wave function. This is shown explicitly in Chapter 4 when we derive the wave function for an odd mass nucleus in more detail.

The relative wave function may be expanded in terms of radial and angular parts

$$\psi_{\alpha' d'}(\mathbf{r}) = \sum_{L'M'} \frac{u_{L'}(r)}{r} \, Y_{L'M'}(\theta, \phi) \tag{2.1.7}$$

where L' here represents the orbital angular momentum of the alpha particle relative to the daughter nucleus, and the angles are defined in the intrinsic frame of the daughter nucleus. For an even–even nucleus, the projection of the alpha particle orbital angular momentum must be zero in the intrinsic frame of the daughter and so the quantum number $M' = 0$. This is a consequence of the parent spin being zero for such a nucleus. We shall therefore make use of the function $\Theta_{L0}(\theta)$ which is the normalized θ-dependent part of the spherical harmonic defined by

$$Y_{LM}(\theta, \phi) = \Theta_{LM}(\theta) \left(\frac{\exp(iM\phi)}{\sqrt{2\pi}} \right). \tag{2.1.8}$$

With these assumptions, we can write the relative wave function in the form

$$\begin{aligned} \psi_{\alpha' d'}(\mathbf{r}) &= \sum_{L'} \frac{u_{L'}(r)}{r} \, \Theta_{L'0}(\theta) \\ &\equiv \sum_{L'} \frac{u_{L'}(r)}{r} \, |L'0\rangle. \end{aligned} \tag{2.1.9}$$

The results are easily generalized for odd mass nuclei where M' may be non-zero.

The total wave function with the condition $M' = 0$ can therefore be written

$$\Psi = \sum_{d'L'} \phi_{d'}\ \psi_{\alpha}\ \frac{u_{L'}(r)}{r}\ |J'_d M'_d\rangle\ |L'0\rangle. \tag{2.1.10}$$

Since the state vectors represent the angular momentum of the daughter nucleus and the relative orbital angular momentum of the alpha particle, they can be combined to describe the angular momentum of the parent,

$$\Psi = \sum_{d'L'J'_pM'_p} \phi_{d'}\ \psi_{\alpha}\ \frac{u_{L'}(r)}{r}\ \langle J'_d L' M'_d 0 | J'_p M'_p\rangle\ |J'_p M'_p\rangle. \tag{2.1.11}$$

This Clebsch-Gordon coefficient allows different parent spins to be created by the vector addition of J'_d and L'. The wave function above is therefore a sum of terms representing different states of the parent nucleus, with different energies. In our work we are only interested in the ground state of the parent with spin J_p, so all terms corresponding to excited states will be ignored,

$$\Psi = \sum_{d'L'} \phi_{d'}\ \psi_{\alpha}\ \frac{u_{L'}(r)}{r}\ \langle J'_d L' M'_d 0 | J_p M_p\rangle\ |J_p M_p\rangle. \tag{2.1.12}$$

We now decompose the state vector of the parent into its two constituent parts again. For an even–even nucleus, the parent spin and projection must be zero and this restricts the angular momentum of the daughter such that $J'_d = L'$. With this condition, the Clebsch-Gordon coefficient reduces to a factor $(2L'+1)^{1/2}$ which is incorporated into the radial wave function $u_{L'}$. The total wave function for an even–even nucleus with $J_p = 0$ may therefore be written as

$$\Psi = \sum_{d'L'} \phi_{d'}\ \psi_{\alpha}\ \frac{u_{L'}(r)}{r}\ |J'_d M'_d\rangle\ |L'0\rangle\ \delta_{J'_d L'}\ \delta_{M'_d 0}. \tag{2.1.13}$$

Now we return to the Schrödinger equation of Equation (2.1.4), and substitute in

Equations (2.1.1 – 2.1.3) and (2.1.13),

$$\sum_{d'L'} \left[-\frac{\hbar^2}{2\mu}\nabla^2 + V(\mathbf{r}) - (E - E_\alpha - E_{d'}) \right] \phi_{d'}\ \psi_\alpha\ \frac{u_{L'}(r)}{r}\ |J'_d M'_d\rangle\ |L'0\rangle\ \delta_{J'_d L'}\ \delta_{M'_d 0} = 0. \tag{2.1.14}$$

The energy term $E - E_\alpha - E_{d'}$ varies only through the rotational energy of the daughter $E_{d'}$ which depends upon the spin J'_d. Since we have $L' = J'_d$ we can replace this energy term by a single value $E_{L'}$. Multiplying by $\psi^*_\alpha\ \phi^*_d\ \langle J_d M_d|$ and integrating over all internal co-ordinates, we obtain

$$\sum_{L'} \left[-\frac{\hbar^2}{2\mu}\nabla^2 + V(\mathbf{r}) - E_{L'} \right] \frac{u_{L'}(r)}{r}\ |L'0\rangle\ = 0. \tag{2.1.15}$$

Finally, we derive the Schrödinger equation for the relative radial wave function $u_L(r)$ by multiplying by $\langle L0|$ and integrating over all angles,

$$-\frac{\mathrm{d}^2 u_L(r)}{\mathrm{d}r^2} + \frac{L(L+1)}{r^2}\ u_L + \frac{2\mu}{\hbar^2} \sum_{L'} V_{LL'}(r)\ u_{L'} = \frac{2\mu}{\hbar^2}\ E_L\ u_L. \tag{2.1.16}$$

We calculate E_L from the observed kinetic energy of the alpha particle, corrected for the recoil of the daughter nucleus and the screening effect of the electron cloud [9]. The matrix element is defined by

$$\begin{aligned} V_{LL'}(r) &= \langle\ L\ |\ V(\mathbf{r})\ |\ L'\ \rangle \\ &= \int_0^\pi \Theta_{L0}(\theta)\ V(\mathbf{r})\ \Theta_{L'0}(\theta)\ \sin\theta\ \mathrm{d}\theta \end{aligned} \tag{2.1.17}$$

and the off-diagonal elements indicate coupling between the alpha particle and excited states of the daughter nucleus.

2.2 Spherical barrier

First let us consider how to calculate the transmission probability through a spherical barrier, i.e. where there is no coupling between the alpha particle and daughter nucleus.

In this case, the potential is a function of the radius r between alpha particle and daughter nucleus, and the off-diagonal matrix elements in Equation (2.1.16) are zero. The radial wave equation may be written more simply as

$$\frac{\mathrm{d}^2 u_L(r)}{\mathrm{d}r^2} - \kappa_L^2(r)\, u_L(r) = 0 \tag{2.2.1}$$

where

$$\kappa_L^2(r) = \frac{2\mu}{\hbar^2}\left(V(r) + V_L - E_L\right) \tag{2.2.2}$$

and the centrifugal term is

$$V_L = \frac{\hbar^2}{2\mu}\frac{L(L+1)}{r^2}. \tag{2.2.3}$$

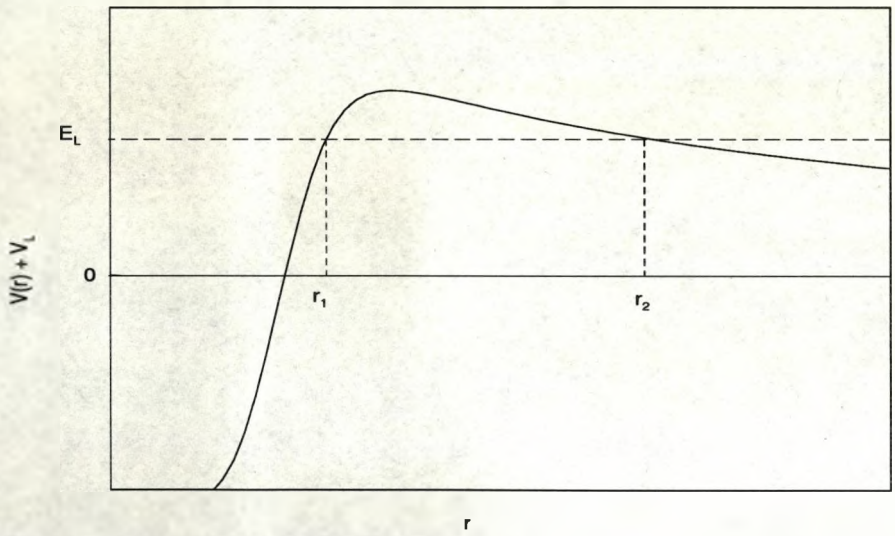

Figure 2.1: General barrier shape for an alpha particle of energy E_L and a potential $V(r)$. The radii r_1 and r_2 are solutions of $\kappa_L(r) = 0$.

We shall briefly review the results of the WKB approximation in the case of a spherical potential. For a general barrier shape as shown in Figure 2.1, the radial equation cannot

be solved analytically. To obtain an approximate solution to Equation (2.2.1), we take a trial wave function of the form

$$u_L(r) = A_L \ \exp(iS_L(r)) \tag{2.2.4}$$

where A_L is a constant for each partial wave and S_L is the function we wish to find. (Other derivations start with a wave function of the form $u_L(r) = \exp(iS_L/\hbar)$ and assume that S_L may be expanded in powers of $\hbar$, e.g. Refs. [20] and [21].) Substituting this trial wave function into Equation (2.2.1) gives

$$iS_L'' - (S_L')^2 - \kappa_L^2 = 0, \tag{2.2.5}$$

where the treatment is still exact. Now if we neglect the second derivative of S_L with respect to r, we get the WKB approximation

$$iS_L(r) = \pm \int_c^r \kappa_L(r)\ \mathrm{d}r \tag{2.2.6}$$

where $r > c$. The limits of integration will depend on the details of the problem being studied. Our aim in this work is to find an expression relating the alpha particle wave function inside and outside the potential barrier. So the region we are interested in is that between the classical turning points r_1 and r_2, as shown in Figure 2.1. In this region the wave function is decaying exponentially from left to right, so we take the negative sign in Equation (2.2.6).

So we have obtained an approximate solution to the radial wave equation. Let us now substitute this solution back into Equation (2.2.1):

$$\frac{\mathrm{d}^2 u_L(r)}{\mathrm{d}r^2} - \kappa_L^2(r)\ u_L(r) = \pm i\ u_L(r)\ \frac{\mathrm{d}\kappa_L}{\mathrm{d}r}. \tag{2.2.7}$$

Thus our solution is a good approximation to the exact wave function if

$$\left|\frac{\mathrm{d}\kappa_L}{\mathrm{d}r}\right| \ll \kappa_L^2. \tag{2.2.8}$$

In practise, this means that the approximation is valid provided that the change in the local wavelength $(1/\kappa_L)$ is small over a few wavelengths, which for our problem is true everywhere except near the turning points r_1 and r_2, which are the solutions of $\kappa_L(r) = 0$. This could obviously create a problem, since it is the wave function between the turning points that we are interested in using. The problem may be solved formally by considering the wave function in each region separately and matching them up using connection formulae, e.g. ([20], page 371).

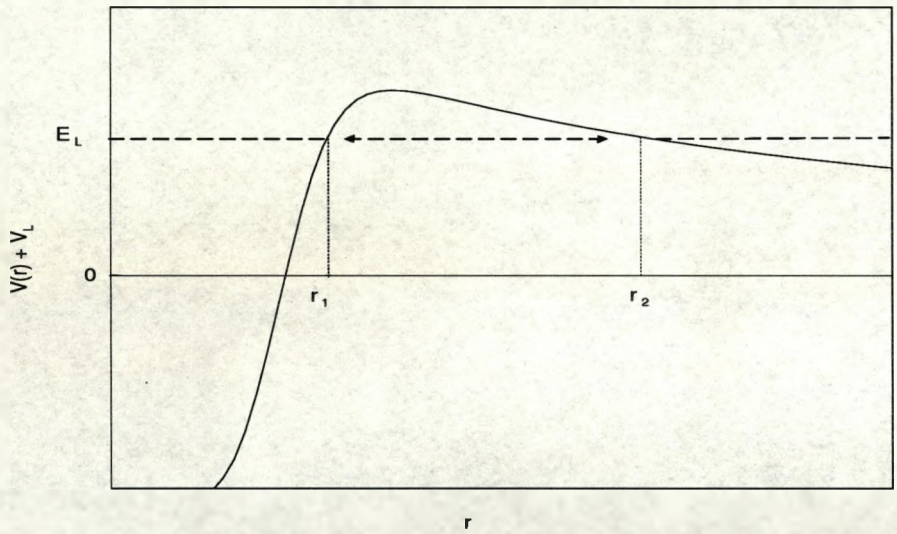

Figure 2.2: The WKB approximation is not valid very close to the turning points r_1 and r_2. In deriving the barrier penetration probability we consider the integral to be done between points just inside each turning point, where the WKB wave function is valid.

We can, however, obtain the same result by a less rigorous approach. The WKB wave function is valid for all values of r under the barrier except those very close to the turning points. We can therefore write down a valid relationship between the radial wave function $u_L(r)$ at radii just within the extent of the barrier, as shown in Figure 2.2.

The relationship between the two wave functions is given by

$$\begin{aligned} u_L(r_2) &= A_L \exp\left(iS_L(r_2)\right) \\ &= A_L \exp\left(iS_L(r_1) + iS_L(r_2) - iS_L(r_1)\right) \\ &= \exp\left(iS_L(r_2) - iS_L(r_1)\right)\ u_L(r_1) \\ &= \exp\left(-\int_{r_1}^{r_2} \kappa_L(r)\ \mathrm{d}r\right)\ u_L(r_1). \end{aligned} \tag{2.2.9}$$

We see from this result that the significant quantity is the integral of κ_L between the two radii. Extending the area of integration then in Figure 2.2 to the actual turning points will not contribute significantly to the integral in Equation (2.2.9), so the result may be used for the barrier penetration problem, where it is the exponential term and not the actual value of the wave functions that is important. This justification is similar to that given by Schiff ([21], page 278).

Thus the wave function of an alpha particle is attenuated by an exponential factor as it penetrates the potential barrier. Consider the square of the wave function in Equation (2.2.9), which is related to the probability of finding the alpha particle at r_2,

$$|u_L(r_2)|^2 = \left| \exp\left(-\int_{r_1}^{r_2} \kappa_L(r)\ \mathrm{d}r\right)\ u_L(r_1) \right|^2. \tag{2.2.10}$$

The physical interpretation of Equation (2.2.10) is that the probability of finding the alpha particle at r_2 is equal to the probability of finding it at r_1 multiplied by the probability of transmission through the barrier.

So we can summarize our result by saying that the probability of transmission of the alpha particle through a spherical barrier is the Gamow factor

$$P = \exp(-2I_L) \tag{2.2.11}$$

where I_L is defined by

$$I_L = \int_{r_1}^{r_2} \kappa_L(r)\, \mathrm{d}r. \tag{2.2.12}$$

The values of r_1 and r_2 are dependent upon the particular form chosen for the potential $V(r)$, as we shall discuss in Section 2.4. For a general barrier shape, the calculation of I_L cannot be done exactly and numerical integration is required. We note again that other derivations obtain exactly the same probability of barrier transmission by a rigorous treatment of the WKB wave functions using connection formulae [20].

2.3 Deformed barrier

If the nucleus is deformed, the potential between the alpha particle and daughter nucleus will be angle dependent. The equation of the surface of an axially symmetric deformed nucleus may be defined by

$$R(\theta) = R_0 \left(1 + \sum_{L=2,3\ldots} \beta_L Y_{L0}(\theta) \right) \tag{2.3.1}$$

where $Y_{L0}(\theta) \equiv Y_{L0}(\theta, 0)$. The term corresponding to $L = 1$ is not present because it describes a displacement of the centre of mass, not a deformation of the nucleus. If the nucleus is also reflection symmetric, only even values of L are included in the sum. Figure 2.3 shows an arbitrary nuclear shape that is both reflection symmetric (in the x-y plane) and axially symmetric (about the z-axis). If we included an octupole term ($L = 3$) for example, the nucleus would be pear shaped and would not be reflection symmetric. The angle θ is measured with respect to the z-axis of the nucleus as shown in Figure 2.3. R_0 is deformation dependent in order to conserve the nuclear volume and in the limit as the nuclear deformation tends to zero R_0 is just the radius of the spherical nucleus.

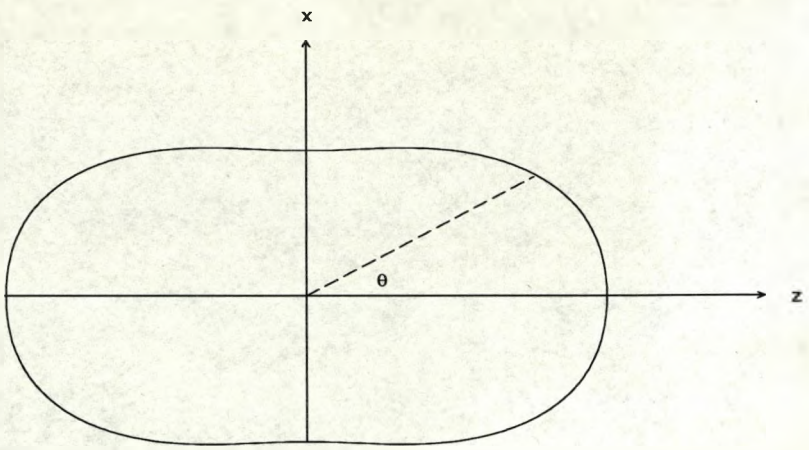

Figure 2.3: Schematic diagram of a deformed nucleus which is both axially symmetric (about the z-axis) and reflection symmetric (in the x-y plane).

2.3.1 Coupled channels equations

We have shown in Equation (2.1.15) that in the even–even case, the relative wave function $\psi(\mathbf{r})$ between the alpha particle and daughter nucleus satisfies

$$\sum_L \left[-\frac{\hbar^2}{2\mu}\nabla^2 + V(\mathbf{r}) - E_L \right] \psi_L(\mathbf{r}) = 0 \tag{2.3.2}$$

where we defined

$$\psi_L(\mathbf{r}) = \frac{u_L(r)}{r}\, \Theta_{L0}(\theta). \tag{2.3.3}$$

By making this partial wave expansion we showed that the radial equations are coupled (Equation (2.1.16)). Physically, the coupling under the barrier may be explained by the deformed daughter nucleus having electric multipole moments due to the asymmetry of the charge distribution. Thus the alpha particle and daughter may exchange energy and angular momentum for some distance after the separation has taken place.

For a general barrier shape the coupled equations are impossible to solve analytically. We could however solve the problem using a numerical integration technique with fixed boundary conditions. These conditions would be that the wave function was regular at the origin i.e. $u_L(0) = 0$, and that outside the barrier there should only be outgoing waves. In our work, we are not interested in solutions of the coupled equations near the origin, since it is not clear that the alpha particle even exists in this region: it is the solutions on the nuclear surface that we are concerned with. We therefore integrate the coupled equations inwards through the barrier, subject only to conditions on the asymptotic wave function.

2.3.2 WKB approximation

Although the exact coupled channels equations can be integrated numerically, approximations such as the WKB technique have often been used in the past because they can be calculated more quickly and easily. In this section we shall use a WKB approach and derive an approximate solution to the wave function for the deformed system. The derivation follows much the same steps as in the spherical case.

Let us write down a general expression for $\psi_L(\mathbf{r})$ which we expect to hold some validity

$$\psi_L(\mathbf{r}) = \frac{1}{r}\, A_L\, \exp(iS_L(r,\theta))\, \Theta_{L0}(\theta) = \frac{1}{r}\, \Phi_L. \tag{2.3.4}$$

Using the properties of the spherical harmonics ([21], page 82) we find

$$\begin{aligned} \nabla^2\psi_L &= \frac{1}{r}\left(\frac{\partial^2\Phi_L}{\partial r^2} + \frac{1}{r^2\sin\theta}\frac{\partial}{\partial\theta}\left(\sin\theta\frac{\partial\Phi_L}{\partial\theta}\right)\right) \qquad (2.3.5)\\ &\approx \frac{1}{r}\left(\left(i\frac{\partial S_L(r,\theta)}{\partial r}\right)^2 + i\frac{\partial^2 S_L(r,\theta)}{\partial r^2} - \frac{L(L+1)}{r^2}\right) A_L\, \Theta_{L0}(\theta)\, e^{iS_L(r,\theta)} \end{aligned}$$

where we have assumed that the derivatives of $S_L(r,\theta)$ with respect to θ are small and so these terms are neglected. If we also ignore the second derivative of $S_L(r,\theta)$ with respect

to r as in the spherical case, and substitute Equation (2.3.5) into Equation (2.3.2) we obtain

$$\frac{1}{r}\sum_L \left(-\left(\frac{\partial S_L(r,\theta)}{\partial r}\right)^2 - \frac{L(L+1)}{r^2} - \frac{2\mu}{\hbar^2}\left(V(r,\theta) - E_L\right)\right) A_L\ \Theta_{L0}(\theta)\ e^{iS_L(r,\theta)} = 0. \tag{2.3.6}$$

The coupled equations that can be obtained from this expression are very complicated because of the angular dependence of S_L in the partial derivatives. We therefore choose the angular dependence of S_L such that it satisfies

$$-\left(\frac{\partial S_L(r,\theta)}{\partial r}\right)^2 - \kappa_L^2(r,\theta) = 0 \tag{2.3.7}$$

where

$$\kappa_L^2(r,\theta) = \frac{2\mu}{\hbar^2}\ \left(V(r,\theta) - E_L\right) + \frac{L(L+1)}{r^2}. \tag{2.3.8}$$

We are able to choose this solution because the function S_L is not unique. In fact we could have chosen S_L to have no angular dependence at all, in which case the expansion would be equivalent to that in Equation (2.3.3). If this were the case, Equation (2.3.6) would reduce to coupled equations as in Equation (2.1.16). A formal proof of Equation (2.3.7) is given in Ref. [5] (Appendix B). Here, Fröman also finds that a WKB approximation for a deformed barrier requires one extra assumption than that for a spherical barrier.

The equation for $S_L(r,\theta)$ becomes

$$iS_L(r,\theta) = \pm \int \kappa_L(r,\theta)\ \mathrm{d}r. \tag{2.3.9}$$

In this case, we choose to carry out the integration from the outer turning point r_2 to some inner radius r such that $r_1 \leq r \leq r_2$. The reasons for this choice will be discussed later. Note that now the turning points are solutions of $\kappa_L(r,\theta) = 0$ and so they also must be angle dependent. The angular dependence of the outer turning point is negligible, but that of r_1 is important and must be considered.

So, finally, we have obtained an approximate wave function

$$\psi(\mathbf{r}) \approx \frac{1}{r} \sum_{L} A_L \exp\ (iS_L(r_2, r(\theta)))\ \Theta_{L0}(\theta) \tag{2.3.10}$$

where

$$iS_L(r_2, r(\theta)) = -\int_{r_2}^{r(\theta)} \kappa_L(r, \theta)\, \mathrm{d}r. \tag{2.3.11}$$

The overall value of iS_L must be positive this time because we are integrating from right to left in Figure 2.1 and the wave function is exponentially increasing as r decreases. The minus sign in Equation (2.3.11) thus cancels out the negative value of the integral. This result is what one might have guessed by generalizing Equation (2.2.6) in the spherical case. The derivation has proceeded in exactly the same way, except that we have had to make one additional approximation – that the derivatives of S_L with respect to θ are negligible. We have calculated values of $iS_L(r, \theta)$ for the ground state of the nucleus ^{238}U and for a range of values of θ, using the potentials defined in Section 2.4 (Equation (2.4.6)). The limits of integration are taken to be r_1 and r_2 and the results are shown in Figure 2.4. We find that the integral is indeed not very sensitive to changes in θ, which shows that our approximation is a good one.

Now we shall derive an expression relating the wave functions just inside and outside the potential barrier, as we did in the spherical case. We can write down two different partial wave expansions of ψ:

$$\begin{aligned} \psi(\mathbf{r}) &= \frac{1}{r} \sum_{L''} u_{L''}(r)\, \Theta_{L''0}(\theta) \\ &= \frac{1}{r} \sum_{L} A_L\, e^{iS_L(r_2, r(\theta))}\, \Theta_{L0}(\theta). \end{aligned} \tag{2.3.12}$$

We have said that the inner turning point r_1 is angle dependent, so we cannot define the radial wave function $u_L(r)$ at this point. We must look for an inner radius which is close to r_1 but does not depend upon θ. We therefore choose the inner radius to be the

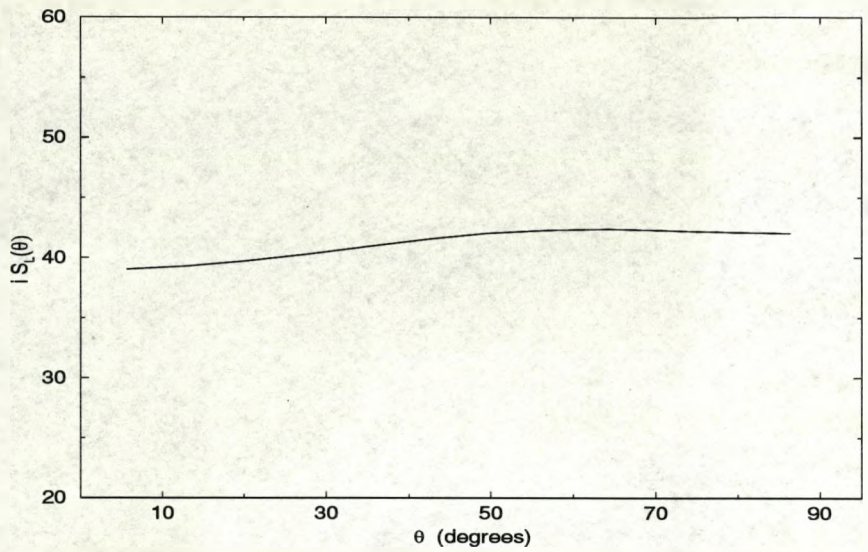

Figure 2.4: Values of $iS_0(r_2, r_1, \theta)$ calculated for ^{238}U using Equation (2.3.11) for a range of angles.

radius R_0 in Equation (2.3.1), which may be thought of as the "average" value of $r_1(\theta)$, and write

$$\sum_{L''} u_{L''}(R_0)\ \Theta_{L''0}(\theta) = \sum_{L} A_L\ e^{iS_L(r_2,r_1,\theta)}\ \Theta_{L0}(\theta). \tag{2.3.13}$$

At the outer turning point $r = r_2$,

$$\begin{aligned} \sum_{L''} u_{L''}(r_2)\ \Theta_{L''0}(\theta) &= \sum_{L} A_L\ e^{iS_L(r_2,r_2,\theta)}\ \Theta_{L0}(\theta) \\ &= \sum_{L} A_L\ \Theta_{L0}(\theta) \end{aligned} \tag{2.3.14}$$

and so $A_L = u_L(r_2)$. Now Equation (2.3.13) becomes

$$\sum_{L''} u_{L''}(R_0)\ \Theta_{L''0}(\theta) = \sum_{L} e^{iS_L(r_2,r_1,\theta)}\ \Theta_{L0}(\theta)\ u_L(r_2). \tag{2.3.15}$$

Multiplying each side by $\Theta_{L'0}(\theta)$ and integrating over all θ gives rise to a term $\delta_{L'L''}$ on the left hand side,

$$u_{L'}(R_0) = \sum_L Q_{L'L}\, u_L(r_2) \tag{2.3.16}$$

where

$$\begin{aligned} Q_{L'L} &= \int_0^\pi \Theta_{L'0}(\theta)\, e^{iS_L(r_2,r_1,\theta)}\, \Theta_{L0}(\theta)\, \sin\theta\, \mathrm{d}\theta \\ &= \int_0^\pi \Theta_{L'0}(\theta)\, e^{I_L(\theta)}\, \Theta_{L0}(\theta)\, \sin\theta\, \mathrm{d}\theta \end{aligned} \tag{2.3.17}$$

and

$$I_L(\theta) = -\int_{r_2}^{r_1} \kappa_L(r,\theta)\, \mathrm{d}r = \int_{r_1}^{r_2} \kappa_L(r,\theta)\, \mathrm{d}r \tag{2.3.18}$$

from Equation (2.3.11). In making the decision to integrate inwards through the barrier we effectively chose to have the angular momentum L rather than L' in the centrifugal potential, thus the matrix Q has I_L not $I_{L'}$ in the exponent. We can justify this by considering the strength of the various expressions in the effective potential $V(r,\theta)+V_L$. The term $V(r,\theta)$ contains the nuclear and Coulomb potentials. The nuclear potential dominates for small values of the radius r, but falls away quickly as r increases. The centrifugal potential V_L will therefore be more important near the outer turning point r_2 where the nuclear potential has less effect, and so the angular momentum of the final state L is used. Having to make this choice is a consequence of our semi-classical approximation to the barrier penetration problem. We shall see later how good the choice is by comparing results with those from the exact coupled channels equations.

The matrix element $Q_{L'L}$ is related to the probability of an alpha particle changing orbital angular momentum from L outside the barrier to L' inside. We now want to obtain a similar expression when we are integrating from inside to outside, as is the case

in many calculations on alpha decay. We can do this by inverting Q so that

$$u_L(r_2) = \sum_{L'} (Q^{-1})_{LL'}\ u_{L'}(R_0). \tag{2.3.19}$$

Alternatively, let us assume that

$$u_L(r_2) = \sum_{L'} \mathcal{K}_{LL'}\ u_{L'}(R_0) \tag{2.3.20}$$

where

$$\mathcal{K}_{LL'} = \int_0^\pi \Theta_{L0}(\theta)\ e^{-I_L(\theta)}\ \Theta_{L'0}(\theta)\ \sin\theta\ \mathrm{d}\theta \tag{2.3.21}$$

and again it is the final state L that appears in the exponent.

Then we should find that

$$\mathcal{K}_{LL'} = (Q^{-1})_{L'L} \tag{2.3.22}$$

where

$$\mathcal{K}_{LL'} = \langle\ L\ |\ e^{-I_L(\theta)}\ |\ L'\ \rangle \tag{2.3.23}$$

and

$$Q_{L'L} = \langle\ L'\ |\ e^{I_L(\theta)}\ |\ L\ \rangle. \tag{2.3.24}$$

Consider the product of these two matrices

$$\begin{aligned} W_{LL''} &= \sum_{L'} \mathcal{K}_{LL'}\ Q_{L'L''} \\ &= \sum_{L'} \langle\ L\ |\ \mathrm{e}^{-I_L(\theta)}\ |\ L'\ \rangle\ \langle\ L'\ |\ \mathrm{e}^{I_{L''}(\theta)}\ |\ L''\ \rangle \\ &= \langle\ L\ |\ \mathrm{e}^{-(I_L(\theta)-I_{L''}(\theta))}\ |\ L''\ \rangle. \end{aligned} \tag{2.3.25}$$

This does not give the unit matrix but the diagonal elements are close to unity (provided we sum over a large number of L'). W is the unit matrix only in the special cases where the integral I is independent of θ (i.e. when the nucleus is spherical) or independent of

L. We have already shown in Figure 2.4 that I_L is not very dependent upon the angle θ. Table 2.1 shows the first six rows and columns of the matrix W for the nucleus ^{238}U considering angular momentum states up to $L = 18$. The more states considered in the calculation, the better the approximation. We find that the matrix elements above the diagonal are much larger than those below. This is because in the upper half of the matrix $L < L''$, making the exponent in Equation (2.3.25) positive and thus magnifying any errors.

Table 2.1: The first six rows and columns of the matrices W and Z for the nucleus ^{238}U including values of L up to 18. We have used the potentials given in Section 2.4 (Equation (2.4.6)).

$$W = \begin{pmatrix} 1.000 & -0.024 & -0.146 & 0.196 & -0.004 & -0.203 \\ 0.007 & 1.000 & -0.107 & -0.131 & 0.503 & -0.591 \\ 0.003 & 0.007 & 1.000 & -0.108 & -0.153 & 0.762 \\ 0.000 & 0.002 & 0.018 & 1.000 & -0.178 & -0.396 \\ 0.000 & 0.000 & 0.003 & 0.016 & 0.999 & -0.277 \\ 0.000 & 0.000 & 0.000 & 0.002 & 0.013 & 1.005 \end{pmatrix}$$

$$Z = \begin{pmatrix} 1.000 & -0.087 & -0.050 & -0.010 & -0.039 & -0.054 \\ -0.014 & 1.031 & -0.001 & 0.038 & 0.059 & 0.049 \\ 0.031 & 0.025 & 1.014 & -0.070 & -0.016 & 0.015 \\ 0.025 & 0.068 & 0.060 & 1.042 & -0.069 & -0.059 \\ -0.018 & -0.035 & 0.001 & 0.018 & 1.038 & 0.006 \\ -0.017 & -0.026 & -0.032 & 0.002 & -0.011 & 0.947 \end{pmatrix}$$

If we consider the matrix multiplication in a different order, this problem of errors in

the upper half of the matrix does not exist. Table 2.1 also shows the first six rows and columns of the matrix Z defined by

$$\begin{aligned} Z_{L'L''} &= \sum_{L} Q_{L'L}\, \mathcal{K}_{LL''} \\ &= \sum_{L} \langle\, L' \mid \mathrm{e}^{I_L(\theta)} \mid L \,\rangle \langle\, L \mid \mathrm{e}^{-I_L(\theta)} \mid L'' \,\rangle. \end{aligned} \tag{2.3.26}$$

Notice that in this case the sum over L cannot be done because of the exponential dependence. If the matrix $\mathcal{K}$ is a good approximation to the inverse of Q however, their product should obviously be close to the unit matrix. We find that the matrix Z is indeed reasonably close to being the unit matrix.

We conclude then that the matrix $\mathcal{K}$ is, to a good approximation, the inverse of Q. It may seem unnecessary to define a new matrix at all, since we have derived Q in the first place, and we can always use the inverse matrix to represent the opposite transformation. The reason for introducing the matrix $\mathcal{K}$ is partly historical – later we shall discuss previous work on this subject by Fröman [5], who defined his matrix to transform from inside the barrier to outside. Secondly, most theoretical work on alpha decay has involved devising a particular model and making predictions to be compared with experiment. In this instance, it is the transformation from inside the barrier to outside that is important. It may also be obvious that we could have derived a matrix for this purpose by a different definition of the limits of integration in Equation (2.3.11). However, if we had chosen the limits the other way round, we would have ended up with L' and not L in the exponential of Equation (2.3.17), which we have already discussed. Later we shall confirm that this choice is valid by comparing results with those from the exact coupled channels equations where no choice is necessary.

To summarize the results of our WKB approximation then, we can say that the

relationship between radial wave functions near the classical turning points is given by

$$u_L(r_2) = \sum_{L'} \mathcal{K}_{LL'}\, u_{L'}(R_0). \tag{2.3.27}$$

Comparing this result with that for a spherical barrier (Equation (2.2.9)), we find that the barrier penetration can no longer be described by a simple exponential attenuation. The angular dependence of the nuclear radius causes the alpha particle to couple to the daughter nucleus during tunnelling. The matrix $\mathcal{K}$ is a semi-classical expression describing the mixing of angular momentum states inside and outside the barrier, similar to the matrix element $V_{LL'}$ in the coupled channels equations of Section 2.3.1. If the nucleus is spherical, $\mathcal{K}$ becomes a diagonal matrix with elements equal to the exponential factors defined in Section 2.2.

2.4 Potentials

So far we have written down expressions containing a potential $V(r, \theta)$. In this section we will discuss the possible forms of this potential, starting with the simplest model and extending to more realistic cases.

In a very simple model of alpha decay, we may assume that the alpha particle is held in the (spherical) nucleus by a radial square well potential of strength V_0. Once the alpha particle separates from the daughter, there is obviously a Coulomb potential V_C between the two charged objects,

$$V_C = \frac{Z_\alpha Z_d e^2}{r} \quad , \quad r \geq r_1 \tag{2.4.1}$$

as well as the centrifugal term V_L. This type of potential will be referred to as a "sharp cut-off" potential, and is shown schematically in Figure 2.5. A more realistic model might include a nuclear potential of Woods-Saxon form for example, giving the shape

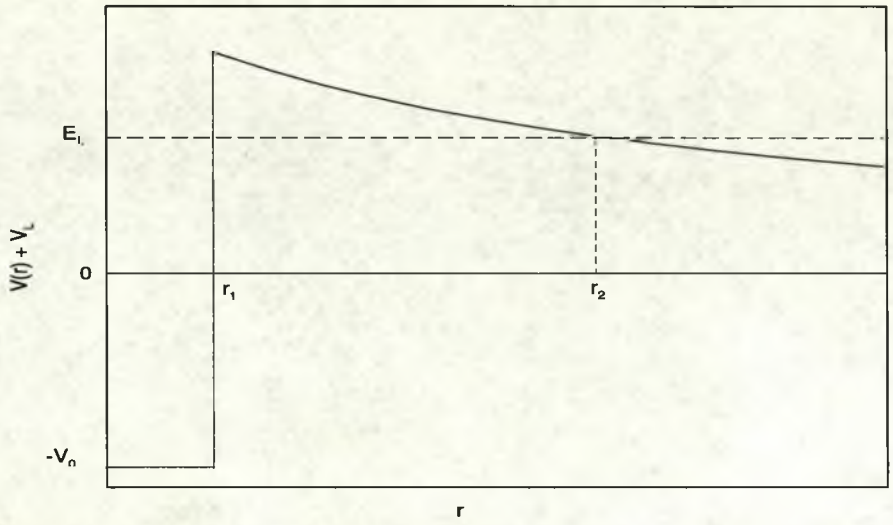

Figure 2.5: Schematic diagram showing the barrier resulting from a sharp cut-off potential.

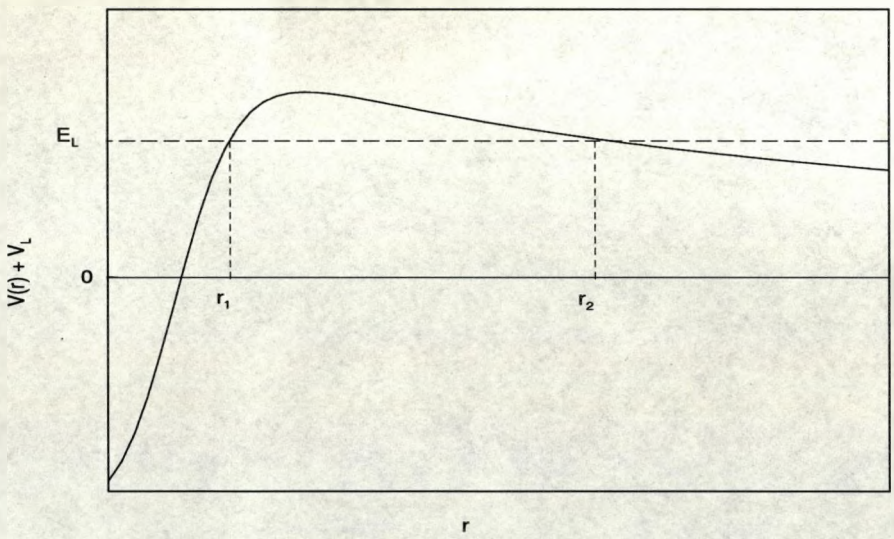

Figure 2.6: Diagram of the barrier resulting from a more realistic potential including a Woods-Saxon term.

shown in Figure 2.6. Note that in this case, the nuclear potential is not cut off at the inner turning point r_1. It is, however, a short range force relative to the Coulomb term and its effects are negligible for large r. Buck *et al.* [8] have used a potential of this type in their work, with a realistic nuclear term but no consideration of nuclear deformation.

The Coulomb potential given in Equation (2.4.1) represents the interaction between two spherically symmetric charged particles, taking no account of their charge distribution. We shall now derive a potential that is more relevant for the system of alpha particle plus deformed daughter nucleus.

The potential at a point $\mathbf{r}$ due to a charge distribution ρ contained in a volume V is given by

$$V_C(\mathbf{r}) = \frac{1}{4\pi\epsilon_0} \int_V \frac{\rho(s)}{|\mathbf{r}-\mathbf{s}|}\, \mathrm{d}^3 s \tag{2.4.2}$$

where $\mathbf{s}$ is a point within the distribution. If the distribution is considered to be uniform, then $\rho(s)$ is constant. The integrand may be expanded as a Taylor series in powers of $1/r$ and integrated term by term. It can be shown that for an axially symmetric charge distribution, the potential takes the form

$$V_C(\mathbf{r}) = \frac{V_1}{r} + \frac{V_3}{r^3}P_2(\theta) + \frac{V_5}{r^5}P_4(\theta) + \ldots \tag{2.4.3}$$

where the angle θ is that between $\mathbf{r}$ and the symmetry axis of the nucleus ([22], page 92). For the system of alpha particle plus deformed daughter nucleus, the first two terms of this potential are usually written in the form

$$V_C(\mathbf{r}) = \frac{Z_\alpha Z_d e^2}{r} + \frac{1}{2}\frac{2e^2 Q_0}{r^3}P_2(\theta) \tag{2.4.4}$$

where Q_0 is the intrinsic quadrupole moment. This is exactly the Coulomb potential used by Fröman [5]. We have derived exact expressions for the multipole moments V_3 and V_5 using the computer algebra package Maple, but we will not present them since they are very complicated. Values for a range of even–even nuclei are given in Appendix A.

We have checked that our expression for V_3 reduces to that given in Equation (2.4.4) if we consider only first order terms in β_2, although considering all orders of β_2 produces a difference of about 10% in its value.

Finally, we shall mention the form of the centrifugal potential. This term is not contained within $V(r,\theta)$, it arises from the kinetic energy term upon the transition from the full wave equation to the radial equation. However, we must modify its form if a WKB approximation is to be used for the wave function ([23], page 35). The appropriate expression to use in this case is the Langer modified form

$$V_L \sim \frac{(L+1/2)^2}{r^2}. \tag{2.4.5}$$

Although this amendment has little effect for large values of L, it is important when L is small.

Unless otherwise stated, all numerical calculations in this thesis are done with the following potentials

$$\begin{aligned}
V(r,\theta) &= V_N + V_C \\
V_N &= -\frac{V_0}{1+\exp\left((r-R(\theta))/d\right)} \quad \text{fm}^{-2} \\
V_C &= \frac{V_1}{r} + \frac{V_3}{r^3}P_2(\theta) + \frac{V_5}{r^5}P_4(\theta) \quad \text{fm}^{-2} \\
V_L &= \frac{(L+1/2)^2}{r^2} \quad \text{fm}^{-2} \\
R(\theta) &= R_0\left(1+\beta_2 Y_{20}(\theta)+\beta_4 Y_{40}(\theta)+\beta_6 Y_{60}(\theta)\right) \quad \text{fm} \\
R_0 &= 1.16\,(A_d{}^{1/3}) \quad \text{fm}
\end{aligned} \tag{2.4.6}$$

where A_d is the mass number of the daughter nucleus. The radius R_0 is consistent with that used in Ref. [19], from which we take all deformation parameters. The octupole

deformation parameter is not considered for any of the work in this thesis, even though $\beta_3 \neq 0$ for some nuclei. We calculate the Coulomb monopole moment V_1 in the same way as Equation (2.4.4). The Woods-Saxon potential is deformation dependent because of the radius $R(\theta)$, and we assume values of $V_0 = 100$ MeV ($= 18.8$ fm^{-2}) and $d = 0.5$ fm for all nuclei. The value of V_0 is important because as the orbital angular momentum increases, V_L becomes larger and the energy decreases – thus if the nuclear potential is not deep enough there will be no inner turning point for large L. This value of V_0 is large enough to enable calculations to be performed for values of $L \leq 18$. Our parameters are very similar to those used by Carjan *et al.* [24] who use $V_0 = 125$ MeV and $a = 0.57$ fm in their Woods-Saxon potential[1]. For a spherical barrier, we use $V_C = V_1/r$ and $R(\theta) = R_0$ in the nuclear potential.

2.5 Fröman's transmission matrix

In 1957, Fröman [5] derived an approximate expression for a semi-classical transmission matrix, using a WKB technique. His results have been used frequently in papers on alpha decay [13] – [16]. He used a deformed nuclear radius of the form

$$R(\theta) = R_0 (1 + \beta_2 Y_{20}(\theta)) \tag{2.5.1}$$

and considered terms only to first order in β_2. His potential is a sharp cut-off type as described in Section 2.4, although the cut-off radius is the angle dependent nuclear radius $R(\theta)$.

[1] We note that these Woods-Saxon parameters and the deformation parameters taken from Ref. [19] are related to nucleon potentials rather than the alpha–nucleus potential, i.e. we do not consider the effects of the charge distribution of the alpha particle. The importance of using more appropriate parameters in our calculations should be investigated.

Fröman's expression represents a different quantity to our matrix $\mathcal{K}$, hence the slightly different notation:

$$k_{LL'} = \int_0^{\pi} \Theta_{L0}(\theta)\ \exp\left(BP_2(\theta)\right)\ \Theta_{L'0}(\theta)\ \sin\theta\ \mathrm{d}\theta. \tag{2.5.2}$$

The term B in the exponent is given by

$$B = 2\eta\sqrt{\frac{5}{4\pi}}\,\beta_2\left(\frac{kR_0}{2\eta}\left(1-\frac{kR_0}{2\eta}\right)\right)^{1/2}\left(1-\frac{1}{5}q_0-\frac{2}{5}q_0\frac{kR_0}{2\eta}\right) \tag{2.5.3}$$

where η is the Sommerfeld parameter and k is related to the energy of the ground state i.e. excitation energies of the daughter states are not considered. In Section 2.8 we shall show that the excitation energies of the daughter states are in fact important and should be considered in the calculation of the transmission matrix. The dimensionless quantity q_0 depends on the charge distribution of the nucleus. Fröman assumes that the nucleus is ellipsoidal and has uniform charge density, thus $q_0 = 1$.

Equation (2.5.2) does not represent the complete barrier penetration process. We can think of this matrix as mapping the alpha particle wave function from a point on the deformed nuclear surface to a point on a sphere around the nucleus. To describe the complete process, these wave functions must then be multiplied by the usual spherical penetration term which takes account of the centrifugal barrier seen by the different partial waves. The full transmission matrix may therefore be written in the form

$$\mathcal{H}_{LL'} = \exp(-I_L)\ k_{LL'} \tag{2.5.4}$$

where the spherical barrier penetration factors I_L are defined in Section 2.2. In other words, Fröman separates the transmission of the deformed barrier into two parts; the matrix $k_{LL'}$ which accounts for all the coupling of angular momenta, and an $L-$dependent factor which contains the purely isotropic terms. In the case of a spherical nucleus, $k_{LL'}$ becomes the unit matrix and the transmission probability reduces to that given in

Section 2.2. For a comparison of our transmission matrix with that of Fröman, it is the full matrix $\mathcal{H}_{LL'}$ that should be considered. The notation is different to avoid confusion between the two.

We can see how this separation of terms comes about by considering our transmission matrix defined by Equation (2.3.21). The integral $I_L(\theta)$ may be expanded in powers of the Legendre polynomial $P_2(\theta)$,

$$I_L(\theta) = I_{L0} + I_{L2}P_2(\theta) + I_{L4}(P_2(\theta))^2 + \cdots \quad . \tag{2.5.5}$$

Let us define τ_L by

$$\tau_L = \exp\left(-I_L(\theta)\right) = \tau_{L0} \exp\left(-\left(I_L(\theta) - I_{L0}\right)\right) \tag{2.5.6}$$

where $\tau_{L0} = \exp(-I_{L0})$ is the purely spherical part, equivalent to the term $\exp(-I_L)$ in Equation (2.5.4). Now we can write the transmission matrix in the separated form

$$\mathcal{K}_{LL'} = \tau_{L0}\ K_{LL'} \tag{2.5.7}$$

where

$$K_{LL'} = \int_0^\pi \Theta_{L0}(\theta)\ \exp\left(-\left(I_L(\theta) - I_{L0}\right)\right)\ \Theta_{L'0}(\theta)\ \sin\theta\ \mathrm{d}\theta. \tag{2.5.8}$$

Fröman's matrix $k_{LL'}$ may be obtained from $K_{LL'}$ by making a first order approximation in $P_L(\theta)$ to the exponent. Thus his parameter B may be compared with the first order term in our expansion, I_{L2}, if we neglect its $L-$dependence. (In Fröman's work all the $L-$dependence is in the spherical part τ_{L0}.)

For example, using data for the ground state of the nucleus ^{238}U and assuming the same form of potential and nuclear radius as Fröman, we obtain

$$I_0(\theta) = 44.553 - 1.786P_2(\theta) - 0.031(P_2(\theta))^2 + \ldots \quad . \tag{2.5.9}$$

The value of $I_{02} = 1.786$ should be compared with $B = 1.760$, which was calculated from Equation (2.5.3). The discrepancy in these values arises from the slightly different value of V_3 to the quadrupole moment defined in Equation (2.4.4).

2.6 Comparison of Fröman and generalized results

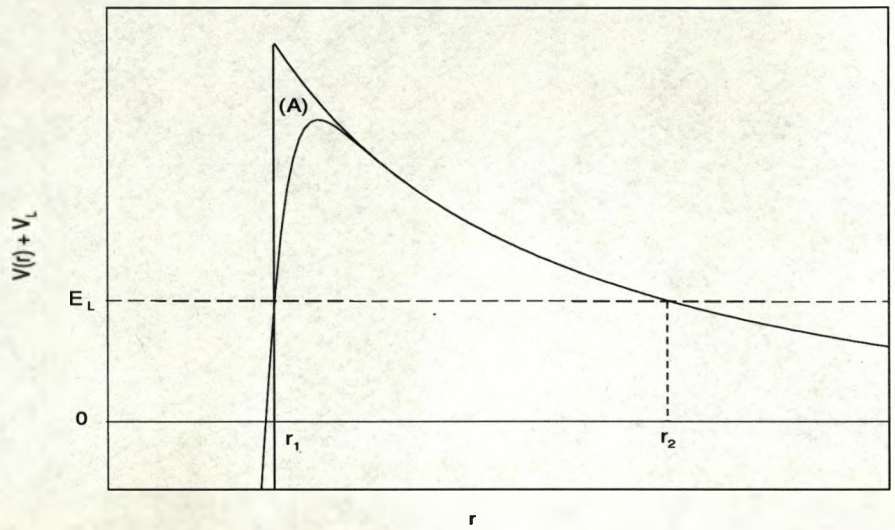

Figure 2.7: Comparison of Fröman's sharp cut-off potential and our realistic one, assuming the same inner turning point r_1 in each case.

In the previous section we showed how our semi-classical transmission matrix compares with that derived by Fröman. We shall now calculate matrices for an even–even nucleus using both methods and investigate the numerical differences. In order to make a comparison, we shall neglect the higher order deformation parameters in our calculation, and consider the nucleus to have a shape given by Equation (2.5.1), in line with Fröman. Now the main difference between the two methods lies in the shape of the potential. Fröman assumes that there is a sharp cut-off in the potential at the nuclear surface, defined by Equation (2.5.1). We include a Woods-Saxon potential which gives the inner turning point at $r_1(\theta)$ (which is a solution of $\kappa_L(r,\theta) = 0$). If we adjust Fröman's cut-off radius to be equal to $r_1(\theta)$, the difference in the barrier is just the region (A) in Figure 2.7

and a comparison of the two approaches is then straightforward. This is easily done by considering $r_1(\theta)$ at two angles and introducing new parameters $\bar{R}_0$ and $\bar{\beta}_2$ into Fröman's formula in place of R_0 and β_2 respectively.

We calculate all transmission matrices in this thesis using the angular integration technique of Kermode and Rowley [25]. Table 2.2 shows the matrices $\mathcal{K}$ and $\mathcal{H}$ for the nucleus ^{238}U. On the left hand side in each case we show the absolute matrix elements. There is a significant difference between the elements in these matrices, caused mainly by the inclusion of a realistic nuclear potential in our calculation. We have also made no approximation to the exponential term in the matrix, and our calculation takes into account the excitation energies of the daughter states. The elements in our matrix are approximately a factor of five larger than those in Fröman's matrix. This is consistent with the findings of Bencze and Sandalescu [26] who report that the WKB approximation with a sharp cut-off potential underestimates barrier penetrabilities by a factor of $2-5$. They reach their conclusions by comparison with results of coupled channels integration, which indicates that our modified WKB approach is a good approximation. On the right we show the same matrix but scaled such that the top left element is equal to one. We find that these scaled matrices are very similar in the two approaches which indicates that any normalized quantities, such as branching ratios, will be much the same in each case. However, the differences in the left hand matrices show us that our more accurate approach will be important in calculations involving absolute values, such as alpha decay widths or lifetimes.

We shall now investigate the effects of the two different matrices on calculated quantities in alpha decay. The quantity most directly dependent on barrier penetration probabilities is the alpha decay width (or lifetime). We shall therefore use widths to compare the effects of our various approximations and assumptions. (All the investigations in the next few sections have also been done for alpha decay branching ratios, since it is these

Table 2.2: Comparison of the transmission matrices $\mathcal{K}_{LL'}$ and $\mathcal{H}_{LL'}$ for ^{238}U, considering only states $L = 0, 2, 4$. The matrix on the left in each case shows the absolute matrix elements, on the right the matrix is scaled such that the top left element is equal to one.

(a) Our matrix $\mathcal{K}_{LL'}$

$$\begin{pmatrix} 0.1092E-17 & 0.9599E-18 & 0.3308E-18 \\ 0.5094E-18 & 0.1050E-17 & 0.5795E-18 \\ 0.4316E-19 & 0.1340E-18 & 0.2207E-18 \end{pmatrix} \quad \begin{pmatrix} 1.000 & 0.879 & 0.303 \\ 0.467 & 0.962 & 0.531 \\ 0.040 & 0.123 & 0.202 \end{pmatrix}$$

(b) Fröman's matrix $\mathcal{H}_{LL'}$

$$\begin{pmatrix} 0.1883E-18 & 0.1764E-18 & 0.6452E-19 \\ 0.9273E-19 & 0.1873E-18 & 0.1060E-18 \\ 0.7593E-20 & 0.2374E-19 & 0.3909E-19 \end{pmatrix} \quad \begin{pmatrix} 1.000 & 0.937 & 0.343 \\ 0.492 & 0.995 & 0.563 \\ 0.040 & 0.126 & 0.208 \end{pmatrix}$$

that will concern us most in Chapter 3 when we study even–even nuclei.)

Consider the wave functions for states of angular momentum L' to the left of the potential barrier at the point $r = R_0$. Let the relative amplitudes of the radial wave functions be represented by $a_{L'}$. The corresponding amplitudes c_L at the outer radius $r = r_2$ are given by

$$c_L = \sum_{L'} \mathcal{K}_{LL'}\, a_{L'}. \tag{2.6.1}$$

It is these amplitudes that determine the outgoing flux of alpha particles from the nucleus. Although the amplitudes will in general be complex, in the semi-classical approach we take them to be real. This greatly simplifies the calculation, and in Chapter 3 we shall

show using coupled channels equations that the amplitudes in the alpha decay problem are, to a good approximation, real. It would be possible, however, to consider complex amplitudes within the semi-classical formalism if necessary by writing them in the form $a_L \exp(i\phi_L)$. We shall refer to c_L and $a_{L'}$ as the external (or outer) and internal (or inner) amplitudes respectively.

The total decay width depends on the sum of the squares of the external amplitudes, so for any particular nucleus

$$\Gamma \propto \sum_L |c_L|^2. \tag{2.6.2}$$

The constants of proportionality depend on the velocity and energy of the alpha particle, but for the purpose of our comparisons we can neglect these factors and only consider the term in ${c_L}^2$. Therefore for our comparison we shall consider the term

$$g = \sum_L |c_L|^2. \tag{2.6.3}$$

Any difference in this quantity will reflect the difference in barrier penetrability, since we shall choose the internal amplitudes to be equal in each case.

In theoretical work on alpha decay, the amplitudes $a_{L'}$ may be obtained by various models, for example by assuming a quadrupole-quadrupole interaction between daughter nucleus and alpha particle. For the purpose of this and following sections, it is convenient to simply fix the amplitudes to represent a particular internal nuclear structure. For example, if we consider only angular momentum states with $L = 0$ inside the nucleus, then $a_0 = 1$ and $a_2 = a_4 = 0$. (For all our comparisons we will only report the results for angular momentum states up to $L = 4$, although we have considered the effects of higher states.) As the alpha particle penetrates the deformed barrier, mixing of the states takes place and the outer amplitudes corresponding to $L = 2$ and $L = 4$ will be non zero.

We use this simple case to investigate the accuracy of Fröman's calculation. Using ^{238}U as a model nucleus, we have calculated g for a range of values of β_2. Figure 2.8

shows the results using two approaches:

i) using Fröman's transmission matrix $\mathcal{H}_{LL'}$ which assumes a sharp cut-off potential and only first order terms in β_2,

ii) using our matrix $\mathcal{K}_{LL'}$ with a realistic potential and the full angular integral $I_L(\theta)$.

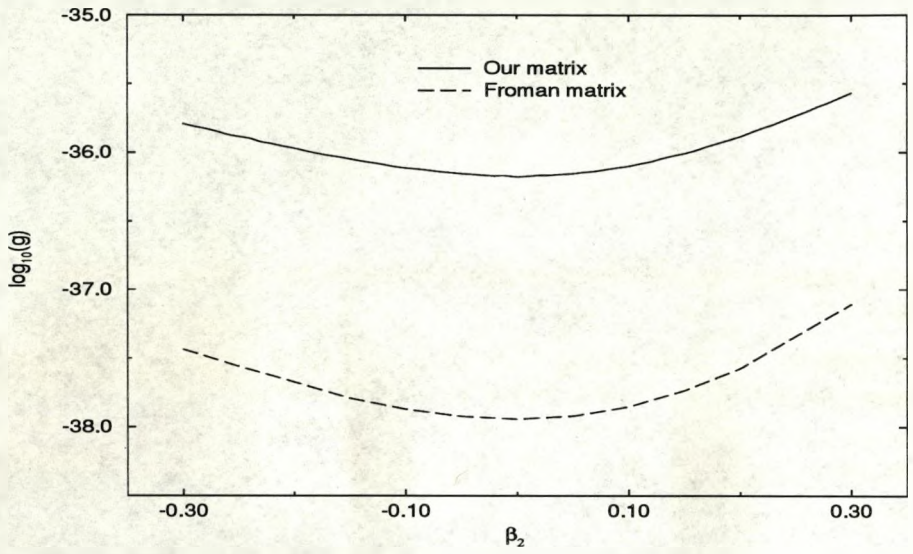

Figure 2.8: Comparison of widths as a function of β_2 using Fröman's and our transmission matrices for ^{238}U. We have assumed the internal amplitudes $a_0 = 1, a_2 = a_4 = 0$ and the potentials shown in Figure 2.7.

We can deduce two results from these curves. Firstly, there is a significant difference in the results obtained using the two methods. The widths calculated using our transmission matrix are over an order of magnitude larger for all deformations than those obtained using Fröman's matrix. This discrepancy is mainly due to the difference in shape of the two potentials shown in Figure 2.7. Since the barrier resulting from the sharp cut-off potential is larger than that due to the realistic potential, the alpha particle

is less likely to escape from the nucleus and thus the decay widths are smaller. This is consistent with the findings of Bencze and Sandalescu [26] who report that calculated decay widths are underestimated by a factor of $10 - 1000$ and this discrepancy is partly due to a WKB approximation in the calculation of barrier penetrabilities. There have been other reports of differences due to the shape of the nuclear potential. Scherk and Vogt [27] find that alpha decay widths are enhanced by using a realistic potential with a diffuse edge rather than assuming a square-edged nucleus. Rowley and Merchant [28] also find a similar enhancement of fusion cross-sections when using a realistic potential instead of a sharp cut-off potential.

Secondly, the calculated widths for our model nucleus obviously depend on the deformation parameter β_2. It has been claimed that the consideration of nuclear deformation during barrier transmission is not important [6, 10]. It is one of the main aims of this thesis to demonstrate the importance of considering the nuclear deformation in the barrier penetration process, and we shall return to this discussion in Chapter 3.

We also calculated branching ratios to the ground state of the daughter and found that there was no real difference in the results using Fröman's method or ours. As we have already discussed, branching ratios are less likely to reflect any differences because the amplitudes c_L are normalized, whereas in the calculation of decay widths it is the absolute values of c_L which are important.

2.7 Sensitivity to the form of the nuclear radius

We have written a general expression for the radius of an axially and reflection symmetric deformed nucleus as

$$R(\theta) = R_0 \left(1 + \beta_2 Y_{20}(\theta) + \beta_4 Y_{40}(\theta) + \beta_6 Y_{60}(\theta) + \ldots\right) \qquad (2.7.1)$$

where R_0 is related to the radius of the equivalent spherical nucleus. For a deformed nucleus, R_0 must be deformation dependent in order to conserve the nuclear volume. This is easily done by defining a modified radius $\bar{R}_0$ and equating the resulting nuclear volume with that obtained in the spherical case. We have found that this correction makes very little difference to calculated widths or branching ratios, but should be included to be strictly correct.

Let us now examine the importance of the higher order deformation parameters β_4 and β_6 in our calculations. We again take ^{238}U as a model nucleus, using all data and parameters from Appendix A unless otherwise stated. We have calculated widths with β_2 only and then included typical values of these parameters, say $\beta_4 = 0.1$ and $\beta_6 = -0.02$. Figure 2.9 shows that the inclusion of β_4 is quite important, but the β_6 term has only a small effect.

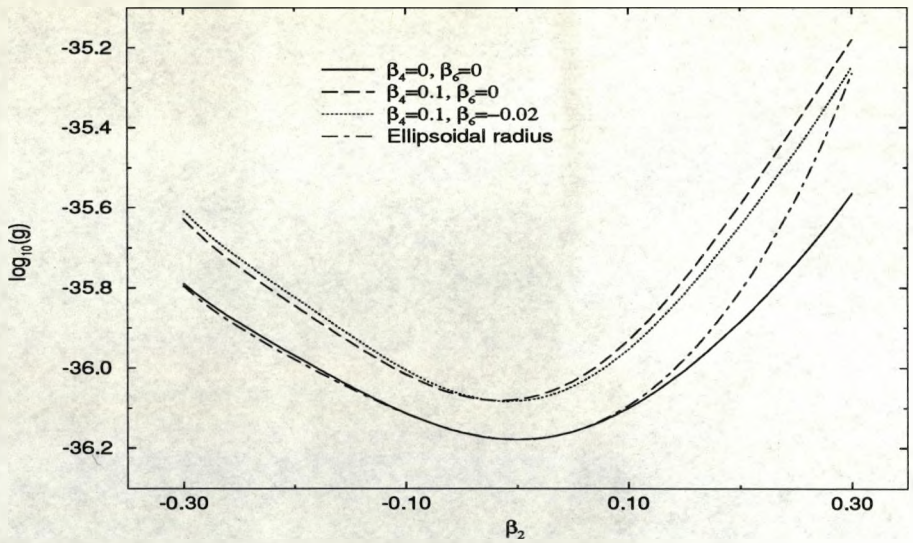

Figure 2.9: Sensitivity of widths to the form of the nuclear radius $R(\theta)$.

It is interesting to look at the shape defined by Equation (2.7.1) as β_2 increases. For

a value of $\beta_2 \approx 0.2$ the shape is ellipsoidal as would be expected. If $\beta_2 > 0.4$ the nucleus defined by Equation (2.7.1) develops a "waist", and for very large β_2 this "peanut" shape is very pronounced.

A nuclear radius that is strictly ellipsoidal may be derived from the equation of an ellipsoid in polar co-ordinates

$$R(\theta) = \frac{R_0}{(1 - 2\beta_2 Y_{20}(\theta))^{1/2}} \tag{2.7.2}$$

where R_0 and β_2 can be expressed as functions of the semi-major and semi-minor axes of the ellipse. Notice that a first order expansion of Equation (2.7.2) in powers of Y_{20} gives exactly the same result as Equation (2.7.1), neglecting higher order deformations. However, if we consider higher order terms in the expansion of Equation (2.7.2), the comparison between the two radii $R(\theta)$ becomes more difficult. For example, if the expansion is made to second order in Y_{20}, we can rewrite the result in terms of Y_{20} and Y_{40},

$$R(\theta) = R_0 \left(1 + \frac{3}{8\pi}\beta_2^2 + \left(\beta_2 + \frac{3}{7}\sqrt{\frac{5}{4\pi}}\beta_2^2\right) Y_{20} + \left(\frac{9}{7}\frac{1}{\sqrt{4\pi}}\beta_2^2\right) Y_{40}\right). \tag{2.7.3}$$

This definition of the nuclear radius therefore results in "effective" values of β_2 and β_4. The more terms included in the expansion, the more these effective terms will differ from the values in Equation (2.7.1).

Figure 2.9 shows widths calculated using the exact ellipsoidal radius in Equation (2.7.2). The results for $\beta_2 < 0$ are only slightly different to those obtained with the conventional radius, with $\beta_4 = \beta_6 = 0$. The asymmetry of the curve with respect to β_2 may be understood by considering the effective quadrupole deformation $\bar{\beta}_2$ in Equation (2.7.3),

$$\bar{\beta}_2 = \beta_2 + \frac{3}{7}\sqrt{\frac{5}{4\pi}}\beta_2^2. \tag{2.7.4}$$

For negative values of β_2, $|\bar{\beta}_2|$ is less than $|\beta_2|$, whereas for positive β_2 its magnitude is

larger. We conclude, therefore, that there is little difference between the two representations. In all our calculations we shall use the radius defined by Equation (2.7.1), since this is the most widely adopted form and the deformation parameters of Ref. [19] are defined in this way.

2.8 Sensitivity to other parameters

We shall end this chapter by investigating the sensitivity of alpha decay widths to the remaining parameters in our model. In each case we use ^{238}U as a model nucleus, using data and parameters from Appendix A unless otherwise stated. We note that the scales of each figure are different in order to highlight the changes resulting from each parameter variation.

In Section 2.5 we remarked that Fröman did not consider the excitation energies of rotational daughter states in his work. We shall see if this is a good approximation. If the angular momentum states of the daughter form a rotational band their excitation energies may be written in the form

$$\epsilon_L^* = fL(L+1) \quad \text{MeV} \tag{2.8.1}$$

(ϵ_L^* is the difference between the energy of the excited daughter state E_L and that of the ground state E_0). The value of f is related to the quadrupole deformation β_2 and so is fixed for a particular nucleus, but varying f for a model nucleus allows us to investigate the sensitivity of our results to differences in excitation energy. We calculated values of g for the nucleus ^{238}U for a range of realistic values of f, and for three different values of β_2, with the other deformation parameters set to zero (Figure 2.10). We found that the consideration of excitation energy is more important as β_2 increases. This is because the coupling of angular momentum states is more likely for larger values of β_2, and so changes in the energy of excited states have more effect on the widths. We conclude

therefore that the consideration of excitation energies, although a small effect, does make some difference to our calculations. Since experimental data is available for most of the nuclei we shall study, we include these energies in all our work.

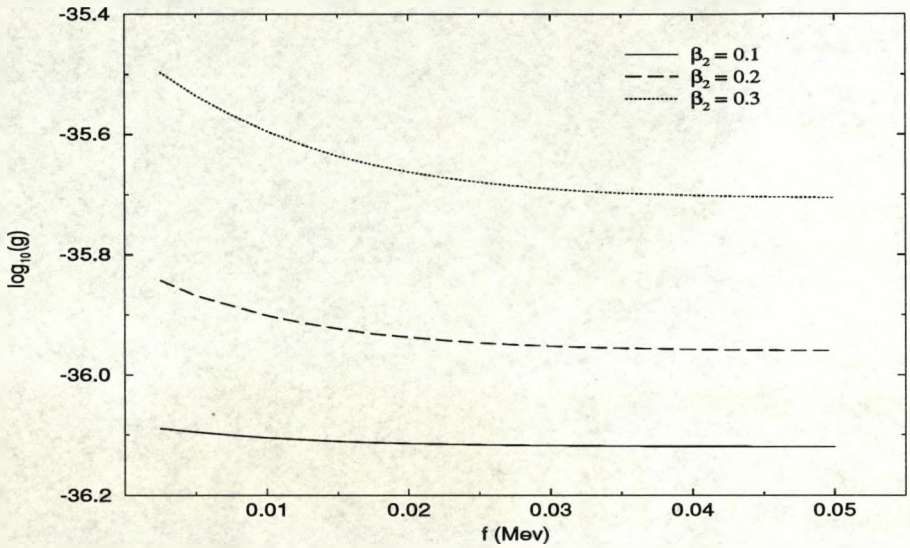

Figure 2.10: Sensitivity of widths to the inclusion of excitation energies $\epsilon_L^* = fL(L+1)$ of the daughter states for three values of β_2.

Next we investigate the importance of the higher order Coulomb terms derived in Section 2.4. It can be seen from Figure 2.11 that the term V_3/r^3 makes a significant difference to the widths for deformed nuclei. The effects of the next term V_5/r^5, however, are found to be very small, so we neglect all terms higher than V_5 in subsequent work.

To complete our investigations we have looked at the effects of varying the Woods-Saxon parameters V_0 and d. For the calculations in this thesis we have chosen a potential depth of 100 MeV and a diffuseness of 0.5 fm (see Section 2.4). Figure 2.12 shows the value of g as a function of the depth V_0, and for three different values of diffuseness. We find that the decay widths are sensitive to large changes in these parameters. We

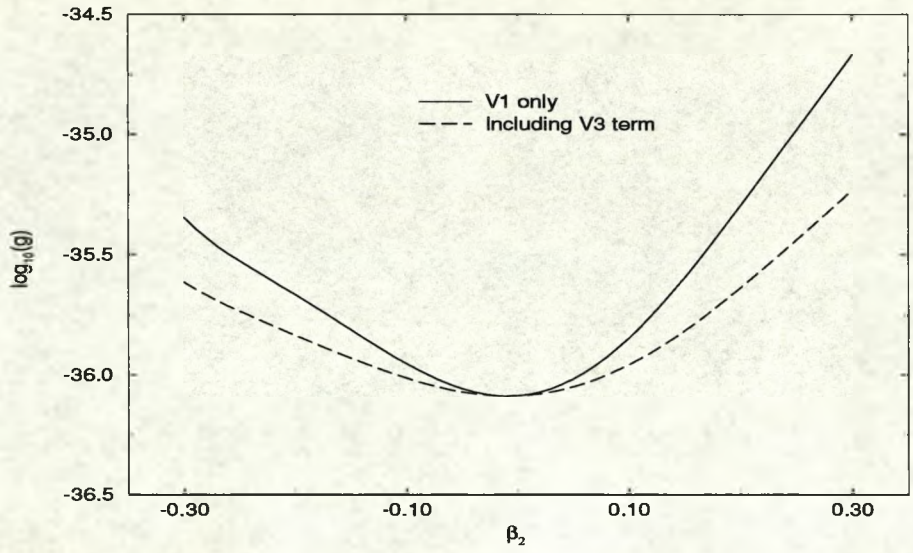

Figure 2.11: Sensitivity of widths to the inclusion of higher order Coulomb terms for a range of β_2.

note however, that for all of the parameters discussed in this section, the alpha decay branching ratios are insensitive to even large variations. It is only in the consideration of absolute lifetime values in Section 3.5 that the exact values of the parameters will be important for even–even nuclei.

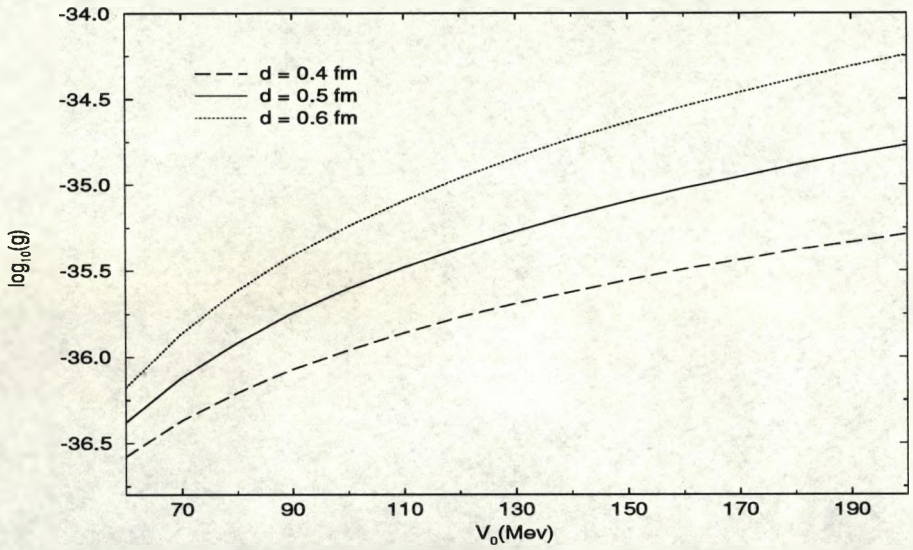

Figure 2.12: Sensitivity of widths to parameters V_0 and d in the Woods-Saxon potential.

Chapter 3

Even–even nuclei

In this chapter we shall study the alpha decay of even–even nuclei, in particular the branching ratios to different states of the daughter nucleus. All even–even nuclei exhibit the same level structure, as shown in Figure 3.1. Since the spin of the parent is always zero, the alpha particle in its final state must carry an orbital angular momentum equal to the spin of the daughter state to which it decays i.e. $L = J_d$.

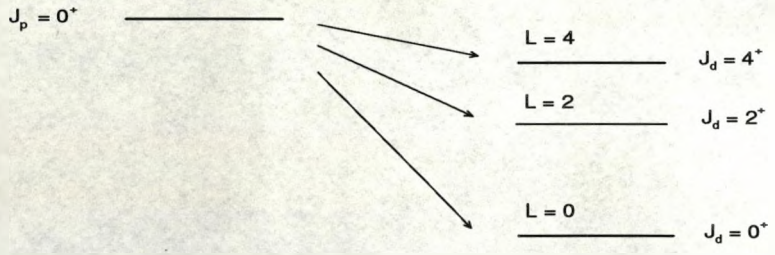

Figure 3.1: Alpha decay of even–even nuclei.

In the previous chapter we defined a transmission matrix $\mathcal{K}$ which relates amplitudes just inside and just outside the deformed barrier. So far we have concentrated mainly on the barrier penetration problem and have not considered how to obtain the internal amplitudes. In this chapter we will investigate some possible models for the alpha particle formation process and compare our results with experimental data.

3.1 Alpha decay branching ratios

In Section 2.6, we derived an expression for the amplitudes of the radial wave function outside the potential barrier

$$c_L = \sum_{L'} \mathcal{K}_{LL'}\, a_{L'}. \tag{3.1.1}$$

The branching ratios tell us the percentage of alpha particles decaying to each state of the daughter, and must therefore be related to the probability of finding an alpha particle outside the barrier. We define the branching ratios by

$$Z_L = \frac{|c_L|^2}{\sum_L |c_L|^2} \times 100\%. \tag{3.1.2}$$

Throughout this chapter, we will be looking at even–even actinide nuclei in the mass range $A_d = 220 - 250$ and $Z_d = 88 - 96$. There are several reasons for this choice of nuclei. Firstly, experimental branching ratios and alpha particle energies are available for angular momentum states up to $L = 4$. Secondly, they have considerable deformations ranging from $\beta_2 = 0.1$ to 0.24 [19] and so offer a good opportunity to investigate the importance of including the barrier deformation. Most of the nuclei have daughter state energies that may be described as rotational, i.e. $\epsilon^*(4^+)/\epsilon^*(2^+) \approx 3.33$, as shown in Figure 3.2.

First, let us consider some simple models for the internal structure of these nuclei. For example, it is possible that only alpha particles with $L = 0$ are formed inside the

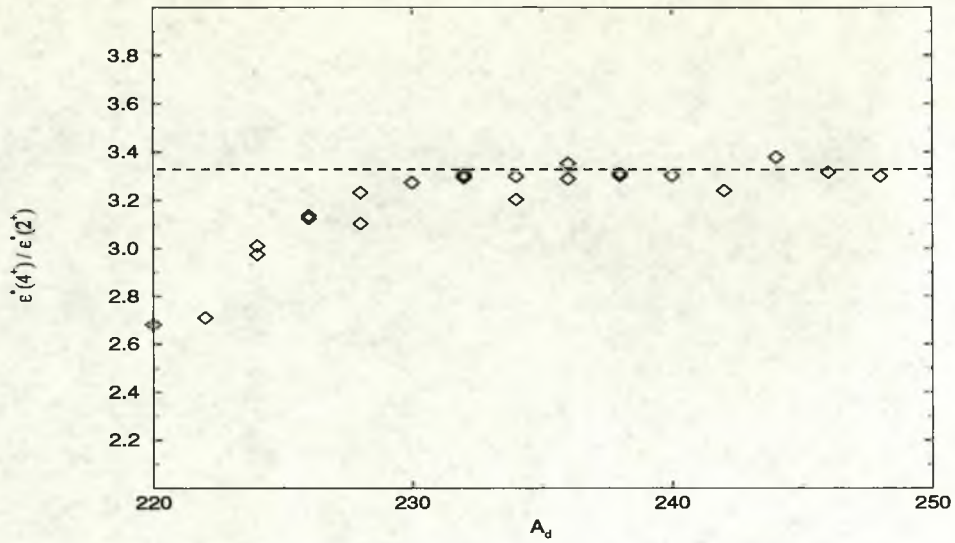

Figure 3.2: Values of $\epsilon^*(4^+)/\epsilon^*(2^+)$ for a range of even–even actinide nuclei. Nuclei with $A_d \geq 230$ have values ≈ 3.33 as expected for a rotational band.

nucleus and it is the mixing of angular momentum states through the deformed barrier that causes alpha particles with $L \geq 2$ to be detected. This situation is represented by the relative amplitudes $a_0 = 1$, $a_2 = a_4 = 0$. It is perhaps more likely that there will be some alpha particles formed with $L \neq 0$, e.g. $a_0 = a_2 = 1$, $a_4 = 0$. Figure 3.3 shows calculated $L = 0$ branching ratios for the range of nuclei, with three different sets of the amplitudes $a_{L'}$. (When comparing our theoretical results with experimentally measured branching ratios, we shall put the greatest importance on agreement in the $L = 0$ state. In most of these nuclei almost all of the intensity goes to the $L = 0$ and $L = 2$ states of the daughter anyway.) We find that the experimental trends are not reproduced by any of these sets of amplitudes. In the following sections we investigate some more complicated models of alpha decay.

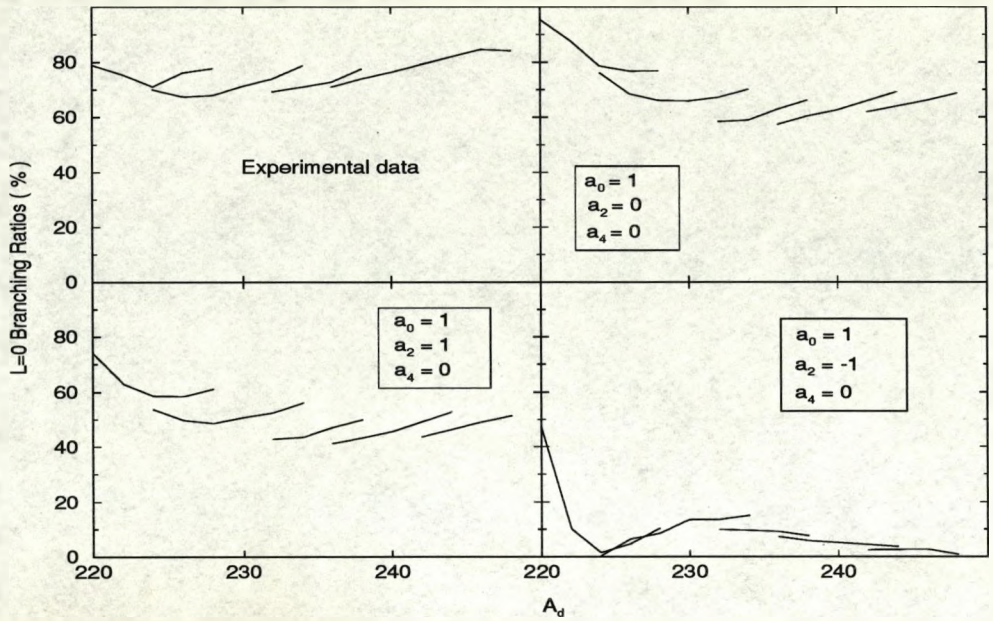

Figure 3.3: Calculated $L = 0$ branching ratios for different sets of the internal amplitudes $a_{L'}$. The experimental trends are not reproduced by any of these sets.

3.2 Quadrupole-quadrupole interaction

Consider the alpha decay of an even–even parent nucleus with angular momentum and projection $J_p = M_p = 0$. The spin of the daughter nucleus J_d must equal the orbital angular momentum L of the alpha particle. However, throughout most of this section we retain the label J_d to make it clear where the various terms are derived from.

We can write a vector to represent this state in terms of the alpha particle and daughter nucleus

$$|J_p M_p\rangle = \sum_{L'} \chi_{L'} \mid (J'_d L')\ J_p M_p\rangle. \tag{3.2.1}$$

This state vector must satisfy the Schrödinger equation

$$H\ |J_p M_p\rangle = E\ |J_p M_p\rangle \tag{3.2.2}$$

where E is the total energy of the parent which remains constant. As discussed in Section 2.1, the Hamiltonian may be divided into two parts, one representing the relative alpha-daughter interaction and the other corresponding to the internal states of the alpha and daughter. The internal energy of the alpha particle does not change, so we do not consider it here.

Our aim is to obtain the coefficients $\chi_{L'}$. In simpler notation, Equation (3.2.2) may be written as

$$H \sum_{L'} \chi_{L'}\ |L'\rangle = E \sum_{L'} \chi_{L'}\ |L'\rangle. \tag{3.2.3}$$

Taking the scalar product with another state vector $|L\rangle$ gives the eigenvalue equation for the system

$$\sum_{L'} (H_{LL'} - E\ \delta_{LL'})\ \chi_{L'} = 0. \tag{3.2.4}$$

So to find the coefficients we diagonalize the matrix $H_{LL'}$ to obtain eigenvalues and eigenvectors. Of course there are L sets of these eigenvectors corresponding to different energy states of the system, so we have a choice in the set of coefficients $\chi_{L'}$.

Now let us discuss the actual form of the Hamiltonian. The interaction between alpha particle and daughter nucleus may be described by a quadrupole-quadrupole term [11, 29]. This is an approximation to the exact interaction which may be written as a series of "multipole-multipole terms". In the notation of Rowley *et al.* [29], the quadrupole interaction may be written

$$\mathcal{V}_2 = Y_2(\hat{\mathbf{r}}_\alpha) \cdot \sum_i V_2(r_\alpha, r_i)\ Y_2(\hat{\mathbf{r}}_i) \tag{3.2.5}$$

where the sum over i runs over all daughter nucleons. We need to calculate the reduced matrix elements of this quadrupole interaction in the basis of Equation (3.2.1)

$$(\mathcal{V}_2)_{LL'} \equiv \mathcal{V}_{LL'} = \langle\ (J_d L) J_p \ ||\ \mathcal{V}_2\ ||\ (J'_d L') J_p\ \rangle. \tag{3.2.6}$$

Using formulae for the reduced matrix elements of tensor operators ([30], page 81), we obtain

$$\mathcal{V}_{LL'} = v_{LL'}\ G_{LL'} \tag{3.2.7}$$

with the geometrical factors

$$G_{LL'} = \hat{L}\ W(J_d J'_d L L'; 2 J_p)\ \langle L || Y_2 || L' \rangle \tag{3.2.8}$$

and the dynamical factors

$$v_{LL'} = \hat{J}_d \int \Phi_L(r_\alpha)\ V_{\text{eff}}(r_\alpha)\ \Phi_{L'}(r_\alpha)\ r_\alpha^2\ \mathrm{d}r_\alpha \tag{3.2.9}$$

where

$$V_{\text{eff}}(r_\alpha) = \sum_i \langle\ \psi_d\ ||\ V_2((r_\alpha, r_i)\ Y_2(\hat{\mathbf{r}}_i)\ ||\ \psi'_d\ \rangle. \tag{3.2.10}$$

The dynamical factors contain unknown quantities such as the radial wave function of the daughter (ψ_d) and the radial wave function of the alpha particle relative to the daughter (Φ_L). Note that the geometrical part $G_{LL'}$ is symmetric with respect to L and L'.

The second part of the Hamiltonian arises from the internal energy of the daughter nucleus, which changes due to its rotational motion. The excitation energies of these rotational states can be written in the form

$$\epsilon^*_L = f L(L+1) \tag{3.2.11}$$

where f is a parameter, as introduced in Section 2.8. So to obtain the coefficients $\chi_{L'}$ we must diagonalize the Hamiltonian matrix

$$H_{LL'} = \mathcal{V}_{LL'} + \epsilon^*_{L'} \delta_{LL'}. \tag{3.2.12}$$

We define this expression to be dimensionless in a similar way to Ref. [29]. Since the values of the coefficients are not affected by a constant factor in $H_{LL'}$ we can divide through by a term with the appropriate dimensions.

Finally, we shall replace the label J_d by L for the even–even nucleus and simplify the dynamical factors to give an interaction of the form

$$\mathcal{V}_{LL'} = -\beta_2 \, \hat{L}^2 \, W(LL'LL';20) \, \langle L||Y_2||L'\rangle^2. \tag{3.2.13}$$

We have assumed that the radial integrals in the dynamical factors are constant for each angular momentum state, and so they will not affect our calculations. We have also assumed that the potential V_{eff} is proportional to the quadrupole deformation of the daughter nucleus as a whole. The negative sign occurs because we will be considering prolate nuclei (for which β_2 is positive) and the overall sign of the quadrupole term must be negative.

This quadrupole interaction may be extended to include higher multipole components of the same form,

$$\mathcal{V} = \mathcal{V}_2 + \mathcal{V}_4 + \mathcal{V}_6 \tag{3.2.14}$$

where the dynamical factors for $\mathcal{V}_i$ are proportional to β_i. We find that the inclusion of the term in β_4 has quite a significant effect on calculated branching ratios, as in Section 2.7, but that the next term in the expression has a negligible effect.

We can now use this model to calculate the coefficients $\chi_{L'}$ for our even–even nuclei. The semi-classical transmission matrix in Equation (3.1.1) can then be used to calculate branching ratios Z_L. We must first consider the variables in this work. The parameter f in the energy term may be constant for all the nuclei considered or varied from nucleus to nucleus. There are also a number of different solutions for the coefficients $\chi_{L'}$, corresponding to different eigenvectors of the matrix in Equation (3.2.12). As we are considering angular momentum states $L = 0, 2, 4$ there will be three different solutions.

Solution 1 corresponds to the eigenvector with the lowest eigenvalue, i.e. the lowest energy state.

Figure 3.4 shows $L = 0$ branching ratios for even–even nuclei with the value of f fixed at 0.015. A comparison of these curves with the experimental ones shows that none of the solutions are in agreement with empirical data. Changing the value of f within the range $0 < f < 0.02$ does not affect the trends for any of the solutions, it merely shifts the values slightly.

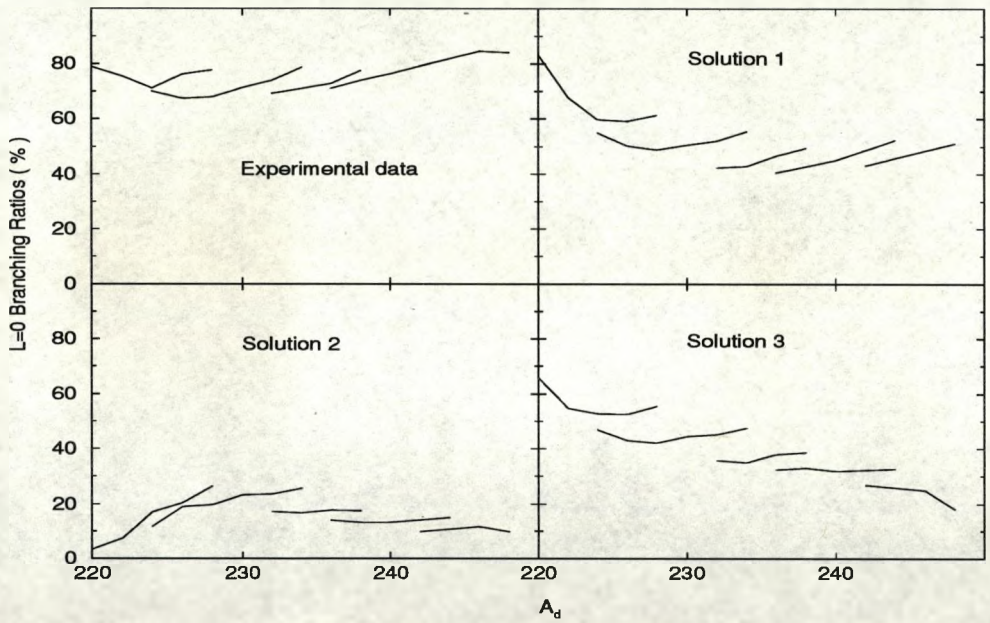

Figure 3.4: Calculated L=0 branching ratios using a quadrupole interaction for a range of even–even nuclei. The three solutions correspond to different energy states of the parent nucleus.

The only option not considered so far is to vary the value of f from nucleus to nucleus. We find that the variations required to fit the experimental branching ratios are very unpredictable; there is no smooth dependence on this parameter from nucleus to nucleus.

We therefore conclude that this model is not a good description of the physical process of alpha decay in this region of even–even nuclei.

Similar calculations using a quadrupole-quadrupole interaction have been done by Berggren and Olanders [11], although they assume a spherical barrier in their work. They also found that it was necessary to vary the solution number and other parameters in order to fit the experimental data. The reasons for having to take a higher energy solution are not clear; it is suggested that the solution which fits the empirical data must correspond to the ground state of the parent nucleus, with all lower energy states being forbidden due to Pauli blocking i.e. the nucleons in the alpha particle may not occupy the same states as those remaining in the daughter nucleus.

3.3 Eigenchannel formalism

There has been much recent work on the penetration of deformed Coulomb barriers in the opposite direction i.e. in the fusion of heavy nuclei [31]. Here it is evident that there exists a distribution of fusion barriers and that at sub-barrier energies, the lowest barrier yields the largest contribution to the fusion cross-section. In this section we investigate the possibility that such a "filter" mechanism may play a role in the alpha decay process.

There are, however, some obvious differences between these two problems. Firstly, for fusion we know precisely the form of the incident wave since this corresponds to the asymptotic wave function. In the alpha decay problem the incident wave is inside the potential barrier and is not known. Secondly, fusion is measured at energies above, or close to the top of, the Coulomb barrier. Here the small differences in the centrifugal barriers and the small energy losses due to target excitation are essentially negligible. This allows the use of the isocentrifugal and adiabatic approximations [32], in which the presence of eigenchannels with different barrier heights and weights can be proved ana-

lytically. For the alpha decay problem the isocentrifugal approximation is inapplicable, and at the energies where alpha decay takes place even the small ϵ_L^* are not negligible due to the large width of the potential barrier. We shall, therefore, first address the problem of how to define eigenchannels in such a situation.

In this section we shall perform calculations using the numerical integration of coupled channels equations, as introduced in Section 2.3.1. The asymptotic wave function in the intrinsic frame of the daughter nucleus must contain only outgoing waves, and may therefore be written in the form

$$\begin{aligned} \psi^{outside} &= \sum_L C_L \, \mathcal{O}_L^{outside}(k_L, \mathbf{r}) \\ &= \sum_L C_L \, \left(G_L(k_L, r) + iF_L(k_L, r)\right) \, \Theta_{L0}(\theta) \, \chi_{L0}, \end{aligned} \tag{3.3.1}$$

where F_L and G_L are the regular and irregular Coulomb wave functions. The $\mathcal{O}_L^{outside}$ represent outgoing alpha particles with orbital angular momentum L coupled to total angular momentum zero with a state χ_{L0} of the daughter. The wavenumbers k_L are related to the energies of the different rotational states. Using such an outgoing wave, we perform coupled channels calculations to obtain the wave function on the other side of the barrier. This must have both incoming and outgoing components

$$\psi^{inside} = \sum_L \left(A_L \, \mathcal{O}_L^{inside}(k_L, \mathbf{r}) + B_L \, \mathcal{I}_L^{inside}(k_L, \mathbf{r})\right). \tag{3.3.2}$$

The corresponding currents are shown schematically in Figure 3.5. Note that we use capital letters for amplitudes in the coupled channels formalism and lower case for the equivalent semi-classical ones.

The above problem is solved numerically to obtain the outside coefficients C_L in terms of those inside, $A_{L'}$. One may thus define a transformation matrix M, where

$$C_L = \sum_{L'} M_{LL'} \, A_{L'}. \tag{3.3.3}$$

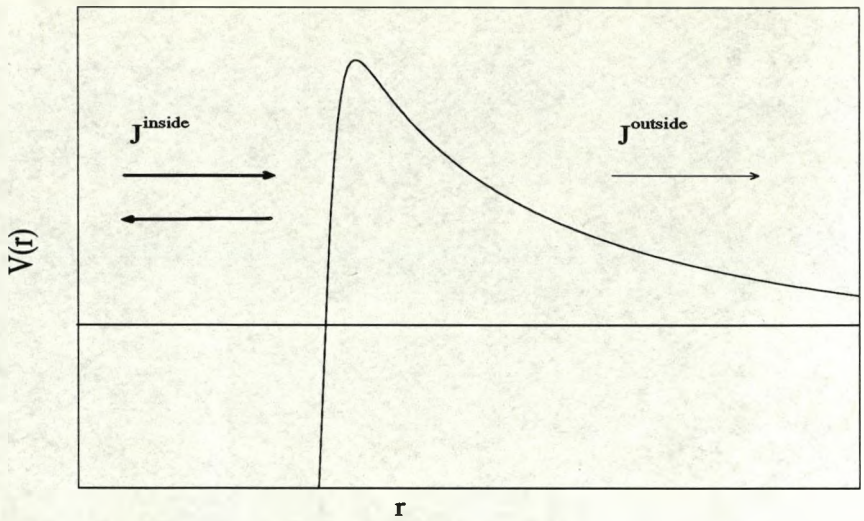

Figure 3.5: Schematic diagram of the potential V and the incoming and outgoing currents J on either side of the barrier.

This is analogous to Equation (3.1.1) in the semi-classical approximation.

Of course there is no reason for M to be hermitian and indeed it is not. We cannot, therefore, diagonalize the above equation to obtain eigenchannels. However, the physical quantities of interest are not so much the outgoing amplitudes as the outgoing fluxes, or currents, for each L. Neglecting the small differences in k_L, these currents are simply proportional to $|C_L|^2$ and from Equation (3.3.3) we obtain a total current

$$\begin{aligned} J \propto \sum_L C_L^\dagger C_L &= \sum_{LL'L''} A_{L''}^\dagger M_{L''L}^\dagger M_{LL'} A_{L'} \\ &\equiv \sum_{L'L''} A_{L''}^\dagger T_{L''L'} A_{L'} \\ &= \sum_\alpha \tilde{A}_\alpha^\dagger \Lambda_\alpha \tilde{A}_\alpha, \end{aligned} \tag{3.3.4}$$

where we have used the fact that the matrix T is hermitian to define the diagonal matrix

element $\Lambda_\alpha = \sum_{L'L''} U^\dagger_{\alpha L''} T_{L''L'} U_{L'\alpha}$. The amplitudes in the physical channels are related to those in the eigenchannels by $A_{L'} = \sum_\alpha U_{L'\alpha} \tilde{A}_\alpha$. We label the eigenchannels $\alpha = 1, 2, 3$ in order of decreasing Λ for our system with three partial waves $L = 0, 2, 4$.

We now consider the possibility that the physical channel corresponds to that with the maximum outgoing flux. This is equivalent to the idea that more alpha particles must be emitted from the poles of a prolate nucleus because here the barrier is lower and thinner. In order to maximize the outgoing flux, we need to maximize the expression

$$\sum_\alpha \tilde{A}^\dagger_\alpha \Lambda_\alpha \tilde{A}_\alpha = \tilde{A}^2_1 \Lambda_1 + \tilde{A}^2_2 \Lambda_2 + \tilde{A}^2_3 \Lambda_3 \tag{3.3.5}$$

subject to the constraint

$$\tilde{A}^2_1 + \tilde{A}^2_2 + \tilde{A}^2_3 = 1 \tag{3.3.6}$$

which arises because the eigenvectors are normalized. This requires the internal coefficients $A_{L'}$ to be the eigenvector of T corresponding to the largest eigenvalue Λ_1 i.e. $\tilde{A}^\dagger_\alpha = \tilde{A}^\dagger_1 \equiv (1\,0\,0)$.

For the maximum-flux channel, the amplitudes in the different physical channels may be obtained from Equation (3.3.3) i.e.

$$C_L = \sum_{L'} M_{LL'} U_{L'1} \tag{3.3.7}$$

and the corresponding branching ratios evaluated. We have performed such calculations for ^{238}U over a range of quadrupole deformations β_2, with $\beta_4 = \beta_6 = 0$. The radial functions $\mathcal{O}^{outside}_L$ are integrated to well inside the barrier where the nuclear potential is almost flat. In order to separate the wave function into incoming and outgoing parts, the numerical values are used to identify equivalent Riccati-Hankel functions from which we obtain unique sets of coefficients $\{A_L\}$ and $\{B_L\}$. This calculation is performed three times with different boundary conditions, i.e. with $\{C_0\ C_2\ C_4\} = \{1\ 0\ 0\}, \{0\ 1\ 0\}$ and $\{0\ 0\ 1\}$, to evaluate the transmission matrix elements $M_{LL'}$.

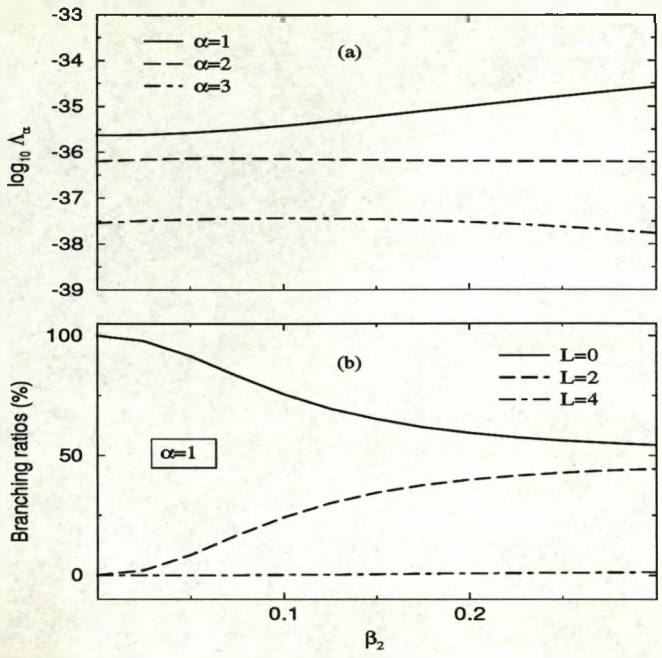

Figure 3.6: Eigenchannel calculations using coupled channels technique: (a) Eigenvalues Λ_α as a function of β_2 for a model ^{238}U nucleus. (b) Branching ratios corresponding to the maximum-flux channel. The experimental branching ratios for $L = 0, 2, 4$ are indicated by crosses at $\beta_2 = 0.215$.

Figure 3.6 shows the calculated eigenvalues Λ_α and branching ratios for eigenchannel 1 as a function of β_2. The experimental branching ratios for ^{238}U, for which $\beta_2 = 0.215$ [19], are indicated by crosses. At this value of β_2, we see that the eigenvalue for eigenchannel 1 is at least one order of magnitude larger than the others, and so one would expect to obtain reasonable results by considering only this channel. This is not the case, however: the branching ratios are not reproduced by the assumption that the physical channel is the one with maximum outgoing flux. The admixture of angular momentum states predicted by eigenchannel 1 is clearly not the one present in the nuclear ground state, suggesting a strong dependence on structure effects. This conclusion is not affected by the inclusion of the hexadecapole deformation $\beta_4 = 0.093$ [19], for which the

eigenchannel 1 branching ratios are 46.2%, 50.3% and 3.5% for $L = 0, 2$ and 4.

We believe therefore that for these actinide nuclei, effects such as strong pairing correlations in the nuclear ground state must force the alpha particle to exist in a configuration which cannot make use of the low potential barrier at the poles of the nucleus. The same will not necessarily be the case for all other nuclei. For example, the nuclei produced in fusion-evaporation reactions will be strongly deformed and highly excited. Then, the statistical distribution of the alpha particle wave function will almost certainly lead to configurations which can readily tunnel in the expected manner.

Let us now take this opportunity to test the accuracy of the semi-classical transmission matrix derived in Section 2.3.2. First, we compare the matrices M and $\mathcal{K}$ calculated in the coupled channels and semi-classical formalisms respectively. Since the coupled channels matrix M is complex, we calculate the modulus of each element M_{ij} for our comparison. The two matrices are shown in Table 3.1, scaled so that the top left element is equal to one. We find that the matrix elements in the semi-classical case are generally smaller than those in the coupled channels matrix, which could be related to the imaginary parts present in the complex coupled channels approach. However, it is more important to see the effects of each matrix in the prediction of alpha decay quantities.

We have therefore performed the same calculations as before using the semi-classical technique. First, we diagonalize the matrix

$$T_{L''L'} = \sum_{L} \mathcal{K}^{\dagger}_{L''L}\, \mathcal{K}_{LL'} \tag{3.3.8}$$

to obtain eigenvalues and eigenvectors. The maximum flux amplitudes are then equal to the eigenvector corresponding to the largest eigenvalue, and branching ratios are calculated using

$$c_L = \sum_{L'} \mathcal{K}_{LL'}\, U_{L'1}. \tag{3.3.9}$$

Table 3.1: Comparison of transmission matrices for ^{238}U, scaled such that the top left element is equal to one.

(a) Coupled channels matrix $M_{LL'}$

$$\begin{pmatrix} 1.0000 & 1.7090 & 1.3973 \\ 1.0270 & 1.6966 & 1.2365 \\ 0.2576 & 0.3992 & 0.1828 \end{pmatrix}$$

(b) Our matrix $\mathcal{K}_{LL'}$

$$\begin{pmatrix} 1.0000 & 1.1491 & 0.9077 \\ 0.6203 & 1.3467 & 1.0111 \\ 0.1128 & 0.2317 & 0.2990 \end{pmatrix}$$

We see from Figure 3.7 that there is very good agreement with the coupled channels results. The branching ratios are almost identical in each case, even though the absolute values of the eigenvalues are slightly different. This confirms that our approximations and assumptions in the derivation of the semi-classical matrix must be good ones. In particular, it proves that the form of our matrix given in Equation (2.3.21) and the choice of angular momentum in the exponent are good. We can now continue our discussion of the eigenchannel formalism using the semi-classical technique for our calculations.

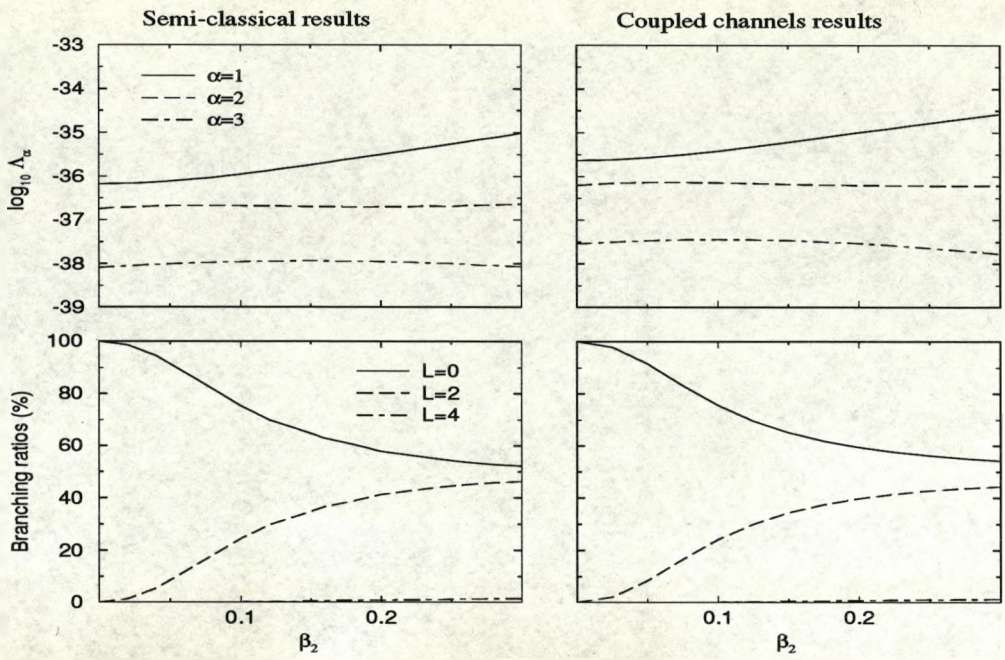

Figure 3.7: Eigenchannel calculations using the semi-classical technique to be compared with the previous results using coupled channels integration. The upper graphs show the eigenvalues Λ_α as a function of β_2 for a model ^{238}U nucleus. Branching ratios corresponding to the maximum-flux channel are shown in the lower graphs.

We have found that the maximum-flux eigenchannel does not reproduce experimental branching ratios for the nucleus ^{238}U. Let us now evaluate branching ratios for the whole range of even–even nuclei and for all three eigenchannels, using deformation parameters given in Ref. [19]. Figure 3.8 shows $L = 0$ branching ratios in the three channels. These results confirm that the experimental trends are not reproduced by assuming that decay proceeds by the channel which maximizes the outgoing flux, or indeed by any of the other channels.

We next consider the possibility that the correct admixture of angular momentum

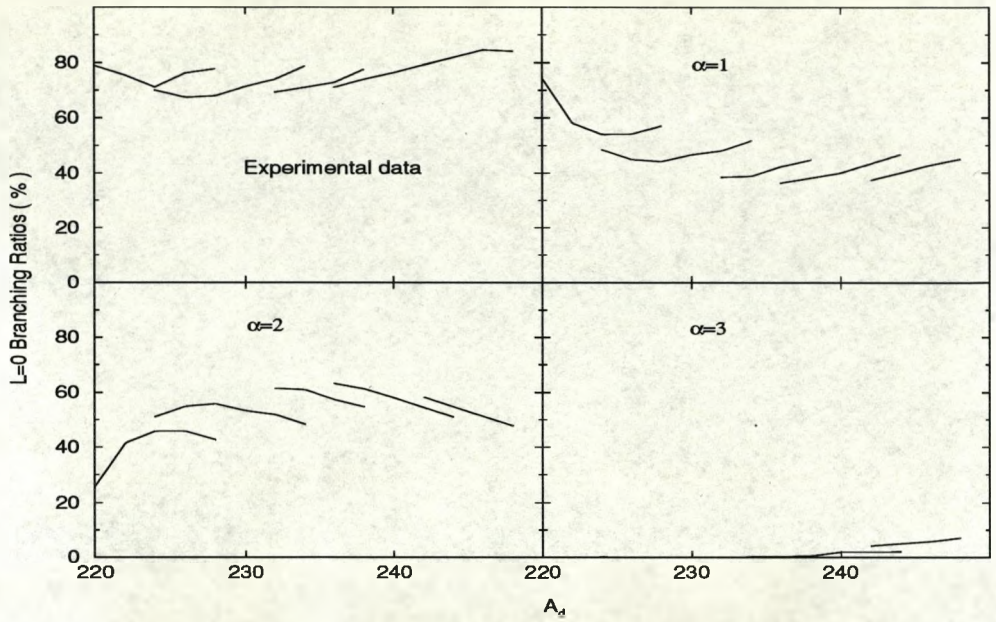

Figure 3.8: Calculated $L = 0$ branching ratios using an eigenchannel formalism and semi-classical transmission matrix. The three different solutions correspond to eigenchannels $\alpha = 1, 2, 3$.

states can be obtained by a simple linear combination of the first two eigenchannels. If we take the normalized internal amplitudes to be given by the formula

$$a_{L'} = x\ U_{L'1} + y\ U_{L'2} \tag{3.3.10}$$

where $y = \pm\sqrt{1 - x^2}$, we can vary x for each nucleus to fit the experimental branching ratios. The results are shown in Figure 3.9. We find that the value of x required to reproduce the experimental data is almost constant for most of the nuclei, although the sign of y must change in the last two cases. This suggests that there may be some common nuclear structure in these actinide nuclei. We note that for nuclei with $A_d < 230$ the value of $\epsilon^*(4^+)/\epsilon^*(2^+) < 3.33$ and so these are not "rotational" nuclei, which may explain why they do not follow the same pattern so closely.

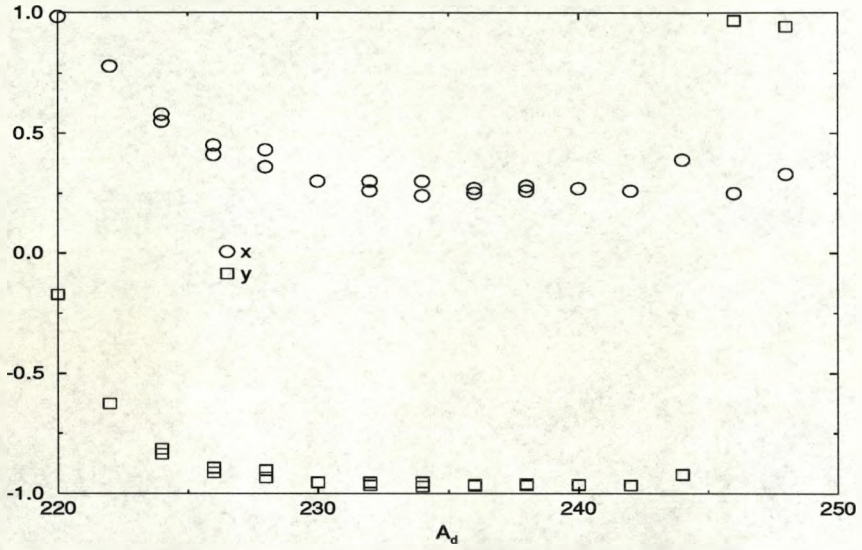

Figure 3.9: Values of x and y from Equation (3.3.10) required to fit the experimental ground state branching ratios for a range of even–even nuclei.

3.4 Systematic study of deformed even–even actinide nuclei

In this chapter we have introduced various models for the alpha decay process and compared their results with experimental data. None of the models investigated so far have been successful in the prediction of branching ratios consistent with experimental trends for even–even actinide nuclei. We will now make use of the semi-classical technique derived in Chapter 2 to perform a systematic study of the even–even actinide nuclei for which data are available, and calculate some possible sets of internal amplitudes consistent with these data.

Since the experimental branching ratios Z_L are derived from the square of the external amplitudes c_L, we can define these amplitudes to within a certain normalization

$$c_L = \exp(i\phi_L)\ \sqrt{Z_L} \tag{3.4.1}$$

where the phase ϕ_L is unknown. To determine the phase experimentally would require a measurement of the angular distribution of alpha particles emitted from oriented nuclei. In the decay of even–even nuclei this is not possible because the parent nuclei have spin zero and so cannot be aligned in the laboratory frame. In our semi-classical calculations, we consider only real amplitudes. The internal amplitudes are obtained by inverting Equation (3.1.1)

$$a_{L'} = \sum_L (K^{-1})_{L'L}\ c_L. \tag{3.4.2}$$

We can justify this choice of real amplitudes by comparison with the full complex coupled channels calculations. Preston and Bhadhuri [3] discuss similar calculations using a coupled channels approach, but with a potential similar to Fröman i.e. purely Coulomb barrier and a sharp cut-off potential. We can put a limitation on the phase ϕ_L by realizing that the imaginary parts of the wave function at the nuclear surface

should be close to zero. This is because experimental lifetimes indicate that the net outgoing current of alpha particles at the nuclear surface is very small. The remaining small imaginary amplitude is then indicative of the slight leakage of current in a quasi-stationary state. Preston and Bhadhuri report that in order for this condition to be met, the external amplitudes should be nearly real as well. We have confirmed this using our coupled channels integration. Figure 3.10 shows the real and imaginary parts of the $L = 0$ wave function inside the potential barrier for the nucleus ^{238}U, using the experimental branching ratios as asymptotic boundary conditions. We find that the imaginary components are much smaller compared with the real parts when the external phases are $\phi_L = 0$ or π, i.e. the wave function shown in Figure 3.10 (a) looks the most like a standing wave. A thorough investigation of all possible phases ϕ_L showed that to minimize the imaginary wave function at the nuclear surface for ^{238}U, ϕ_0 is always within 1° and ϕ_2 always within 10° of 0° or 180°. The asymptotic phase of the $L = 4$ wave function deviates more than the other phases but this has little effect on the results.

Thus in the semi-classical approximation, we are justified in using only the phases $\phi_L = 0$ or π, i.e. $c_L = \pm\sqrt{Z_L}$. We shall again restrict our calculations to $L \leq 4$ since few nuclei have measured branches to the 6^+ state. (We have, however, considered the inclusion of 6^+ and 8^+states and found that our conclusions are essentially unaffected.) We therefore consider four possibilities for the relative signs of $\{c_0\ c_2\ c_4\}$, i.e. $\{+++\}$, $\{++-\}$, $\{+-+\}$ and $\{+--\}$.

For all the decays we consider, the Sommerfeld parameters are large ($\eta \approx 25$) and the Coulomb phases then ensure that for the case $\{+++\}$ the spherical harmonics in Equation (3.3.1) are in phase along the symmetry axis. To show this we consider the radial component of the current density at a fixed radius asymptotically. The asymptotic

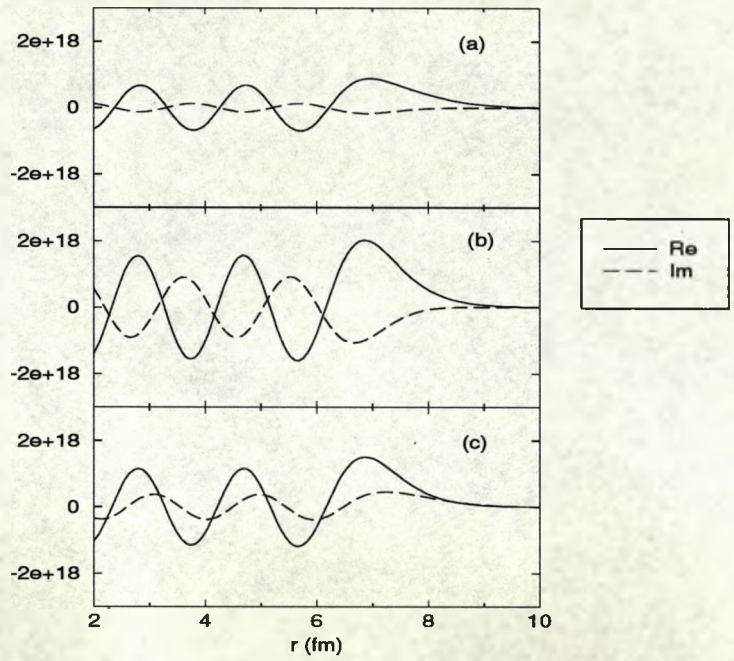

Figure 3.10: Real and imaginary parts of the $L = 0$ wave function in the nuclear interior, obtained by coupled channels calculation. The phases of the external amplitudes $\{c_0\ c_2\ c_4\}$ in each case are (a) $\{0\ 0\ 0\}$, (b) $\{0\ \pi/2\ \pi\}$, (c) $\{\pi/4\ \pi/2\ \pi\}$.

wave function may be written in the form

$$\psi = \sum_L c_L\ (G_L + iF_L)\ \Theta_{L0}(\theta) \tag{3.4.3}$$

where G_L and F_L are the regular and irregular Coulomb wave functions, whose asymptotic forms may be written

$$\begin{aligned} F_L &= \sin\left(k_L r - \frac{L\pi}{2} - \eta \ln(2k_L r) + \sigma_L\right), \\ G_L &= \cos\left(k_L r - \frac{L\pi}{2} - \eta \ln(2k_L r) + \sigma_L\right). \end{aligned} \tag{3.4.4}$$

The radial current density is obtained from

$$j_r \propto \left(\psi^* \frac{\partial \psi}{\partial r} - \psi \frac{\partial \psi^*}{\partial r}\right) \tag{3.4.5}$$

which gives

$$j_r \propto \sum_{LL'} c_L \, c_{L'} \, \cos(\alpha_{LL'}) \, \Theta_{L0}(\theta) \, \Theta_{L'0}(\theta) \tag{3.4.6}$$

where $\alpha_{LL'} = \frac{1}{2}(L' - L)\pi + \sigma_L - \sigma_{L'}$. For large values of η, we can write down the relationship ([33], page 540)

$$\sigma_{L+2} - \sigma_L = \arctan\left(\frac{\eta}{L+2}\right) + \arctan\left(\frac{\eta}{L+1}\right) \approx \pi. \tag{3.4.7}$$

Thus, since $L = 0, 2, 4...$, it follows that $\alpha_{LL'} \approx 0$ and

$$j_r \propto \sum_{LL'} c_L \, c_{L'} \, \Theta_{L0}(\theta) \, \Theta_{L'0}(\theta). \tag{3.4.8}$$

Since the amplitudes c_L add coherently, with the relative signs $\{+++\}$ the outgoing flux would be axial in the intrinsic frame. In the even–even system the outgoing flux in the laboratory frame is always isotropic after integrating over all orientations of the daughter. However, we shall see in the next chapter that the above consideration is important for odd mass systems which may be polarized to yield anisotropic alpha decay.

First we shall check again that the WKB approximation is good by comparing results with the coupled channels case. In the coupled channels calculation, the experimental data provides the asymptotic boundary condition and the wave function (Equation (3.4.3)) is integrated inwards through the barrier to obtain corresponding internal wave functions. For comparison with results from the semi-classical method, we must assume that there is no coupling of angular momentum states inside the inner radius R_0. This is because the semi-classical method maps external amplitudes in through the barrier to R_0, it makes no prediction of the behaviour of the wave function inside the nucleus. The only reason we integrate further inwards in the coupled channels calculation is

to enable us to define incoming and outgoing components where the nuclear potential is nearly flat. With no coupling inside the inner turning point, the outgoing current in this region is constant, and therefore the corresponding amplitude A_L in Equation (3.3.2) is also constant inside the barrier. It is this amplitude that is comparable with the semi-classical amplitude $a_{L'}$, because both are related to the outgoing current on the inside of the barrier. Since the coupled channels amplitude is complex, we calculate the normalized amplitudes

$$\frac{|A_L|}{\sqrt{\sum_L |A_L|^2}} \tag{3.4.9}$$

for our comparison. The sign of each amplitude is taken to be that of the real component.

In Table 3.2 we show the calculated amplitudes using each method for three nuclei, and for each of the four phase combinations. We find very good agreement for the phases $\{+-\pm\}$, but the comparisons for the phase choices $\{++\pm\}$ are not as close. This is due to the larger imaginary parts in the coupled channels wave function for these choices of phase, as shown in Figure 3.11. In cases (a) and (b) the imaginary parts are less than an order of magnitude smaller than the real parts, whereas in the other cases the difference is nearly two orders of magnitude. Since our semi-classical approach allows only real wave functions there should be a larger difference in the amplitudes where the imaginary parts are significant. It is evident however that the trends of the amplitudes obtained from each approach are very similar in all cases and the discrepancy in the actual values of $a_{L'}$ will not affect any of our conclusions.

These results, together with the comparisons made in Section 3.3, confirm that the semi-classical approach is a good approximation. In the derivation of the transmission matrix $\mathcal{K}$, we argued that the value of L used in the centrifugal potential should be that of the final state rather than the initial state. In reality, there is mixing of these angular momentum states during barrier transmission and so there will be no single value of L. We have calculated the internal amplitudes for ^{238}U using the angular momentum of

Table 3.2: Comparison of internal amplitudes obtained using two approaches. The phase combination indicated is that of the outer amplitudes, which are deduced from experimental branching ratios.

	Coupled channels			Semi-classical		
	A_0	A_2	A_4	a_0	a_2	a_4
$\{+++\}$						
^{222}Ra	0.66	0.74	0.11	0.75	0.10	0.65
^{238}U	0.69	0.14	-0.71	0.91	0.17	-0.39
^{248}Cm	0.79	-0.53	-0.30	0.97	-0.23	0.01
$\{++-\}$						
^{222}Ra	0.40	0.41	-0.82	0.46	0.51	-0.73
^{238}U	0.58	0.17	-0.80	0.71	0.36	-0.61
^{248}Cm	0.75	-0.16	-0.65	0.90	0.05	-0.42
$\{+-+\}$						
^{222}Ra	0.44	-0.70	0.56	0.43	-0.71	0.56
^{238}U	0.80	-0.56	0.22	0.76	-0.61	0.22
^{248}Cm	0.78	-0.58	0.24	0.76	-0.60	0.24
$\{+--\}$						
^{222}Ra	0.90	-0.25	-0.35	0.87	-0.28	-0.41
^{238}U	0.88	-0.47	0.05	0.83	-0.55	0.08
^{248}Cm	0.86	-0.50	0.10	0.82	-0.56	0.09

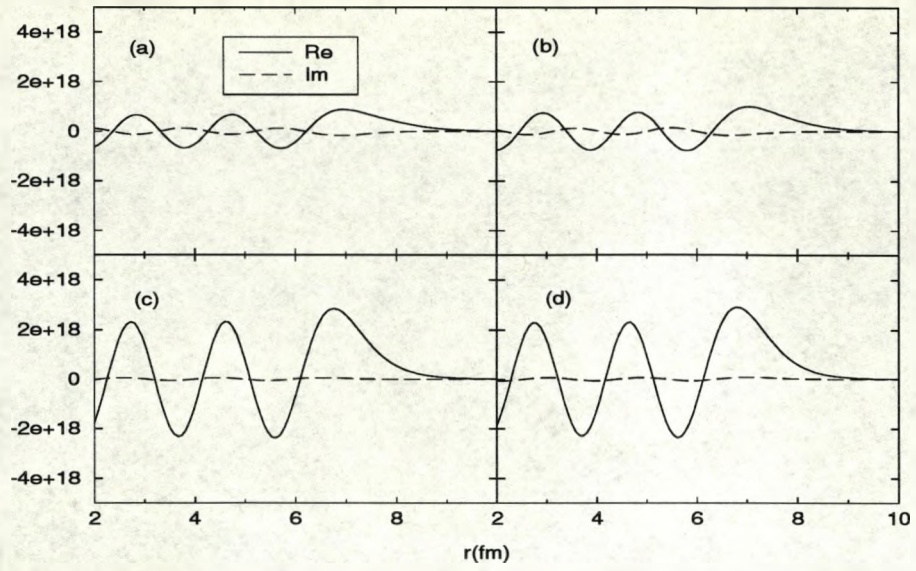

Figure 3.11: Real and imaginary parts of the $L = 0$ wave function near the nuclear surface for four combinations of signs for the external amplitudes $\{c_0\ c_2\ c_4\}$: (a)$\{+++\}$, (b)$\{++-\}$, (c)$\{+-+\}$, (d)$\{+--\}$.

the initial state L' in the centrifugal term, to compare the two results. For the phase combination $\{+--\}$, we obtain $\{a_0\ a_2\ a_4\} = \{0.59\ -0.67\ 0.44\}$, which does not agree so well with the coupled channels amplitudes given in Table 3.2. We therefore conclude that the alpha particle penetrates most of the potential barrier with its final state angular momentum L i.e. the mixing of angular momentum states must take place mainly near the inner turning point.

Now we have confirmed the accuracy of the semi-classical technique, we can use it to gain some information on internal nuclear structure in the actinide region. For each of the above phase combinations, we have determined the amplitudes $a_{L'}$ using Equation (3.4.2) for the even–even nuclei listed in Appendix A. Although this is not a new idea, we are not aware of any previous systematic study of actinide nuclei using experimental data and realistic deformation parameters. Figure 3.12 shows the four sets of $a_{L'}$, normalized such that the sum of the squares are equal to one. The uncertainty on these amplitudes which result from the experimental errors in the branching ratios will be discussed later. One immediate observation to be made is that the signs of the amplitudes can change during barrier transmission. For example, in Figure 3.12 (a) the asymptotic signs $\{+++\}$ become $\{+--\}$ inside the barrier for some nuclei.

It is important to note that in the nuclear interior, none of the four sets of solutions resembles eigenchannel 1, which maximizes the outgoing flux. Indeed for ^{238}U this solution has $\{a_{L'}\} = \{0.43, 0.70, 0.57\}$, i.e. all the amplitudes are *positive*, which is not the case in any of our solutions. This is not surprising since we have already shown that this eigenchannel does not reproduce experimental trends in the branching ratios. In particular, we note that if the alpha width of the spherical problem is Γ_0, then eigenchannel 1 has a width of around $17\,\Gamma_0$. The solutions which reproduce the experimental branching ratios, however, only have $\Gamma/\Gamma_0 = 3.4, 1.9, 0.4, 0.4$ for $\{++\!+\}, \{++\!-\}, \{+-\!+\}, \{+--\}$ respectively. These widths are all within a factor of four of the spherical value. This may be why reasonable lifetimes (e.g. Buck *et al.* [6] – [9]) can be obtained without considering the deformation of the daughter.

However, from Figure 3.13 we can see that the amplitudes obtained are quite different if we neglect the deformation of the nucleus and consider a spherical barrier. In this case, there is no mixing of angular momentum states through the barrier and the signs of the inner amplitudes remain the same as the asymptotic ones. Thus $|a_{L'}|$ is the same for each

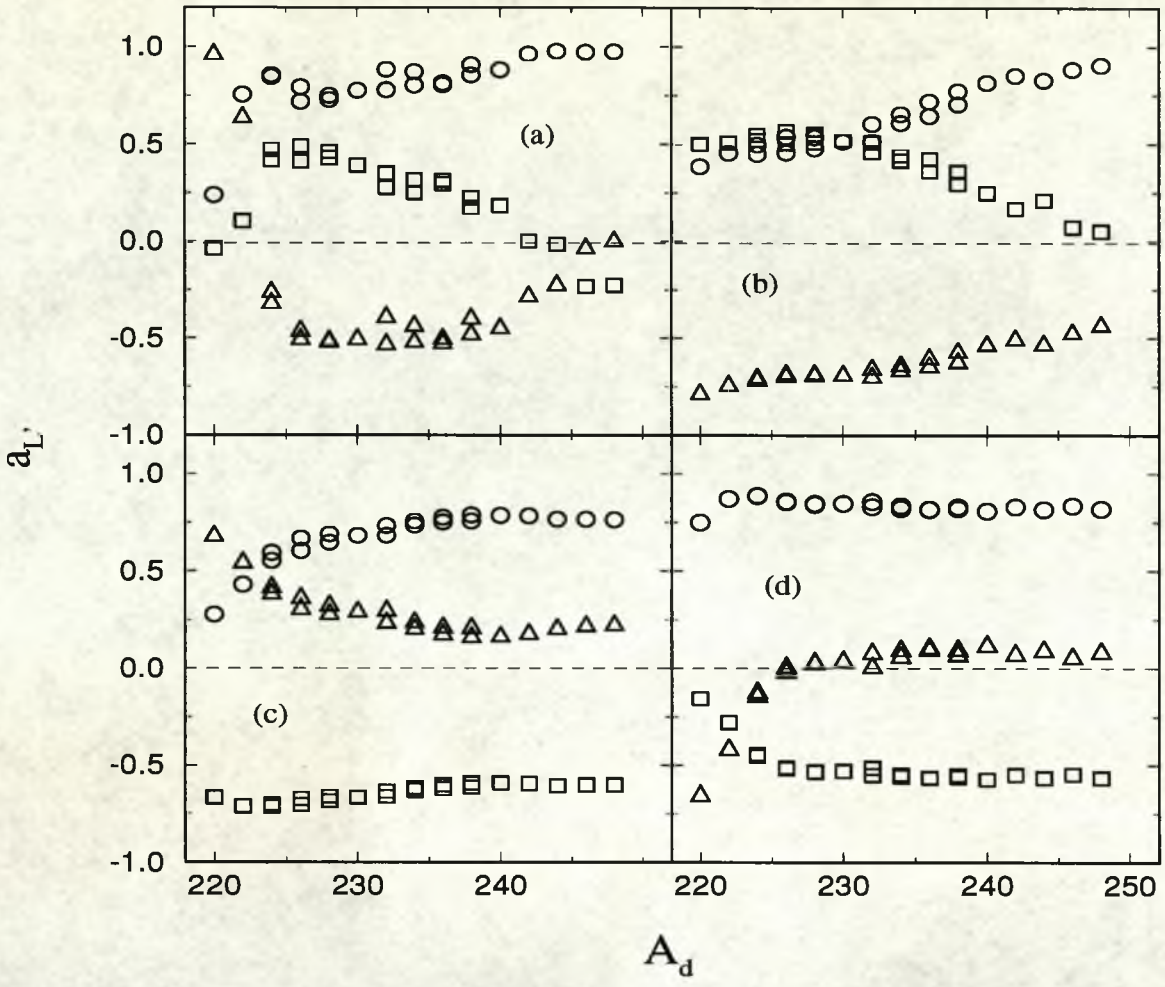

Figure 3.12: Normalized amplitudes $a_{L'}$ for even–even actinide nuclei with four choices of relative signs for $\{c_0\ c_2\ c_4\}$: (a) $\{+++\}$, (b) $\{++-\}$, (c) $\{+-+\}$, (d) $\{+--\}$. The amplitudes are calculated using experimental branching ratios and our semi-classical transmission matrix. The circles, squares and triangles represent $L' = 0, 2$ and 4 respectively.

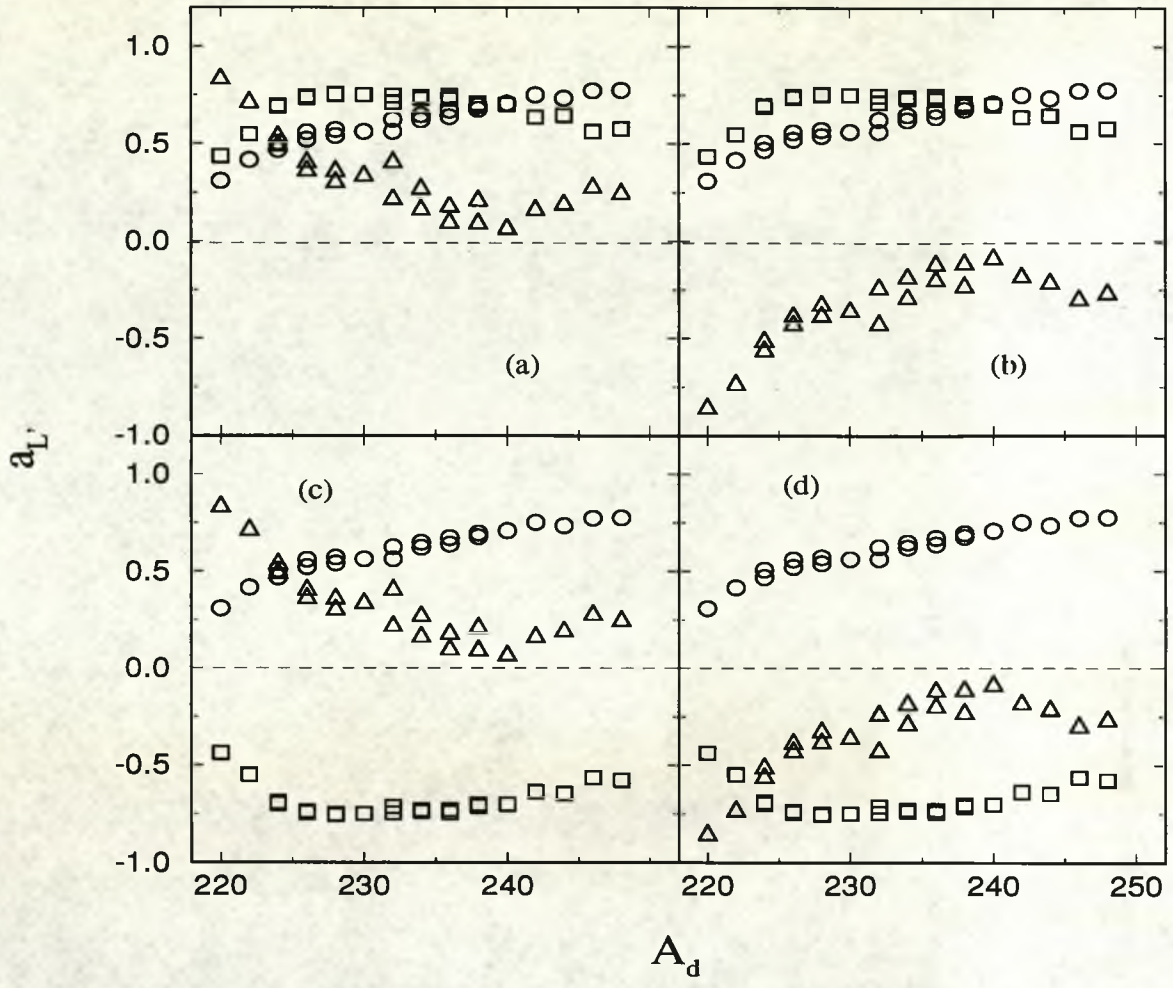

Figure 3.13: Normalized amplitudes $a_{L'}$ for even–even actinide nuclei calculated in the same way as Figure 3.12 but with a spherical barrier. The four choices of relative signs outside the barrier are (a) $\{+++\}$, (b) $\{++-\}$, (c) $\{+-+\}$, (d) $\{+--\}$. The circles, squares and triangles represent $L' = 0, 2$ and 4 respectively.

case in Figure 3.13. Neglecting the barrier deformation is obviously an approximation since we know that for a deformed nucleus there must be mixing of angular momentum states during barrier transmission. It has been claimed that this mixing is unimportant as long as the nuclear deformation is considered in the calculation of internal amplitudes [10]. If this suggestion is correct, the internal amplitudes calculated by Berggren and Olanders [11] should correspond to one of the solutions given in Figure 3.13. We do not find the deformation of the potential barrier to be negligible in our work, however.

Since the deformation of the daughter varies smoothly with A_d, we expect that just one set of the amplitudes shown in Figure 3.12 corresponds to the physical amplitudes i.e. it is likely that neighbouring nuclei will have similar nuclear structure. One particularly interesting solution is that obtained with the combination $\{+ - -\}$ (Figure 3.12 (d)) since the amplitudes $a_{L'}$ are practically nucleus-independent even though β_2 varies from around 0.10 to 0.24 and the alpha particle energies vary from around 4 to 7 MeV over this mass region. Similar results are obtained from the combination $\{+ - +\}$, although the amplitudes are slightly less constant. We find that almost identical trends are obtained by using Fröman's transmission matrix in these calculations – the lower two graphs of Figure 3.12 again show nearly constant amplitudes. This is because the differences in the transmission matrices are not so significant in the calculation of relative, normalized quantities. We have already shown that they are significant in the calculation of absolute alpha decay widths.

We note that for the constant solution a_2 (and c_2) are always negative. This indicates that the flux density of outgoing alpha particles is greater at the equator than at the poles of the nucleus, which may seem to be contrary to the suggestion of Hill and Wheeler [4] for a prolate system. However, Hill and Wheeler only showed that transmission is enhanced near the poles for a prolate nucleus where the barrier is lower and thinner. The angular distribution of alpha particles outside the barrier depends primarily on the

distribution at the nuclear surface, it is only modified by the barrier penetration. (This is also discussed in Ref. [10]). Therefore the solutions with $a_2 < 0$ do not conflict with Ref. [4] and cannot be ruled out.

At first sight, $a_2 < 0$ might also imply that if the same solution prevailed for odd mass nuclei, then alpha emission would take place mainly in the equatorial plane – a result which would not be consistent with measured anisotropies. We shall show in Chapter 4 that this is not necessarily the case i.e. that taking the solution with $a_2 < 0$ in the even–even case need not be ruled out by the experimental results from odd–A decays.

This evidence of some constant nuclear structure in actinide nuclei may be consistent with the findings of Buck *et al.* [8], who calculated decay widths for the favoured decay of over a hundred even–even nuclei. They used a realistic nuclear potential similar to ours, but did not consider the nuclear deformation in their calculations. A fixed set of four parameters for all nuclei in our mass range was used, chosen from a global fit to the experimental data. The nuclear radius was then varied for each nucleus subject to the Bohr-Sommerfeld quantization condition which ensures that the decaying state has the correct energy. With these fixed parameters, experimental alpha decay widths were reproduced to within a factor of ≈ 2 for all the nuclei considered.

We must now consider what physical model could generate such constant amplitudes. The best candidate would appear to be the notion that the alpha particle wave function should be projected from the pair-correlated neutron and proton Nilsson-model states i.e. a BCS calculation similar to that of Delion *et al.*. In the mass region we are considering, the level density is high and the pair forces lead to a rather diffuse Fermi surface. One might then expect that the ground state wave function should vary rather slowly with the Fermi energy, or in other words with the number of nucleons in the system. This model therefore can account for the nearly constant amplitudes found in Figure 3.12 (d). Since nucleons couple pairwise to zero as far as the Pauli principle allows, this model

would also be expected to give internal amplitudes with the property $|a_0| > |a_2| > |a_4|$. This trend is most apparent in the constant solution we have discussed.

Let us consider alternatively the model of a preformed alpha particle moving in the deformed field of the daughter nucleus. One would expect that the amplitudes in this case would show some dependence upon the value of the quadrupole deformation parameter β_2, which would effectively rule out the solutions in Figures (3.12) (c) and (d). One would also expect that as β_2 increases the $L = 0$ amplitudes would decrease as we move further away from spherical symmetry. It is therefore difficult to see how such a model could explain any of the solutions in Figure 3.12.

There have been some attempts to gain nuclear structure information in this way in the past. Chasman and Rasmussen [34] performed similar calculations on actinide nuclei using an analytic approximation to the coupled channels equations and considering different phase combinations as we have done. They included angular momentum states up to $L = 6$ in their work, but did not have any detailed information on the deformation parameters for their nuclei and so they performed their calculations for three different values of the intrinsic quadrupole moment Q_0. Since this amounts to keeping β_2 fixed for each nucleus, we cannot expect our results to be comparable as the values of β_2 used in our calculation vary from nucleus to nucleus. Their results do not show any constant pattern for any of the solutions considered. We have performed one calculation for the decay of ^{232}U, including states up to $L = 6$ and taking a value of $\beta_2 = 0.26$ consistent with a quadrupole moment of $Q_0 = 14$ b. We took alpha particle energies and branching ratios from Ref. [34] and calculated relative internal amplitudes to be compared with their values, using the relative signs $\{+ + +\}$. It can be seen from Table 3.3 that our results agree reasonably well, considering the different techniques employed.

Other work has used the same approach of working backwards from experimental data, but concentrating on one or two nuclei rather than a systematic study [35, 36, 37].

Table 3.3: Comparison of internal alpha particle amplitudes with results taken from Ref. [34] for the parent nucleus ^{232}U.

	a_0	a_2	a_4	a_6
Chasman and Rasmussen	1.00	1.57	0.94	0.31
Our calculation	1.00	1.18	0.42	-0.19

In these papers, angular distributions at the nuclear surface are calculated for each phase combination. They show that the combination $\{+++\}$ gives a distribution that is peaked around the poles of the nucleus, whereas in the cases with $L = 0$ and $L = 2$ waves out of phase, the peak shifts towards the equator. As we have already mentioned, in the favoured alpha decay of odd mass nuclei it is evident that for most nuclei in this mass region the $L = 0$ and $L = 2$ partial waves are in phase asymptotically. The authors in Refs. [35, 36, 37] have assumed that the same relative phases are present in the even–even case, at the nuclear surface. We stress again however that for an even–even decay the angular distribution of emitted alpha particles is a theoretical concept, it cannot be measured experimentally because it is not possible to align the parent nuclei. Even if we could assume the same amplitudes for even–even and odd–A nuclei asymptotically, we have already seen that the relative signs may be different at the nuclear surface.

There have also been attempts to predict alpha particle wave functions in the actinide region by calculation using various models, e.g. Poggenburg *et al.* [38] use shell model calculations to predict relative amplitudes. They adopt Fröman's approach to barrier

penetration which splits up the process into an isotropic part and a non-spherical part. The amplitudes listed in their tables correspond to those on a sphere outside the deformed nuclear surface, and so are not comparable with ours. However, we can comment on the relative signs of their external amplitudes, since the spherical penetration term will not affect their signs. For all the nuclei they consider, the asymptotic signs of the $L = 0, 2$ and 4 partial waves are $\{++\pm\}$ respectively. We shall comment further on their results in the next chapter when we calculate alpha decay anisotropies for odd mass nuclei.

Finally in this section, we shall make some comments concerning experimental errors. The data used for even–even nuclei in this chapter are given in Appendix A. First, we consider the errors on the internal amplitudes $a_{L'}$ arising from the experimental uncertainty in the branching ratios. We have calculated errors for each case shown in Figure 3.12, and find that for most nuclei the errors are less than the size of the symbols. Figure 3.14 shows the amplitudes together with their error bars for two out of the four phase combinations that we consider. Although for some nuclei the errors are larger in Figure 3.14 (a) than (b), they are not significant enough to alter any of our conclusions.

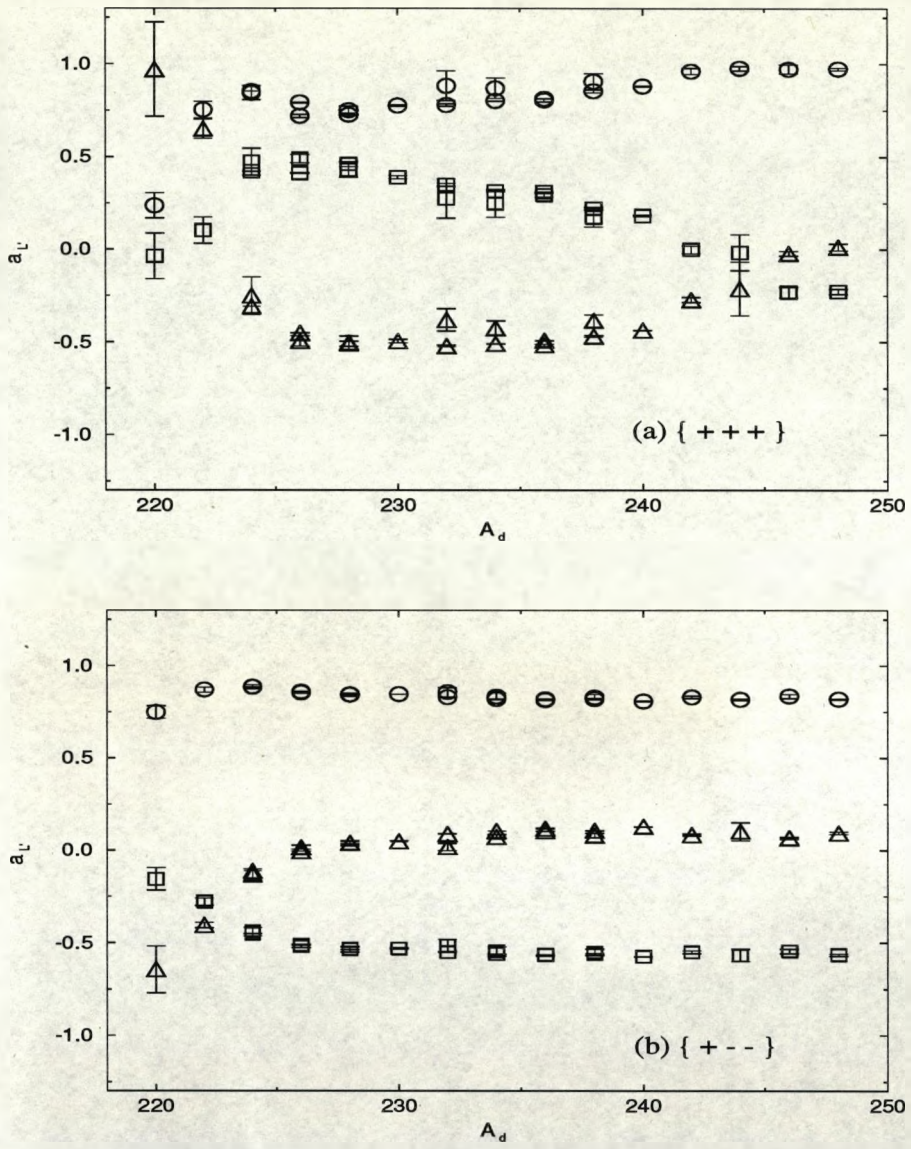

Figure 3.14: Internal amplitudes derived from experimental branching ratios using a semi-classical transmission matrix. Two of the four possible sign combinations are shown with errors which arise from experimental uncertainty in the branching ratios. The circles, squares and triangles correspond to $L' = 0, 2, 4$ respectively.

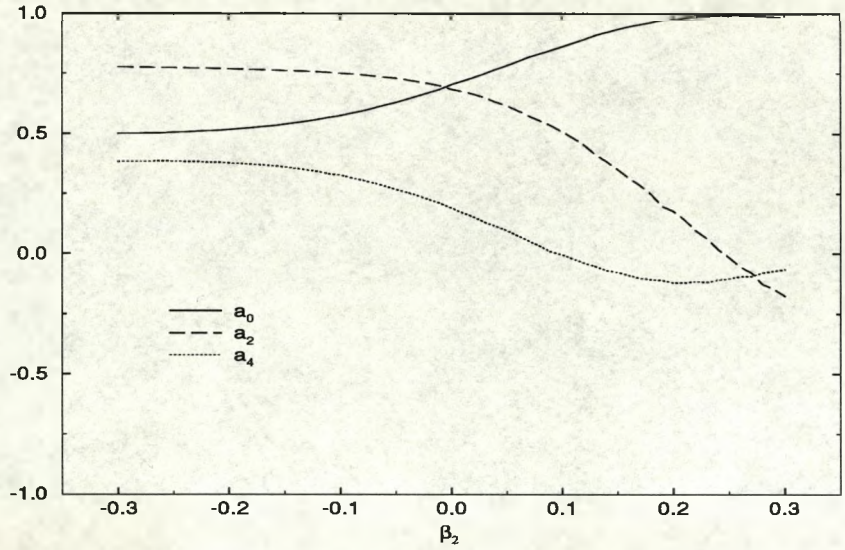

Figure 3.15: Internal amplitudes derived from experimental branching ratios, plotted as a function of the quadrupole deformation parameter β_2. We have used ^{238}U as a model nucleus and set $\beta_4 = \beta_6 = 0$.

As discussed in Chapter 1, we take deformation parameters from the compilation by Möller *et al.* [19]. Since there are no errors quoted on these parameters, we shall investigate the sensitivity of our results to changes in their values. We use ^{238}U as a model nucleus and take all data from Appendix A unless otherwise stated. In Figure 3.15 we show the dependence of $a_{L'}$ on β_2, with $\beta_4 = \beta_6 = 0$. The amplitudes are calculated as before by taking the experimental branching ratios with relative signs $\{+++\}$ and using Equation (3.4.2) to factor out the effects of the barrier transmission. We find that the amplitudes are not very sensitive to small changes in β_2 e.g. a fairly large change of β_2 from 0.15 to 0.20 would change a_0 from 0.93 to 0.98. We have also verified that reasonable variations of all other parameters used in our work, i.e. β_4, β_6, Woods-Saxon parameters and energies have negligible effect on the calculated amplitudes.

3.5 Alpha decay lifetimes

In the previous section we calculated relative amplitudes near the nuclear surface which are consistent with experimentally measured branching ratios. There are four solutions of this type corresponding to different combinations of asymptotic phases, but it is not experimentally possible to find out which are the correct phases.

However, we do have experimental data on alpha decay lifetimes for these nuclei. It may be possible to establish the physical solution by calculating quantities to be compared with these lifetimes. In a simple model of alpha decay, one can picture the alpha particle moving around inside the nucleus until it manages to penetrate the potential barrier of the daughter. The probability of an alpha particle being emitted from the nucleus therefore depends on several factors; a preformation factor describing the probability of an alpha particle being formed in the first place (e.g. by considering the Nilsson-model states of the individual nucleons), the number of times per second that the alpha particle "hits" the nuclear surface (knocking frequency), and the probability that it will be transmitted through the barrier and escape to infinity. The last factor will be related to the square of the external amplitudes c_L, so the alpha decay rate R may be written in the form

$$R = fP\sum_L |c_L|^2 \tag{3.5.1}$$

where P is the preformation factor and f is the knocking frequency in units of s^{-1}. The lifetime in seconds is then calculated from

$$\tau = \frac{\ln 2}{R}. \tag{3.5.2}$$

We might expect there to be little variation in preformation factors and knocking frequencies across the mass range in question, in which case these would just appear as

a constant factor for all nuclei. Therefore, we have calculated values of

$$\tau_{th} = \frac{1}{\sum_L |c_L|^2} \tag{3.5.3}$$

using each of the four sets of normalized internal amplitudes found in the previous section and our semi-classical transmission matrix. This calculation effectively maps the amplitudes in through the barrier then out again in order to obtain absolute values of c_L rather than normalized ones. The results are then compared with experimental alpha decay lifetimes. As expected, the theoretical values follow the trends of the experimental data very closely, but are shifted by an almost constant factor. Unfortunately this does not help in our aim of finding a particular physical solution since all four sets of amplitudes create almost identical results.

We can look more closely at the lifetimes obtained with the four solutions by plotting the difference between the theoretical values τ_{th} and the experimental lifetimes, which are represented by Equation (3.5.2). We define the difference Δ_τ by

$$\begin{aligned} \Delta_\tau &= \log_{10}(\tau_{th}) - \log_{10}(\tau) - 22 \\ &= \log_{10}\left(\frac{fP}{\ln 2}\right) - 22. \end{aligned} \tag{3.5.4}$$

The factor 22 is subtracted to make the points lie around zero and highlight any differences between the results. It is also a convenient factor to remove if we assume that the knocking frequency is constant for this range of nuclei, since the value of f may be taken to be $\approx 10^{22}$ s^{-1} ([39], page 142). Δ_τ is then equal to

$$\Delta_\tau = \log_{10}\left(\frac{P}{\ln 2}\right). \tag{3.5.5}$$

Figure 3.16 shows plots of Δ_τ for the four solutions of internal amplitudes, and also those using a purely spherical barrier. We find that the plots in Figure 3.16 (c) and (d) are again nearly constant across the range, which from Equation (3.5.5) suggests that the

preformation factor P must also be constant. The exact value of P cannot be uniquely determined because there are several parameters in our work. Firstly, we have chosen to normalize the amplitudes $a_{L'}$ to one when the normalization could be to any number in principle. Secondly the value of P will depend on the parameters V_0 and f in our Woods-Saxon potential. With the current values of $V_0 = 100$ MeV and $d = 0.5$ fm, the average value of Δ_τ from Figure 3.16 (d) is approximately 1.6. Using Equation (3.5.5), this gives a value of the preformation factor $P = 28$. If we change the parameters to fairly large values of $V_0 = 200$ MeV and $d = 0.6$ fm, P becomes 1.1. A realistic value of P would lie between 0 and 1, so this result suggests that our arbitrarily chosen normalization of the internal amplitudes is not correct and we cannot deduce absolute values. (Of course this normalization does not affect any other results in this thesis.) Alternatively, it may indicate that the simple model of alpha decay presented in this section is incorrect.

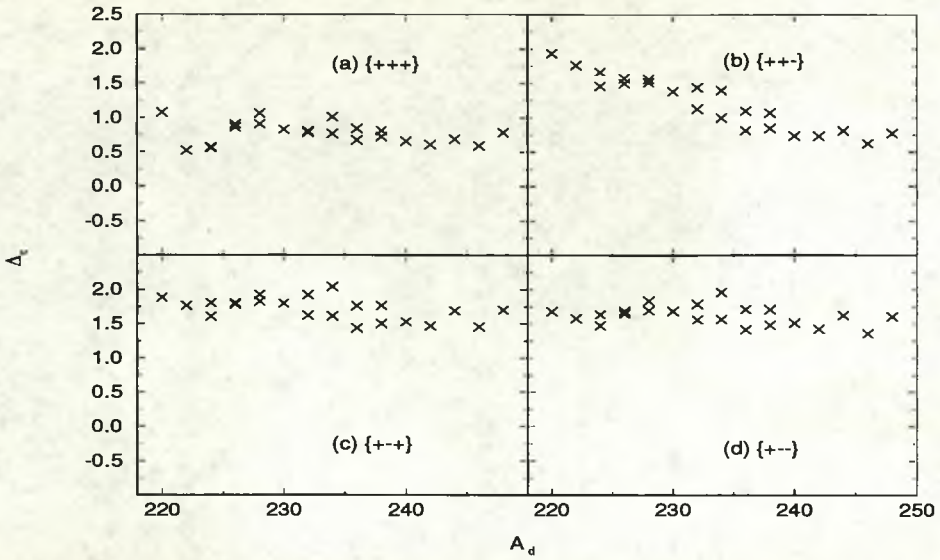

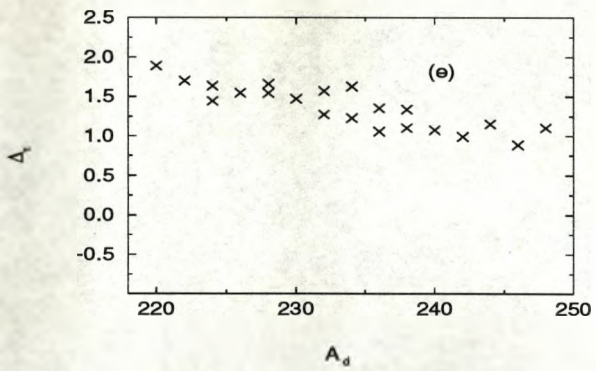

Figure 3.16: Plots of the difference between calculated lifetimes and experimental values, with a constant factor removed. Graphs (a) – (d) are obtained using a deformed barrier and four solutions of internal amplitudes. Graph (e) assumes a spherical barrier.

Chapter 4

Odd–A nuclei

The alpha decay of odd mass nuclei is potentially more difficult to model than that of even–even nuclei, since we no longer have the condition $L = J_d$. For each daughter state in the odd–A nucleus, the alpha particle may carry an orbital angular momentum given by $J_p + J_d \leq L \leq |J_p - J_d|$. Thus the energy of the emitted alpha particle is no longer directly related to its orbital angular momentum L. If the parity of parent and daughter states remains the same, only even values of L are allowed. An example of a decay from $J_p = 5/2^+$ is shown schematically in Figure 4.1.

There is, however, an interesting physical phenomenon arising from this, in that the superposition of partial waves in the favoured daughter state leads to an anisotropy in the alpha emission. Recently, there has been renewed interest in this subject because of new experimental techniques to measure this anisotropy for several odd mass nuclei. For odd mass nuclei, we shall calculate two quantities to be compared with experimental data: the anisotropy of alpha emission to the favoured daughter state and the branching ratios to all states.

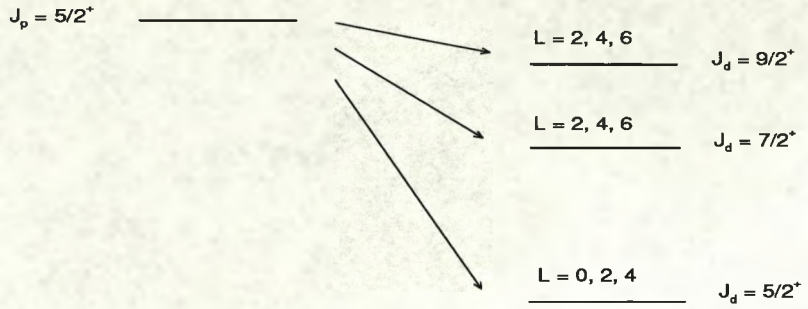

Figure 4.1: Alpha decay of an odd–A nucleus with $J_p = 5/2^+$.

4.1 Derivation of the wave function for odd mass nuclei

Let us consider a simple model to describe the internal wave function of an odd–A nucleus. We assume that the odd mass nucleus consists of an even–even core plus an odd nucleon. If the odd nucleon has no effect on the alpha decay process, then the wave function of the decaying odd–A nucleus must be closely related to that of the neighbouring even–even one. This idea has previously been discussed in the papers by Fröman [5] and Buck *et al.* [7, 8]. With this model, we can make use of our results from Section 3.4 to predict amplitudes for odd–A nuclei in the actinide region.

We write the normalized wave function of the parent nucleus in the same notation as Bohr and Mottelson ([40], page 10)

$$\Psi^{J_p}_{MK} = \sqrt{\frac{2J_p+1}{16\pi^2}}\left(\Phi^{J_p}_{MK} + (-1)^{J_p+K}\Phi^{J_p}_{M\bar{K}}\right) \tag{4.1.1}$$

where J_p is the angular momentum of the parent and M and K represent its projection onto space-fixed and body-fixed axes respectively. $\Phi^{J_p}_{M\bar{K}}$ is the wave function $\Phi^{J_p}_{MK}$ rotated by π about an axis perpendicular to the symmetry axis. It is included to make the total wave function rotationally invariant.

We can write each wave function as a product of terms involving the parent nucleus, odd nucleon and alpha particle,

$$\begin{aligned} \Phi^{J_p}_{MK} &= D^{J_p}_{MK}(\Omega)\, \phi_K(\mathbf{r_n}')\, \psi(\mathbf{r}_\alpha') \\ \Phi^{J_p}_{M\bar{K}} &= D^{J_p}_{M-K}(\Omega)\, \phi_{\bar{K}}(\mathbf{r_n}')\, \psi(\mathbf{r}_\alpha'). \end{aligned} \tag{4.1.2}$$

In the following work we shall only consider the first term $\Phi^{J_p}_{MK}$ since all manipulations apply equally to the second term.

Throughout this chapter we use primed angles and co-ordinates for the intrinsic frame and unprimed ones for the laboratory frame. Thus the rotation matrix describes the collective rotational motion of the parent nucleus in the laboratory frame. The function $\phi_K(\mathbf{r_n}')$ represents the intrinsic motion of the odd nucleon, and $\psi(\mathbf{r}_\alpha')$ is the wave function of the alpha particle relative to the daughter which is also defined in the intrinsic frame of the parent nucleus. We assume that the odd nucleon has no effect on the alpha decay and that its wave function in the intrinsic frame remains the same. The quantum number K therefore does not change, since the nucleon is always aligned with the even–even core. This situation corresponds to the "strong coupling" model of Rowe [41], where the odd nucleon wave function is independent of the rotational motion. Thus in the work that follows, we shall not write down the wave function of the odd nucleon.

Let us first consider the parent wave function inside the barrier. The alpha particle wave function for the decay of an odd mass nucleus may be written as a linear

combination of spherical harmonics

$$\Phi^{J_p}_{MK} = D^{J_p}_{MK}(\Omega) \sum_{L'n} a_{L'n}\, Y^*_{L'n}(\hat{\mathbf{r}}'_\alpha) \tag{4.1.3}$$

with expansion coefficients $a_{L'n}$. In the even–even case, the quantum number $n = 0$ because the parent has zero spin. We now assume that the odd nucleon has no effect on the alpha particle and thus the wave function of the alpha particle must be identical for odd mass and even–even nuclei. With this assumption, $n = 0$ and the expansion coefficients must be the same as the amplitudes $a_{L'}$ present in the even–even case,

$$\Phi^{J_p}_{MK} = D^{J_p}_{MK}(\Omega) \sum_{L'} a_{L'}\, Y^*_{L'0}(\hat{\mathbf{r}}'_\alpha). \tag{4.1.4}$$

In the work that follows, all formulae involving spherical harmonics and rotation matrices are taken from Ref. [42], page 79. The spherical harmonic is taken to be the complex conjugate in order to simplify some of the algebra.

The equivalent expression for the wave function outside the barrier must depend upon the final daughter state J_d as well as the orbital angular momentum L. In the even–even case we did not encounter this problem because of the special relationship $L = J_d$. If we transform the spherical harmonics into the laboratory frame, using

$$Y^*_{L'0}(\hat{\mathbf{r}}'_\alpha) = \sum_{m'} D^{L'}_{m'0}(\Omega)\, Y^*_{L'm'}(\hat{\mathbf{r}}_\alpha) \tag{4.1.5}$$

we obtain

$$\Phi^{J_p}_{MK} = \sum_{L'm'} a_{L'}\, D^{J_p}_{MK}(\Omega)\, D^{L'}_{m'0}(\Omega)\, Y^*_{L'm'}(\hat{\mathbf{r}}_\alpha). \tag{4.1.6}$$

The contraction formula for two rotation matrices then gives

$$\Phi^{J_p}_{MK} = \sum_{L'J'_dm'} a^{m'}_{L'J'_d}\, D^{J'_d}_{(M+m')K}(\Omega)\, Y^*_{L'm'}(\hat{\mathbf{r}}_\alpha) \tag{4.1.7}$$

where

$$a^{m'}_{L'J'_d} = a_{L'}\, \langle J_p L' M m' | J'_d M + m' \rangle\, \langle J_p L' K 0 | J'_d K \rangle. \tag{4.1.8}$$

In the even–even case, $J_p = 0$ and $J_d = L$ and the amplitudes $a_{L'}$ and $a^{m'}_{L'J'_d}$ are the same. However, for odd–A nuclei these amplitudes are very different in the two frames. Note that by switching from the intrinsic frame of the nucleus to the laboratory frame, we have produced an explicit dependence upon the daughter angular momentum (and thus implicitly on the energy of the alpha particle). Now we can write the equivalent expression for the wave function outside the barrier:

$$\Phi^{J_p}_{MK} = \sum_{LJ_dm} c^m_{LJ_d}\, D^{J_d}_{(M+m)K}(\Omega)\, Y^*_{Lm}(\hat{\mathbf{r}}_\alpha) \tag{4.1.9}$$

where

$$c^m_{LJ_d} = c_L\, \langle J_p L M m | J_d M + m \rangle\, \langle J_p L K 0 | J_d K \rangle. \tag{4.1.10}$$

(We do not label the amplitudes with J_p, M or K since they are constant in our work.) This equation describes the wave function of the odd mass nucleus outside the barrier and in the laboratory frame. The coefficients c_L are not related to the equivalent amplitudes in the even–even case, because the barrier penetration factors depend upon the energy of the alpha particle during transmission and these energies will be different in neighbouring nuclei. It is only inside the barrier, before the decay takes place that we assume a direct relationship between the wave functions of odd–A and even–even nuclei. Fröman [5] has considered a model where the external coefficients are assumed to be the same as the neighbouring even–even case. As well as employing the wrong alpha particle energies, this model leads to other errors as we shall show in the next section.

4.2 Angular distributions

First we consider the angular distribution of alpha particles in the decay to one particular state J_d, starting from Equation (4.1.9). The angular distribution is obtained by taking the modulus square of the wave function and integrating over all orientations Ω, which

gives

$$W(\theta) \propto |\Phi^{J_p}_{MK}|^2 = \sum_m \mid \sum_L c_L \, \langle J_d L M - m m | J_p M \rangle \, \langle J_p L K 0 | J_d K \rangle \, Y_{Lm}(\hat{\mathbf{r}}_\alpha) \mid^2 . \tag{4.2.1}$$

This expression for the angular distribution is relevant only for fully aligned systems where the projection $M = J_p$ for all nuclei. A more general expression for systems that are not completely aligned may be found for example in Ref. [29].

We note that so far we have only considered one part of the total wave function in Equation (4.1.1). If we considered the total wave function, the full expression for $W(\theta)$ would contain three parts; one each for the square of the two parts $\Phi^{J_p}_{MK}$ and $\Phi^{J_p}_{M\bar{K}}$ and an interference term between the two. This interference term becomes zero when we integrate over all orientations. The full expression for $W(\theta)$ therefore contains a second term of the same form but with $\bar{K} = -K$ throughout. Since the quantity is squared, the value of this second term will be the same as the first. Equation (4.2.1) is therefore the complete expression for the angular distribution if we neglect all constant factors (we can do this because we shall always be concerned with ratios of $W(\theta)$ at two angles).

We define the alpha decay anisotropy by $W(0)/W(\frac{1}{2}\pi)$. Thus an anisotropy greater than one would mean that the current density of outgoing alpha particles is larger axially than equatorially (in the laboratory frame), and vice versa for anisotropy less than one. Figure 4.2 shows schematically the angular distribution obtained if the anisotropy is greater than one.

So we have deduced an expression for the angular distribution in terms of the external amplitudes c_L. We must now consider the problem of how to determine the c_L. In the previous chapter, we made use of a simple relationship between the internal and external amplitudes in the even–even case. Our aim is to obtain a similar relationship for the barrier transmission in the odd–A case.

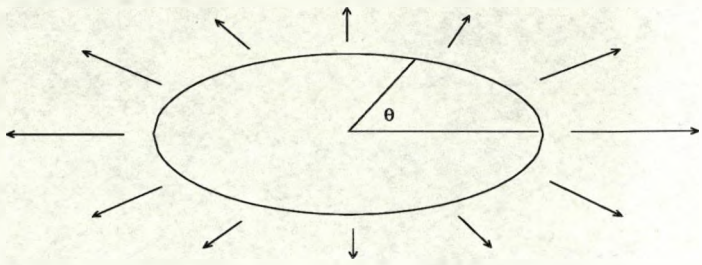

Figure 4.2: Schematic diagram of the angular distribution of emitted alpha particles corresponding to anisotropy > 1.

From Equations (4.1.7) and (4.1.9), we obtain a relationship between the amplitudes:

$$\frac{c^m_{LJ_d}}{2J_d+1} = \sum_{L'J_d'm'} a^{m'}_{L'J_d'} \langle\, D^{J_d'}_{(M+m')K}(\Omega)\, Y^*_{L'm'}(\hat{\mathbf{r}}_\alpha) \mid f_L(\theta') \mid D^{J_d}_{(M+m)K}(\Omega)^*\, Y_{Lm}(\hat{\mathbf{r}}_\alpha) \,\rangle \tag{4.2.2}$$

where

$$f_L(\theta') = \exp\left(-I_L(\theta')\right) \tag{4.2.3}$$

is the barrier transmission factor derived in Section 2.3.2 and θ' is the angle between alpha particle and daughter in the intrinsic frame.

The matrix element $\langle\, Y^*_{L'm'}(\hat{\mathbf{r}}_\alpha) \mid f_L(\theta') \mid Y_{Lm}(\hat{\mathbf{r}}_\alpha) \,\rangle$ is almost the same as $\mathcal{K}_{LL'}$ derived in the even–even case, except that the spherical harmonics must be transformed into the intrinsic frame. This introduces another rotation matrix and another quantum number n. By integrating over all orientations Ω we find

$$\begin{aligned}\frac{c^m_{LJ_d}}{2J_d+1} &= \sum_{L'J_d'm'n} (-1)^{m'+m}\, \langle J_d' M + m' L' - m' | J_p M \rangle\, \langle J_d' L' K - n | J_p K - n \rangle \\ &\quad \times \langle J_d L M + m - m | J_p M \rangle\, \langle J_d L K - n | J_p K - n \rangle\, \mathcal{K}^n_{LL'}\, a^{m'}_{L'J_d'}\end{aligned} \tag{4.2.4}$$

where

$$\mathcal{K}^{n}_{LL'} = \langle\ Ln \mid e^{-I_L(\theta)} \mid L'n\ \rangle. \tag{4.2.5}$$

If we make use of the definitions of $a^{m'}_{L'J_d'}$ and $c^{m}_{LJ_d}$ from Equation (4.1.8) and Equation (4.1.10), we can carry out the sum over m' and simplify the expression further

$$\langle J_p L K 0 | J_d K \rangle\ c_L = \sum_{L'J_d'n} \langle J_p L K - nn | J_d K \rangle\ \langle J_p L' K - nn | J_d' K \rangle\ \langle J_p L' K 0 | J_d' K \rangle\ \mathcal{K}^{n}_{LL'}\ a_{L'}. \tag{4.2.6}$$

Since the spherical harmonics contained in the matrix $\mathcal{K}$ are now defined in the intrinsic frame, their projection must be zero because of our assumption that the odd nucleon does not affect the alpha particle. The quantum number n must therefore be zero as in Equation (4.1.3), and we get the expression

$$c_L = \sum_{L'J_d'} \langle J_p L' K 0 | J_d' K \rangle^2\ \mathcal{K}_{LL'}\ a_{L'}. \tag{4.2.7}$$

Now we cannot perform the sum over J_d' because the matrix $\mathcal{K}_{LL'}$ depends on the energy of the alpha particle during transmission, which in turn depends on both the initial and final state of the daughter. (For even–even nuclei we were able to approximate this energy dependence by arguing that the alpha particle should tunnel with the energy corresponding to the final state. We were able to do this by considering the importance of the centrifugal term and our choice of orbital angular momentum also fixed the tunnelling energy of the alpha particle. In the odd mass case this argument is not so straightforward because the energy of the alpha particle is not directly related to its orbital angular momentum.)

If the daughter states are considered to be degenerate, however, the sum over J_d' can be done and we get the result given in Fröman's paper, and used more recently in the papers by Delion *et al.* [13] – [15]

$$c_L = \sum_{L'} \mathcal{K}_{LL'}\ a_{L'}. \tag{4.2.8}$$

This expression is exactly that used in the even–even case where the alpha particle energy is determined by the orbital angular momentum L. It is not valid for odd–A systems where the alpha particle energy is determined by the initial and final daughter states. By assuming all daughter states to be degenerate, the Clebsch-Gordon coefficients are summed over and do not appear in the barrier transmission factor. We shall show in the next section that these coefficients make a large difference to the mapping of amplitudes from inside to outside the barrier.

Now let us return to Equation (4.2.7). If we assume that there can be no mixing between daughter states during the barrier transmission, then $J_d = J'_d$ and we obtain

$$c_L = \sum_{L'} \langle J_p L' K 0 | J_d K \rangle^2 \, \mathcal{K}_{LL'} \, a_{L'}. \tag{4.2.9}$$

Note that now c_L depends explicitly upon the daughter spin J_d. There is no ambiguity in the tunnelling energy of the alpha particle because $J_d = J'_d$. In the next section we shall calculate anisotropies for the favoured decay of four actinide nuclei. Since these decays are to the ground state of rotational bands, we expect that the contribution of mixing from excited states of the daughter should be small, especially if their excitation energies are high. This is because the alpha particle is unlikely to tunnel through the barrier at a lower energy (where the extent of the barrier is greater) before coupling to the ground state. Thus we use Equation (4.2.9) with no mixing between daughter states during barrier penetration.

4.2.1 Experimental details

Before we go on to calculate theoretical anisotropies, we shall discuss some experimental details that are necessary to make comparisons with the data. There are four odd mass actinide nuclei for which experimentally measured anisotropies are quoted (Table 4.1). For two of these cases (^{241}Am and ^{253}Es) the experiments were performed in the early

1970's using the old techniques of low temperature nuclear orientation. In these experiments, the radioactive nuclei were dissolved in a saturated solution and applied to the face of the host crystal. This resulted in the nuclei being deeply embedded in the crystal, and made resolution of the alpha decay peaks more difficult. The fraction of implanted nuclei at "good sites" i.e. feeling the full strength of the magnetic field, was typically between 0.5 and 0.8 in such experiments. The other two anisotropies have been measured recently using on-line nuclear orientation, where the nuclei are implanted directly into the host material at low temperature. This method reduces the problem of deeply embedded nuclei, and therefore the resolution is improved. The fraction of good sites obtained in this way is typically > 0.95 [43].

The relevant equation to be used in an experimental situation is

$$W(\theta) = 1 + A_2 B_2 Q_2 P_2(\cos\theta) + A_4 B_4 Q_4 P_4(\cos\theta) + \ldots. \qquad (4.2.10)$$

The factor Q_L is an experimental correction taking into account the positioning and angular resolution of the detector. B_L are orientation parameters which also include the temperature dependence of the system. The experimentally determined quantity is actually fA_L, where f is the fraction of implanted nuclei that are in good sites. For comparison with theory, we must assume that $Q_L = f = 1$, which gives a least value for the anisotropy in two of the cases shown in Table 4.1. In the other two cases, the fraction of good sites has already been accounted for in the values of A_L quoted [44] and we include an experimental error.

4.2.2 Results and discussion

We shall now calculate the anisotropy for the favoured decay ($J_p = J_d = K$) of the four odd–even actinide nuclei in our mass region for which experimental data are available. For each nucleus we assume that the internal amplitudes are equal to those present in

the neighbouring even–even nucleus with one less nucleon. For the four cases considered here the odd nucleon is a proton, but in later work we treat cases with odd neutrons – our model is not dependent on whether the odd nucleon is a neutron or a proton.

The first three decays are all examples of $5/2 \rightarrow 5/2$ transitions and so can only proceed with $L = 0, 2$ or 4. The favoured decay of ^{253}Es is a $7/2 \rightarrow 7/2$ transition and so alpha particles with $L = 6$ are permitted. Since we find that the results are not very sensitive to variations in the internal amplitude for $L = 6$ we have taken $a_6 = 0$, but considered mixing of states up to and including $L = 6$ in the transmission matrix. We should also point out that the first two nuclei have non-zero values of the octupole deformation β_3, which we do not consider in our work[1]. Note that three of the nuclei are quoted to have anisotropies greater than one, the other having a value less than one. Although the prediction of anisotropies consistent with these experimental values is important, we are most concerned with reproducing the *trends* of the data.

First, we adopt Fröman's formula (4.2.8) for the transformation of amplitudes during barrier transmission and calculate anisotropies using Equation (4.2.1). From the results in Table 4.1, we see that this formula cannot predict anisotropies both greater than and less than one for these nuclei, for any of the four sets of amplitudes taken from Figure 3.12. This is because the sign of c_2/c_0 is either positive (anisotropy > 1, i.e. solutions (a) and (b)) or negative (anisotropy < 1, i.e. solutions (c) and (d)). We should point out here that in his original paper, Fröman did not explicitly use Equation (4.2.8) for the odd–A case. He obtained the external amplitudes c_L directly from the neighbouring even–even nuclei, by taking the (positive) square root of the experimental branching ratios. This is a more crude approximation than ours, i.e. in our work we calculate the transmission matrix using the correct energies for the odd–A nucleus. Even with these improvements

[1]Since our model assumes rotational nuclei, there may be some question concerning its use for nuclei with small deformations such as ^{221}Fr which may be interpreted as a vibrational nucleus.

Table 4.1: Anisotropies ($W(0)/W(\frac{1}{2}\pi)$) for the favoured decay of four odd–even nuclei, calculated using Fröman's formula (Equation (4.2.8)). The theoretical predictions (a) – (d) are obtained using the four sets of internal amplitudes from Section 3.4.

Parent	(a)	(b)	(c)	(d)	Experiment	Reference
^{221}Fr	3.90	3.90	0.15	0.15	0.37(2)	[44]
^{227}Pa	7.25	6.47	0.03	0.00	3.55(28)	[44]
^{241}Am	5.19	5.08	0.06	0.06	>2.7	[45]
^{253}Es	4.61	4.45	0.11	0.09	>3.8	[46]

Table 4.2: Anisotropies calculated as in Table 4.1 but using our formula (Equation (4.2.9)) to calculate the amplitudes c_L.

Parent	(a)	(b)	(c)	(d)	Experiment	Reference
^{221}Fr	2.11	2.11	0.73	0.73	0.37(2)	[44]
^{227}Pa	5.87	6.58	1.03	2.26	3.55(28)	[44]
^{241}Am	6.84	7.33	3.03	3.51	>2.7	[45]
^{253}Es	6.36	7.98	2.71	3.25	>3.8	[46]

to the model however, we have shown that the experimental trends are not reproduced. We conclude that Fröman's formula, which assumes the final states of the daughter to be degenerate, is not a good approximation for these odd–A decays.

Next we calculate anisotropies using our formula (4.2.9) and each of the four sets of amplitudes from the even–even case. Table 4.2 shows the results of our calculations. The values of the predicted anisotropies in cases (c) and (d) agree well with the experimental trends. In particular, we emphasize the prediction of anisotropies both less than and greater than one, i.e. it is possible to have a larger current density of alpha particles emitted along the symmetry axis than equatorially, despite the fact that $a_2 < 0$. The reason is that the outer amplitude c_2 may become positive, since the Clebsch–Gordan coefficients of Equation (4.2.9) attenuate the effect of the inner amplitude a_2. This effect is not possible if we use the amplitudes from Figure 3.12 (a) or (b), or if we adopt Fröman's formula. It would also not be possible if we employed the solutions of Poggenburg *et al.* [38] discussed in Section 3.4. Since these amplitudes have phases similar to those in Figure 3.12 (a), they would give anisotropies greater than one for all nuclei and so would not reproduce the experimental trends.

We have checked the sensitivity of the result for one nucleus to variations in the Woods-Saxon parameters V_0 and d. We see from Figure 4.3 that the value of the anisotropy for ^{241}Am with internal amplitudes from Figure 3.12 (d) is more sensitive to changes in V_0 than d, but still not enough to alter the trends of our results.

Delion *et al.* have also calculated theoretical anisotropies for two of these nuclei. In their work they calculate the formation amplitudes microscopically for each partial wave and use Fröman's transmission matrix for the barrier penetration. For the favoured decay of ^{241}Am, using slightly different deformation parameters and assuming full alignment of the parent nucleus, they obtain a value of $W(0)/W(\frac{1}{2}\pi) = 2.04$ [13]. Because Fröman's transmission matrix cannot change the sign of the $L = 2$ amplitude during barrier

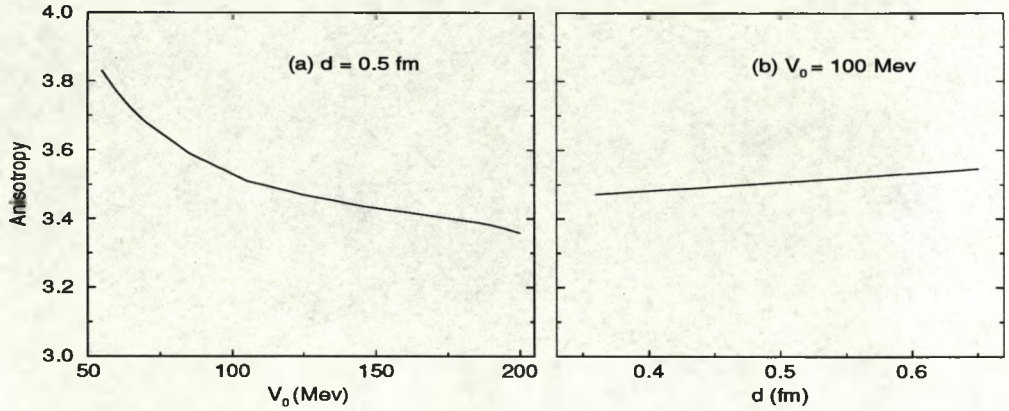

Figure 4.3: Sensitivity of the calculated anisotropy of ^{241}Am to variations in the Woods-Saxon parameters; (a) the depth of the potential V_0 and (b) the diffuseness d. Internal amplitudes are taken from Figure 3.12 (d).

transmission, to get this result the value of a_2 had to be positive. If we use the same deformation parameters, our simple model with $a_2 < 0$ gives $W(0)/W(\frac{1}{2}\pi) = 3.42$. (These deformation parameters correspond to those of the parent nucleus rather than the daughter as we have assumed in our work.) For the favoured transition of ^{221}Fr, Delion *et al.* calculate an anisotropy of 0.63 [15]. To obtain this anisotropy with Fröman's transmission matrix the value of a_2 had to be negative. Using the same quadrupole deformation of $\beta_2 = 0.069$, our model gives a value of 0.89. So to reproduce these two anisotropies Delion *et al.* had to employ different values of a_2, whereas our model can reproduce the experimental trends from one set of internal amplitudes. We notice also that the anisotropy of ^{221}Fr is quoted both experimentally and theoretically to be less than one, even though β_2 is positive. This contradicts the general statement by Delion

et al. that prolate nuclei should have anisotropy greater than one [15]. It has also been discussed in Ref. [10] that the sign of β_2 does not necessarily determine whether the anisotropy is greater than or less than one.

Equation (4.2.9) was derived by assuming that there is no mixing between different daughter states during barrier transmission. This assumption is good if the excitation energies of the higher states are large. However, the excited states of the daughter nuclei we have considered lie at relatively low energies and so we must check that our approximation is valid. We have considered the decay of ^{241}Am again and used Equation (4.2.7) which allows mixing between all daughter states. In the semi-classical formalism, we are forced to choose a single energy for the alpha particle during tunnelling. If we adopt the same approach as for the even–even nuclei and assume that the alpha particle tunnels with its final state energy J_d, Equation (4.2.7) is equal to Fröman's formula since the sum over J'_d can be done. The appropriate anisotropy with mixing included and amplitudes from Figure 3.12 (d) is therefore 0.06 (from Table 4.1). This value is obviously very different from that given in Table 4.2 and is not at all consistent with experimental data. The mixing of daughter states under the barrier therefore does have a large effect on the anisotropy and cannot be neglected due to energy considerations.

However, the success of Equation (4.2.9) does seem to suggest that some other mechanism is present which prevents, or at least weakens coupling between different states of the daughter. The reasons for this diminished coupling in odd mass nuclei are not yet clear. One possible reason could be related to our assumptions about the odd nucleon: we have assumed that its projection K on the body-fixed axis does not change, and that it has no interaction with the alpha particle. So when the core rotates, the odd nucleon must rotate with it in order to maintain the same projection K. It is possible that this restriction in some way reduces the probability of coupling between different daughter states during barrier transmission. An explanation related to the behaviour

of the odd nucleon would be capable of accounting for the good results obtained for odd mass nuclei and still allow all daughter states to mix for even–even decays. Another possibility could be related to the time taken for the alpha particle to tunnel through the barrier. This time is believed to be $\approx 10^{-22}$ s [24], whereas the time taken for the core to rotate is $\approx 10^{-20}$ s ([40], page 116). The alpha particle therefore does not have time to re-orientate, and hence excite, the daughter. Of course, this argument would not apply to energetic nuclei with high spin for which the rotation time would be much smaller. It is also not clear why this argument would not also prevent coupling in even–even decays.

Although we are only aware of four nuclei in the mass range for which quantitative angular distribution information has been obtained experimentally, there exists a good deal of data on level schemes and energies for other nuclei. We have therefore made predictions of the anisotropy of favoured decays for all other odd–A nuclei in the mass range for which we have data. The results are shown in Table 4.3. In all cases we have adopted Equation (4.2.9) and internal amplitudes from Figure 3.12 (d). We find that our model predicts anisotropies greater than one for all these actinide nuclei. Although there are several parameters which vary from nucleus to nucleus, the results show evidence of an increase in anisotropy with J_p, in agreement with Ref. [29]. Experiments have been performed to measure the angular distribution of alpha particles from two of these nuclei, ^{237}Np [47] and ^{249}Cf [48]. Although no absolute values of anisotropy were obtained in either case, the preferential direction of emission was established. In both decays, it was found that emission took place mainly from the poles of the nucleus, and hence anisotropy should be greater than one as we have predicted.

Table 4.3: Anisotropies ($W(0)/W(\frac{1}{2}\pi)$) for the favoured decay of odd–A nuclei, calculated using Equation (4.2.9) which assumes no mixing between daughter states during barrier transmission. These predictions are obtained using internal amplitudes from Figure 3.12 (d).

Parent	J_p	β_2	Anisotropy
^{229}U	3/2	0.165	2.07
^{251}Es	3/2	0.235	2.16
^{233}U	5/2	0.190	3.74
^{237}Np	5/2	0.207	4.14
^{241}Pu	5/2	0.207	3.96
^{243}Cm	5/2	0.223	3.58
^{245}Cm	7/2	0.224	3.39
^{247}Cf	7/2	0.234	3.84
^{247}Es	7/2	0.234	3.63
^{249}Bk	7/2	0.224	3.31
^{249}Cf	9/2	0.234	3.56

4.3 Branching ratios

The calculation of branching ratios is more complicated than that of anisotropies, since we must consider the decay to a larger number of daughter energy levels. To specify the state of the emitted alpha particle uniquely we must label it with both the daughter and alpha particle angular momenta $\{J_d L\}$. For the $J_p = 5/2^+$ decay illustrated in Figure 4.1, there are nine possible final states to be considered. If we were to allow mixing between all nine states our transmission matrix $\mathcal{K}_{LL'}$ would therefore have 9×9 non-zero elements. We have shown in the previous section however that better results are obtained if we do not allow mixing between different daughter states J_d during barrier transmission, only between orbital angular momentum states L within each J_d. We shall make the same assumption in the calculation of branching ratios, which leads to a transmission matrix with three 3×3 blocks of non-zero elements.

We shall now derive an expression for the branching ratios from the wave function in Equation (4.1.9). The first few steps are the same as in Section 4.2, squaring the wave function and integrating over all orientations of the daughter. In this case, however, we must retain the sum over J_d because we are looking at more than one daughter state. Taking Equation (4.2.1) and integrating over all angles $\hat{\mathbf{r}}$, the spherical harmonics simplify and the sum over m can be done. We are left with the following formula

$$\left|\Phi_{MK}^{J_p}\right|^2 = \sum_{J_d L} c_L^2 \, \langle J_p L K 0 | J_d K \rangle^2 \tag{4.3.1}$$

from which we can deduce the branching ratios to each daughter state

$$Z_{J_d} = \frac{\sum_L \mid c_L \, \langle J_p L K 0 | J_d K \rangle \mid^2}{\sum_{L J_d} \mid c_L \, \langle J_p L K 0 | J_d K \rangle \mid^2}. \tag{4.3.2}$$

We have calculated branching ratios for all odd–A actinide nuclei in the mass range for which data on rotational daughter states are available. We use Equation (4.2.9) to calculate the external amplitudes, taking internal amplitudes for the even–even core from

Table 4.4: Branching ratios for a range of odd–A actinide nuclei, calculated using Equation (4.2.9) which assumes no mixing between daughter states during barrier transmission, and Equation (4.3.2) with internal amplitudes from Figure 3.12 (d).

Parent	J_p	J_d	Theory	Experiment
^{229}U	3/2	3/2	88.6	64.0
		5/2	9.7	20.0
		7/2	1.7	11.0
^{233}U	5/2	5/2	85.5	84.4
		7/2	14.3	13.2
		9/2	0.2	1.6
^{239}Pu	1/2	1/2	76.9	73.1
		3/2	7.9	15.0
		5/2	15.2	11.8
^{241}Pu	5/2	5/2	82.7	83.2
		7/2	17.2	12.2
		9/2	0.1	1.2
^{241}Am	5/2	5/2	84.3	85.2
		7/2	15.5	12.8
		9/2	0.2	1.4

Parent	J_p	J_d	Theory	Experiment
^{241}Cm	1/2	1/2	76.3	68.9
		3/2	8.1	18.1
		5/2	15.7	11.8
^{243}Am	5/2	5/2	86.6	87.9
		7/2	13.3	10.7
		9/2	0.2	1.1
^{243}Cm	5/2	5/2	85.3	72.9
		7/2	14.6	11.5
		9/2	0.2	1.6
^{251}Es	3/2	3/2	76.3	81.0
		5/2	15.7	9.4
		7/2	8.1	3.0

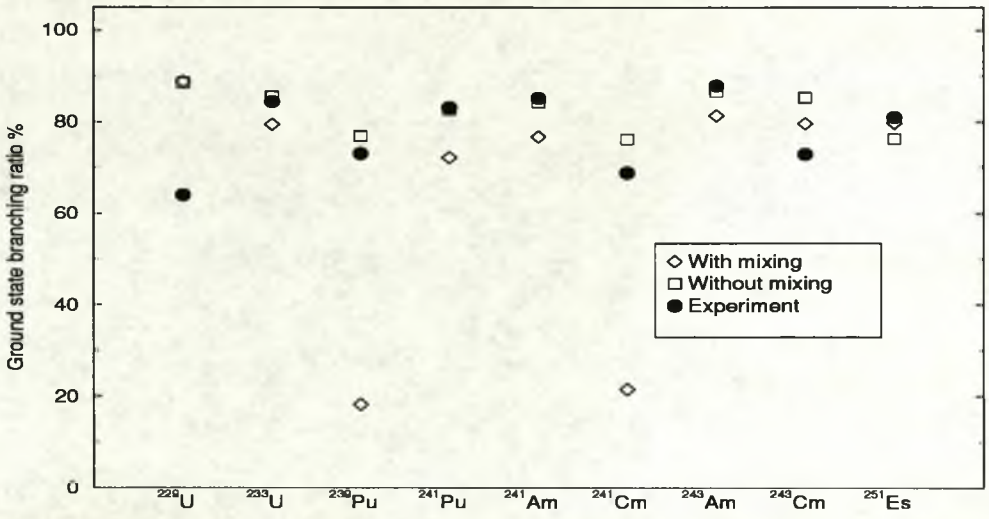

Figure 4.4: Calculated branching ratios to the ground state of odd–A actinide nuclei, using Equation (4.3.2). We show our results in the two cases, with and without mixing between different daughter states J_d during barrier transmission.

Figure 3.12 (d). The results are shown in Table 4.4. Considering the approximations and assumptions involved in this work, the agreement with experiment is quite good. We have also looked at the results obtained by allowing mixing between all daughter states during barrier transmission – they are generally not as good as those in Table 4.4. Figure 4.4 shows the branching ratio to the ground state of each nucleus in the two cases, with and without mixing between daughter states. The branching ratios obtained with mixing included are generally smaller than those without mixing. This is because the relative signs of the internal amplitudes ensure that mixing between daughter states takes more intensity away from the ground state than it adds in. We note that for the $J_p = 1/2$ nuclei in particular, the mixing gives far too much weighting to the excited states of the daughter. These nuclei are different in that there is only one possible

alpha particle angular momentum L for each state of the daughter, and so one might expect them to behave more like even–even nuclei. In the even–even case, we consider mixing between all daughter levels so it is possible that this should also be applicable to the $J_p = 1/2$ nuclei. The poor results, however, seem to support the idea that mixing between different daughter states under the barrier is prohibited for odd–A nuclei.

4.4 Anisotropy of Astatine isotopes

Experiments have recently been performed [43, 49, 50] to measure the anisotropy of the favoured alpha decay of a chain of astatine isotopes, which all have $J_p = J_d = 9/2$. The mass region observed is $199 \leq A \leq 211$ for which the daughter nuclei are believed to be almost spherical in shape. Note that for the final isotope in the sequence, the neutron number is $N = 126$ which corresponds to a closed shell. It is found that the anisotropy varies quite smoothly with mass number for this astatine chain (see Table 4.5).

A number of explanations of this variation have been proposed. Delion *et al.* [15] believe that alpha decay anisotropy is predominantly due to the effects of the deformed barrier, and therefore suggest a strong variation in quadrupole deformation over these isotopes. Berggren [12] takes the opposite point of view that the deformed barrier has very little effect and that the variations must reflect structural changes. He uses a quadrupole-quadrupole interaction similar to that defined in Section 3.2, which produces different solution numbers corresponding to different energy states of the parent nucleus. To reproduce the experimental data there must be a shift in solution number from nucleus to nucleus. This is explained as a consequence of a Pauli blocking mechanism as more neutrons are added to the system. Schuurmans *et al.* [50] also decide upon structural changes as the most likely explanation; since these nuclei are believed to be nearly spherical it is unlikely that barrier deformation is an important effect in this

mass region. To reinforce this point, the authors point out that since the anisotropy increases with increasing mass number, the explanation of Delion *et al.* would require the quadrupole deformation also to be increasing with increasing A. It is unlikely that the deformation would be increasing as one approaches the closed shell at $N = 126$. In this section we aim to find evidence to decide between these explanations of the anisotropy variations.

Obviously this mass range is well outside that which we have investigated in the previous sections but our technique may still be applied, although we realise that for these nearly spherical nuclei a rotational model may not be applicable. According to Ref. [19], these isotopes all have $\beta_2 < 0$ which indicates an oblate shape – all nuclei previously considered have been prolate. It is important to note that the experimental anisotropies are greater than one for some of the nuclei (Table 4.5) even though they are all oblate. This again shows that there is no general relationship between the value of anisotropy and the sign of β_2.

We find that alpha decays to the neighbouring even–even nuclei in this region take place almost always to the $L = 0$ state of the daughter, with a very small percentage to the first excited state. Consequently, there is very little available data for the energy of the $L = 2$ state of the daughter, and no data at all for the $L = 4$ state in most cases. We have therefore tried two approaches to fit the experimental anisotropies.

First, we assume that the internal amplitudes in the even–even case are zero for all partial waves other than $L = 0$ (i.e. $a_0 = 1, a_2 = 0$ etc.). Since the nuclei are known to be nearly spherical and branching ratios to the $L = 0$ state of the daughter are $\approx 100\%$ for all nuclei, this seems to be a reasonable assumption. We then calculate anisotropies for the favoured decay of each isotope using Equation (4.2.1) and Equation (4.2.9). From the results in Table 4.5 (a), we see that this simple idea does not reproduce the experimental anisotropies. If we had assumed a spherical barrier in this calculation, the anisotropies

would all have been equal to one. The deviation from unity therefore reflects the effects of the deformed barrier and we see that these effects are significant, even for these nuclei where β_2 is relatively small.

Secondly, we take one nucleus (^{203}At) and fit the internal amplitudes to reproduce the experimental anisotropy. These amplitudes ($a_0 = 1$, $a_2 = 0.3$, $a_4 = a_6 = a_8 = 0$) are then used to predict values for all other isotopes and the results are given in Table 4.5 (b). We note that the positive value of a_2 can lead to anisotropies both greater than and less than one, even though all nuclei have the same sign quadrupole deformation parameter. This again shows the importance of the Clebsch-Gordon coefficients in Equation (4.2.9). However, the magnitudes of the anisotropies are not consistent with the experimental values.

Thus we find that the results are not very good in either approach. In both cases we have assumed that the internal amplitudes are constant for all isotopes so that the variations seen are due simply to barrier penetration effects. The results clearly show that the variations in anisotropy found experimentally are not just a consequence of barrier effects, but must reflect changes in nuclear structure as well.

We shall now investigate the sensitivity of the anisotropy of one of these nuclei to changes in the internal amplitudes. The calculations have been done using ^{207}At as a model nucleus, and the results are shown in Figure 4.5. We find that the anisotropy is very sensitive to the value of the internal amplitude a_2, but that variations in a_4 have a relatively minor effect. We assume that a_L with $L \geq 6$ will also have little effect on the anisotropies.

We also find that the value of the deformation parameter β_2 is very important. Figure 4.6 shows the anisotropy for ^{207}At as a function of β_2, as well as results for the same nucleus calculated by Delion *et al.* [15]. The results are not exactly comparable because of the difference in internal amplitudes a_L between the two approaches – we have

Table 4.5: Anisotropies for the favoured decay ($J_p = J_d = 9/2$) of a chain of astatine isotopes, together with data used in the calculation for the energy of the alpha particle and quadrupole deformation of the daughter. The theoretical calculations correspond to two different assumptions for internal even–even amplitudes, (a) $a_0 = 1,\ a_2 = a_4 = a_6 = a_8 = 0$, and (b) $a_0 = 1,\ a_2 = 0.3,\ a_4 = a_6 = a_8 = 0$. Experimental data are taken from Ref. [50].

Parent	E_α (MeV)	β_2	(a)	(b)	Experiment
^{211}At	5.870	-0.026	0.79	1.17	1.59(3)
^{209}At	5.647	-0.035	0.73	1.09	1.41(2)
^{207}At	5.785	-0.035	0.70	1.10	1.26(2)
^{205}At	5.902	-0.044	0.67	1.02	1.10(1)
^{203}At	6.088	-0.044	0.67	1.02	1.02
^{201}At	6.344	-0.052	0.63	0.96	0.89
^{199}At	6.643	-0.052	0.63	0.96	0.79(1)

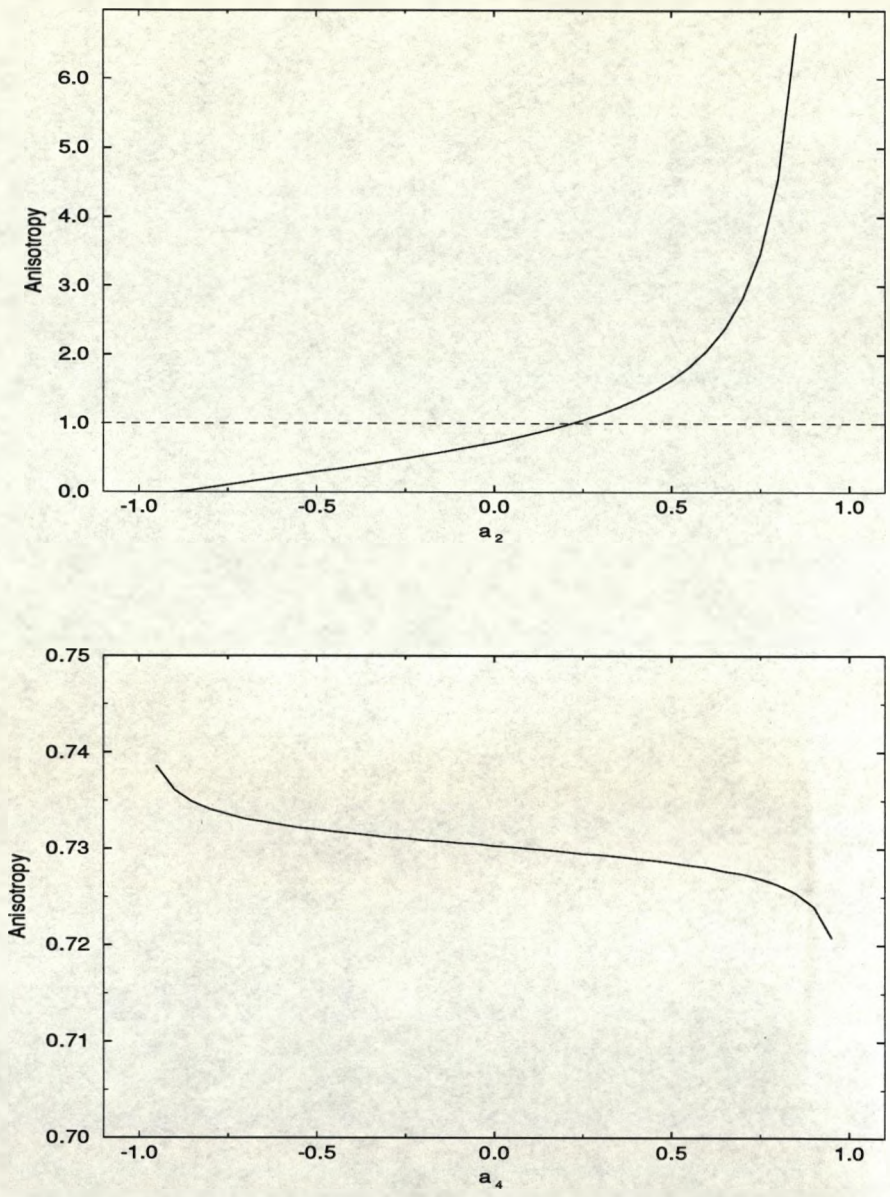

Figure 4.5: Sensitivity of the anisotropy of ^{207}At to the values of the internal amplitudes. In the upper graph, we have assumed $a_0 = \sqrt{(1 - a_2^2)}$ and all other amplitudes equal to zero. In the lower graph $a_0 = \sqrt{(1 - a_4^2)}$ and again all other amplitudes equal zero.

assumed only $L = 0$ alpha particles at the nuclear surface, while Delion *et al.* calculate a_L microscopically for each value of β_2. Even so, the results are in good agreement for $\beta_2 < 0$ which is the region of importance for this particular nucleus. Our method seems to predict a far greater sensitivity for $\beta_2 > 0$ though. Similar investigations by Berggren [12] produce very different results from those shown in Figure 4.6. He finds that the anisotropy is very sensitive to variations in β_2 at values close to zero, but fairly insensitive as its value increases.

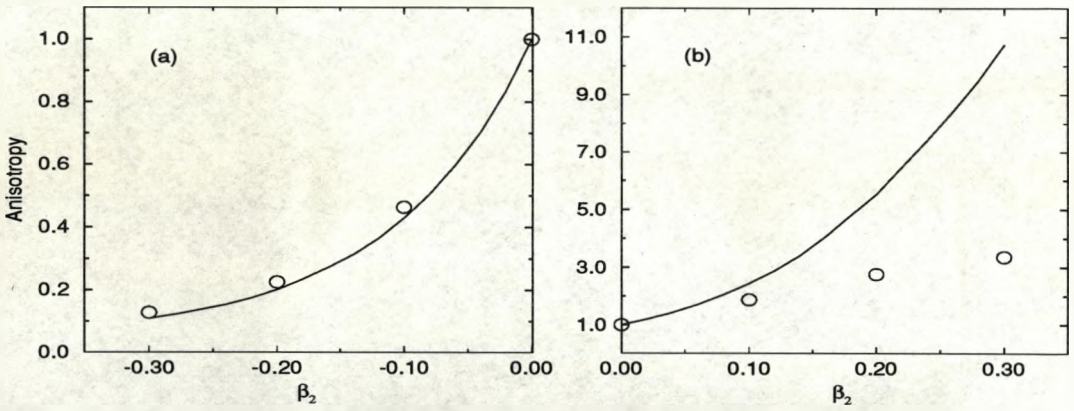

Figure 4.6: Sensitivity of the anisotropy of ^{207}At to the value of β_2, with $\beta_4 = \beta_6 = 0$. We assume internal amplitudes of $a_0 = 1, a_2 = a_4 = a_6 = a_8 = 0$. The results of our calculations are shown as solid lines for (a) $\beta_2 < 0$ and (b) $\beta_2 > 0$. The circles represent anisotropies for the same nucleus calculated by Delion *et al.* [15].

These results indicate that the most important factor in the variation of anisotropy of astatine isotopes is the value of a_2, i.e. structure effects. We therefore agree most closely with the opinions of Schuurmans *et al.* [50] who also believe that the variation of anisotropy in this chain of astatine isotopes is due to structure effects. Since the nuclei considered have neutron numbers close to $N = 126$, it is likely that the structure of these isotopes is changing rapidly as N changes. We do not believe, however that the effects of barrier deformation are negligible, they are only small in this mass region where the nuclei are nearly spherical. For nuclei with appreciable deformations such as those considered in Section 4.2.2 the effects of barrier deformation are at least equally as important as structure effects. Indeed, further away from closed shells, one might expect the structure of a chain of isotopes to vary much less.

Chapter 5

Summary and Conclusions

We have derived a transmission matrix $\mathcal{K}$ which may be applied to a barrier of any shape. The matrix is a more general form of that derived by Fröman in 1957, including higher order deformed Coulomb terms, a realistic Woods-Saxon potential and considering excitation energies of the daughter nucleus. Comparisons have been made between our results and those of Fröman in a number of calculations. We find that in some cases the extra accuracy of our matrix makes little difference to results e.g. in the calculation of branching ratios where it is the relative values of the alpha particle amplitudes that are important. However, in quantities depending upon the absolute values such as decay widths, we find that the more detailed matrix increases values by over an order of magnitude. The use of our matrix in Refs. [13] and [16] for example may therefore go part of the way to resolving differences between experimental and theoretical absolute decay widths. The technique may be of use in barrier penetration problems other than alpha decay e.g. in sub-barrier fusion and proton radioactivity. There is also no limit on the quadrupole deformation of nuclei that may be treated in this way – barrier problems in superdeformed or hyperdeformed nuclei may be considered.

The accuracy of the semi-classical transmission matrix has been confirmed by comparison with results from the numerical integration of the exact coupled channels equations. The only major difference between the two approaches seems to lie in the contribution of imaginary parts in the wave function. In the semi-classical approximation we consider only real wave functions, although it would be possible to extend this work and include imaginary parts if required.

In Chapter 3, we tested several models to explain the alpha decay process by calculating relative amplitudes near the nuclear surface and comparing their predictions with experimental data. One particularly interesting idea was that the alpha decay process could be explained in terms of eigenchannels, as has been done for fusion. In the latter case, the different eigenchannels correspond to barriers of different shape and height. In the alpha decay problem the dimensions of the barrier are fixed by the potentials in the model, so we define the different channels to correspond to different outgoing currents. We tested the idea that the physical channel taken by the alpha particle is that which maximizes the outgoing flux by exploiting the effects of the deformed barrier. Despite its appeal, this idea does not reproduce the experimental branching ratios for a range of even–even actinide nuclei. However, we have shown that the eigenchannel formalism used in fusion may be extended to apply to any barrier penetration problem with any shape of barrier or potential.

In an attempt to resolve the many differing ideas about alpha particle formation and interaction with the daughter nucleus, we made use of our semi-classical transmission matrix and experimental branching ratios and calculated internal amplitudes for a range of even–even actinide nuclei. We are not aware of any previous systematic study of actinide nuclei using experimental data and realistic deformation parameters. By making some assumptions about the asymptotic phases of the wave functions, we found four possible solutions of internal amplitudes that are consistent with the experimental data.

One of these solutions predicts almost constant amplitudes across the range of actinide nuclei. We confirmed that this solution is not a particular result of the form of our transmission matrix by comparing results with those using Fröman's matrix and with the coupled channels calculations. The error bars arising from experimental uncertainty in the branching ratios are negligible for most nuclei. We also checked that the amplitudes are not especially sensitive to the exact values of the deformation parameters taken from Ref. [19], or any other parameters in our model.

Although this constant solution is appealing, we have no way of establishing if these are the "physical" amplitudes. It is not possible to determine the relative phases of the amplitudes experimentally because the angular distribution of emitted alpha particles from an even–even nucleus is isotropic. The model of an alpha particle moving in a deformed field does not seem capable of explaining any of the four solutions found for the amplitudes near the nuclear surface. However, the model of an alpha particle being projected from pair correlated neutron and proton Nilsson-model states does seem to be consistent with the constant solution. The conclusion of our work in Chapter 3 therefore is that the constant solution, as well as being appealing by its very nature is the most likely solution and suggests that a microscopic model of alpha decay similar to that of Delion *et al.* is the most realistic model for this mass region.

Our work on odd mass nuclei tested a number of ideas. First of all, it has been found previously that good results may be obtained by assuming that the structure of the odd–A nucleus is closely related to that of the neighbouring even–even one. By assuming a model of this type we have been able to make use of the results of our work on even–even nuclei. We have also investigated the dependence of alpha decay anisotropy on nuclear deformation and nuclear structure, which is currently a matter of great interest.

Before drawing conclusions on the work contained in Chapter 4, we shall summarize the assumptions and approximations made in the odd–A case:

1. The odd mass nucleus consists of an even–even core plus an odd nucleon, which has no effect on the alpha decay process. Internal amplitudes for the core are taken to be those present in the neighbouring even–even nucleus (only states up to $L = 4$ considered).

2. The parent nucleus is fully aligned and therefore has $M = J_p$. This assumption simplifies our expression for the angular distribution $W(\theta)$ and corresponds to idealized experimental conditions.

3. There is no mixing between different energy levels of the daughter nucleus during barrier transmission, only between orbital angular momentum states within each daughter level.

4. We have not considered the octupole deformation parameter β_3 in this work. The semi-classical transmission matrix could be extended to account for β_3 and its importance established.

For odd–A nuclei in the same mass range as the even–even ones in Chapter 3, we assumed that the relevant amplitudes for the even–even core are those taken from the constant solution in Figure 3.12. The results obtained are in good agreement with the experimental trends, considering the assumptions made above. Further, we find that the amplitudes taken from the constant solution reproduce the experimental data more closely than any of the other solutions. The physical reason for assumption 3 above is not yet clear, although we have discussed some possible explanations. It is likely that the solution of coupled channels equations for odd mass nuclei may help in understanding the dynamics involved.

We emphasize here that these conclusions are only true if we consider the effects of the deformed barrier. If we assumed a spherical barrier for these odd mass nuclei,

the experimental trends could not be reproduced for any of the four solutions found in Chapter 3. Indeed throughout this thesis we have shown that the effects of the deformed barrier are important in all our calculations.

We have investigated the anisotropy of the favoured decay for a chain of astatine isotopes outside the mass range considered in Chapter 3. Our model does not reproduce experimentally measured anisotropies for these nuclei. It is possible that these nuclei are not so closely related to their even–even neighbours that assumption 1 above is valid. We also note that our model of alpha decay assumes rotational rather than vibrational states of the nuclei, which may not be valid for these astatine isotopes. However, our general investigation of the sensitivity of anisotropy to changes in deformation and structure produced some interesting results. We find that both factors are important in the calculation, and our viewpoint therefore lies between that of Delion *et al.* and Berggren who take opposite points of view. It seems that the anisotropy is mainly determined by nuclear structure before the barrier penetration takes place, although even for these nearly spherical nuclei the effect of the deformed barrier is certainly not negligible. For these astatine isotopes, we conclude that structural changes are most likely to be responsible for variations in anisotropy. We stress however that in the actinide region where the quadrupole deformation is much larger, the effects of the deformed barrier are much more important and in our work the experimental trends would not be reproduced if the barrier was considered to be spherical.

Appendix A

Even–even data

Here we present all data and parameters used in our calculations on even–even nuclei. Table A.1 shows branching ratios Z_L with their errors in brackets, and energies E_L for the daughter states of each nucleus up to $L = 4$. These data are all taken from the relevant Nuclear Data Sheets. In Table A.2 we show the daughter deformation parameters β_L which are taken from the compilation by Möller *et al.* [19]. Also given are values of the expansion coefficients in the deformed Coulomb potential, relative to the monopole term V_1 which are defined in Equation (2.4.3). We quote values of the alpha decay half-life $\tau_{1/2}$, which are deduced from the partial half-lives given in Ref. [9].

Table A.1:

Z_d	A_d	Z_0	Z_2 (%)	Z_4	E_0	E_2 (MeV)	E_4
88	220	79.0 (2.0)	19.0 (2.0)	1.20 (0.40)	7.1700	6.9970	6.7060
88	222	75.5 (3.0)	22.8 (2.0)	1.27 (0.05)	6.3375	6.2283	6.0414
88	224	71.1 (1.0)	28.2 (1.0)	0.44 (0.08)	5.4233	5.3405	5.1770
88	226	76.3 (0.3)	23.4 (0.1)	0.12 (0.00)	4.6876	4.6211	4.4798
88	228	77.8 (1.4)	22.1 (1.4)	0.06 (0.01)	4.0100	3.9520	3.8300
90	224	70.0 (0.0)	29.0 (0.0)	0.56 (0.00)	6.6810	6.5890	6.4040
90	226	67.4 (0.4)	32.0 (0.2)	0.38 (0.04)	5.8887	5.8178	5.6663
90	228	68.0 (0.4)	31.7 (0.4)	0.30 (0.02)	5.3203	5.2635	5.1367
90	230	71.4 (0.2)	28.4 (0.1)	0.20 (0.01)	4.7761	4.7238	4.6049
90	232	74.0 (4.0)	26.0 (4.0)	0.26 (0.01)	4.4940	4.4450	4.3320
90	234	78.8 (2.7)	21.2 (2.7)	0.08 (0.00)	4.1960	4.1470	4.0390
92	232	69.3 (0.5)	30.6 (0.5)	0.18 (0.00)	5.7677	5.7210	5.6138
92	234	71.0 (0.0)	28.8 (0.1)	0.10 (0.00)	5.4992	5.4565	5.3583
92	236	72.8 (0.1)	27.1 (0.1)	0.09 (0.00)	5.1682	5.1237	5.0218
92	238	77.5 (3.0)	22.4 (2.0)	0.10 (0.02)	4.9006	4.8564	4.7546
94	236	71.0 (0.6)	28.9 (0.6)	0.05 (0.00)	6.2906	6.2478	6.1470
94	238	74.0 (0.5)	25.0 (0.5)	0.04 (0.00)	6.1129	6.0696	5.9694
94	240	76.4 (0.2)	23.6 (0.2)	0.02 (0.00)	5.8050	5.7628	5.6656
94	244	81.9 (0.4)	18.0 (0.2)	0.08 (0.12)	5.0785	5.0349	4.9311
96	242	79.3 (1.0)	20.6 (1.0)	0.15 (0.02)	6.7501	6.7086	6.6156
96	246	84.6 (1.2)	15.1 (1.2)	0.30 (0.00)	6.0310	5.9889	5.8913
96	248	84.2 (0.3)	15.7 (0.3)	0.24 (0.04)	6.1184	6.0756	5.9771

Table A.2:

Z_d	A_d	β_2	β_4	β_6	V_3/V_1 (fm^2)	V_5/V_1 (fm^4)	$\tau_{1/2}$ (s)
88	220	0.103	0.072	0.007	3.703	185.256	0.1027E+01
88	222	0.130	0.092	0.008	4.856	255.541	0.1888E+04
88	224	0.164	0.112	0.010	6.373	343.688	0.6034E+08
88	226	0.172	0.112	0.007	6.709	352.035	0.2365E+13
88	228	0.180	0.113	0.005	7.063	364.563	0.4389E+18
90	224	0.164	0.112	0.010	6.373	343.688	0.5600E+03
90	226	0.173	0.111	0.034	6.881	379.029	0.1820E+07
90	228	0.182	0.112	0.025	7.239	385.874	0.2195E+10
90	230	0.198	0.115	0.014	7.901	404.874	0.7975E+13
90	232	0.207	0.108	0.003	8.178	384.532	0.7400E+15
90	234	0.215	0.102	-0.007	8.437	367.095	0.1386E+18
92	232	0.207	0.117	0.010	8.311	421.128	0.8853E+08
92	234	0.215	0.110	0.000	8.554	400.331	0.2792E+10
92	236	0.215	0.102	-0.008	8.471	369.249	0.2058E+12
92	238	0.215	0.093	-0.015	8.391	336.762	0.1170E+14
94	236	0.215	0.110	-0.004	8.573	399.013	0.2330E+07
94	238	0.215	0.102	-0.012	8.491	367.875	0.1406E+08
94	240	0.223	0.087	-0.021	8.679	323.393	0.5730E+09
94	244	0.224	0.062	-0.027	8.550	247.350	0.1051E+14
96	242	0.224	0.079	-0.024	8.673	299.472	0.1248E+06
96	246	0.234	0.057	-0.032	8.941	239.110	0.4140E+09
96	248	0.235	0.040	-0.036	8.869	186.959	0.8160E+08

Appendix B

Odd–A data

All data given in Table B.1 are extracted from the relevant Nuclear Data Sheets, except for deformation parameters which are again taken from the compilation by Möller *et al.*. We note here that Ref. [19] quotes non-zero values of the octupole deformation β_3 for many of these odd mass nuclei, but we do not include this parameter in our work.

Table B.1:

Z_d	A_d	β_2	β_4	β_6	J_p	J_d		
						E_α	(MeV)	
217	85	0.039	0.028	0.007	$5/2^-$	$5/2^-$		
						6.126		
223	89	0.147	0.110	0.010	$5/2^-$	$5/2^-$		
						6.466		
225	90	0.165	0.112	0.010	$3/2^+$	$3/2^+$	$5/2^+$	$7/2^+$
						6.360	6.332	6.297
229	90	0.190	0.114	0.020	$5/2^+$	$5/2^+$	$7/2^+$	$9/2^+$
						4.824	4.784	4.729
237	92	0.207	0.117	0.010	$5/2^+$	$5/2^+$	$7/2^+$	$9/2^+$
						4.896	4.853	4.798
237	93	0.215	0.102	-0.009	$5/2^-$	$5/2^-$	$7/2^-$	$9/2^-$
						5.486	5.443	5.388
239	93	0.223	0.095	-0.018	$5/2^-$	$5/2^-$	$7/2^-$	$9/2^-$
						5.275	5.233	5.181
239	94	0.223	0.095	-0.018	$5/2^+$	$5/2^+$	$7/2^+$	$9/2^+$
						5.785	5.742	5.686

Z_d	A_d	β_2	β_4	β_6	J_p	J_d		
						E_α (MeV)		
241	94	0.224	0.079	-0.024	$7/2^+$	$7/2^+$		
						5.362		
243	96	0.234	0.073	-0.030	$7/2^+$	$7/2^+$		
						6.296		
243	97	0.234	0.073	-0.029	$7/2^+$	$7/2^+$		
						7.323		
245	95	0.224	0.062	-0.028	$7/2^+$	$7/2^+$		
						5.417		
245	96	0.234	0.064	-0.031	$9/2^-$	$9/2^-$		
						5.813		
247	97	0.235	0.057	-0.034	$3/2^-$	$3/2^-$	$5/2^-$	$7/2^-$
						6.492	6.462	6.422
249	97	0.235	0.040	-0.037	$7/2^+$	$7/2^+$		
						6.633		

Bibliography

[1] G. Gamow, Z. Phys. **51** (1928) 204.

[2] E. U. Condon and R. W. Gurney, Phys. Rev. **33** (1929) 127.

[3] M. A. Preston and R. K. Bhaduri, *Structure of the nucleus*, Chapter 11 (Addison-Wesley, Massachusetts, 1975).

[4] D. L. Hill and J. A. Wheeler, Phys. Rev. **89** (1953) 1102.

[5] P. O. Fröman, Mat. Fys. Skr. Dan. Vid. Selsk. **1** (1957) 1.

[6] B. Buck, A. C. Merchant and S. M. Perez, Phys. Rev. Lett. **65** (1990) 2975; B. Buck, A. C. Merchant and S. M. Perez, J. Phys. G **17** (1991) 1223.

[7] B. Buck, A. C. Merchant and S. M. Perez, J. Phys. G **18** (1992) 143.

[8] B. Buck, A. C. Merchant and S. M. Perez, Phys. Rev. C **45** (1992) 2247.

[9] B. Buck, A. C. Merchant and S. M. Perez, Atomic Data and Nuclear Data Tables **54** (1993) 54.

[10] T. Berggren, Phys. Lett. B **197** (1987) 1.

[11] T. Berggren and P. Olanders, Nuc. Phys. A **473** (1987) 189.

[12] T. Berggren, Hyperfine Interactions **43** (1988) 407;
T. Berggren, Hyperfine Interactions **75** (1992) 401.

[13] D. S. Delion, A. Insolia and R. J. Liotta, Phys. Rev. C **46** (1992) 884.

[14] D. S. Delion, A. Insolia and R. J. Liotta, Phys. Rev. C **46** (1992) 1346.

[15] D. S. Delion, A. Insolia and R. J. Liotta, Phys. Rev. C **49** (1994) 3024.

[16] H. J. Mang, Ann. Rev. Nucl. Sci. **14** (1964) 1.

[17] T. L. Stewart, M. W. Kermode, D. J. Beachey, N. Rowley, I. S. Grant and A. T. Kruppa, Phys. Rev. Lett. **77** (1996) 36.

[18] T. L. Stewart, M. W. Kermode, D. J. Beachey, N. Rowley, I. S. Grant and A. T. Kruppa, *submitted for publication.*

[19] P. Möller, J. R. Nix, W. D. Myers and W. J. Swiatecki, Atomic Data and Nuclear Data Tables **59** (1996) 185.

[20] E. Anderson, *Modern physics and quantum mechanics*
(W. B. Saunders Company, Philadelphia, 1971).

[21] L. I. Schiff *Quantum mechanics*, Third edition
(McGraw-Hill, New York, 1968).

[22] P. Lorrain, D. Corson and F. Lorrain, *Electromagnetic fields and waves*
(Freeman and company, New York, 1988).

[23] D. M. Brink, *Semi-classical methods in nucleus-nucleus scattering*
(Cambridge University Press, Cambridge, 1985).

[24] N. Carjan, O. Serot and D. Strottman, Japanese Journal of Applied Physics **9** (1992) 86.

[25] M. W. Kermode and N. Rowley, Phys. Rev. C **48** (1993) 2326.

[26] G. Bencze and A. Sandalescu, Phys. Lett. **22** (1966) 473;
G. Bencze, Phys. Lett. **23** (1966) 713.

[27] L. Scherk and E. W. Vogt, Can. J. Phys. **46** (1968) 1119.

[28] N. Rowley and A. C. Merchant, Astrophysical Journal **381** (1991) 591.

[29] N. Rowley, G. D. Jones and M. W. Kermode, J. Phys. G **18** (1992) 165.

[30] D. M. Brink and G. R. Satchler, *Angular Momentum*
(Oxford University Press, Oxford, 1993).

[31] J. X. Wei *et al.*, Phys. Rev. Lett. **67** (1991) 3368;
R. C. Lemmon *et al.*, Phys. Lett. B **316** (1993) 32;
C. R. Morton *et al.*, Phys. Rev. Lett. **72** (1994) 4074.

[32] M. A. Nagarajan *et al.*, J. Phys. G **12** (1986) 529.

[33] *Handbook of mathematical functions* edited by M. Abramowitz and I. A. Stegun
(Dover Publications, New York, 1965).

[34] R. R. Chasman and J. O. Rasmussen, Phys. Rev. **112** (1958) 512.

[35] J. O. Rasmussen and B. Segall, Phys. Rev. **103** (1956) 1298.

[36] E. M. Pennington and M. A. Preston, Can. J. Phys **36** (1958) 944.

[37] J. O. Rasmussen and E. R. Hansen, Phys. Rev. **109** (1958) 1656.

[38] J. K. Poggenburg, H. J. Mang and J. O. Rasmussen, Phys. Rev. **181** (1969) 1697.

[39] N. A. Jelley *Fundamentals of nuclear physics*
(Cambridge University Press, Cambridge, 1990).

[40] A. Bohr and B. R. Mottelson, *Nuclear Structure Vol. II*
(Benjamin, New York, 1975).

[41] D. J. Rowe, *Nuclear Collective Motion*
(Methuen and Co., London, 1970).

[42] A. Bohr and B. R. Mottelson, *Nuclear Structure Vol. I*
(Benjamin, New York, 1975).

[43] J. Wouters, D. Vandeplassche, E. Van Walle, N. Severijns and L. Vanneste, Hyperfine Interactions **22** (1985) 527.

[44] P. Schuurmans, Leuven (*private communication*).

[45] A. J. Soinski and D. A. Shirley, Phys. Rev. C **10** (1974) 1488.

[46] A. J. Soinski, R. B. Frankel, Q. O. Navarro and D. A. Shirley, Phys. Rev. C **2** (1970) 2379.

[47] S. H. Hanauer, J. W. T. Dabbs, L. D. Roberts and G. W. Parker, Phys. Rev. **124** (1961) 1512.

[48] Q. O. Navarro, J. O. Rasmussen and D. A. Shirley, Phys. Lett. **2** (1962) 353.

[49] J. Wouters, D. Vandeplassche, E. Van Walle, N. Severijns and L. Vanneste, Phys. Rev. Lett. **56** (1986) 1901.

[50] P. Schuurmans *et al.*, International conference on nuclear shapes and nuclear structure at low excitation energies, Antibes, France (1994).